

**ARCHIVE COPY  
DO NOT LOAN**

cy.1

J S.C



**NONINTRUSIVE (NONINTERFERING) ULTRASONIC  
TECHNIQUES TO MEASURE GAS MASS  
FLOW RATES**

Lawrence C. Lynnworth, Charles A. Carey and Norman E. Pedersen

Panametrics, Inc.  
221 Crescent Street  
Waltham, Massachusetts 02154

October 1974

Final Report for Period July to December, 1973

Approved for public release; distribution unlimited.

AEDC TECHNICAL LIBRARY



5 0720 00036 6957

Prepared for

ARNOLD ENGINEERING DEVELOPMENT CENTER  
AIR FORCE SYSTEMS COMMAND  
ARNOLD AIR FORCE STATION, TENNESSEE 37389

U.S. AIR FORCE  
AEDC LIBRARY  
F40600-75-C-0001

### NOTICES

When U. S. Government drawings specifications, or other data are used for any purpose other than a definitely related Government procurement operation, the Government thereby incurs no responsibility nor any obligation whatsoever, and the fact that the Government may have formulated, furnished, or in any way supplied the said drawings, specifications, or other data, is not to be regarded by implication or otherwise, or in any manner licensing the holder or any other person or corporation, or conveying any rights or permission to manufacture, use, or sell any patented invention that may in any way be related thereto.

Qualified users may obtain copies of this report from the Defense Documentation Center.

References to named commercial products in this report are not to be considered in any sense as an endorsement of the product by the United States Air Force or the Government.

### APPROVAL STATEMENT

This technical report has been reviewed and is approved.

*Melvin L. Guiou*

MELVIN L. GUIOU  
Captain, USAF  
Research and Development  
Division  
Directorate of Technology

*Robert O. Dietz*

ROBERT O. DIETZ  
Director of Technology

# UNCLASSIFIED

REPORT DOCUMENTATION PAGE		READ INSTRUCTIONS BEFORE COMPLETING FORM
1. REPORT NUMBER AEDC-TR-74-77	2. GOVT ACCESSION NO.	3. RECIPIENT'S CATALOG NUMBER
4. TITLE (and Subtitle)  NONINTRUSIVE (NONINTERFERING) ULTRASONIC TECHNIQUES TO MEASURE GAS MASS FLOW RATES	5. TYPE OF REPORT & PERIOD COVERED Final Report - July to December 1973	
	6. PERFORMING ORG. REPORT NUMBER	
7. AUTHOR(s) L. C. Lynnworth, C. A. Carey, and N. E. Pedersen	8. CONTRACT OR GRANT NUMBER(s) F40600-73-C-0011	
9. PERFORMING ORGANIZATION NAME AND ADDRESS Panametrics, Inc. 221 Crescent Street Waltham, Massachusetts 02154	10. PROGRAM ELEMENT, PROJECT, TASK AREA & WORK UNIT NUMBERS  Program Element 65802F	
11. CONTROLLING OFFICE NAME AND ADDRESS Arnold Engineering Development Center (DYFS) Air Force Systems Command Arnold Air Force Station, Tennessee 37389	12. REPORT DATE October 1974	
	13. NUMBER OF PAGES 127	
14. MONITORING AGENCY NAME & ADDRESS (if different from Controlling Office)	15. SECURITY CLASS. (of this report)  UNCLASSIFIED	
	15a. DECLASSIFICATION/DOWNGRADING SCHEDULE  N/A	
16. DISTRIBUTION STATEMENT (of this Report)  Approved for public release; distribution unlimited.		
17. DISTRIBUTION STATEMENT (of the abstract entered in Block 20, if different from Report)		
18. SUPPLEMENTARY NOTES  Available in DDC		
19. KEY WORDS (Continue on reverse side if necessary and identify by block number)  ducts                      nonintrusive                      ultrasonics 1 flowmeters              subsonic flow                      volumetric flow rate flow velocity              ultrasonic measurements mass flow rate              ultrasonic transducers		
20. ABSTRACT (Continue on reverse side if necessary and identify by block number)  An analytic and experimental effort was conducted to determine the range of applicability of ultrasonic flowmeters for gases, and in particular, to determine the optimum nonintrusive ultrasonic flowmeter design for the Propulsion Wind Tunnel (PWT) facilities at Arnold Engineering Development Center (AEDC). This effort included evaluations of six types of ultrasonic flowmeter approaches (1) Transmission, (2) Reflection/Doppler Scatter, (3) Beam Drift, (4) Correlation, (5) Noise, and (6) Vortex-Shedding. For a class of duct applications		

UNCLASSIFIED

20. ABSTRACT Continued

represented by the PWT facilities, we concluded that a transmission measurement would be optimum. To achieve the required accuracy of 0.5% in gas mass flow rate, for Mach Numbers up to at least 0.5, it appears essential to utilize coherent detection. The ultrasonic flowmeter design which is recommended for use in the PWT facilities uses flush-mounted electrostatic transducers, a 50-kHz amplitude-modulated cw carrier, and a phase comparison of two waves, preferably launched simultaneously, upstream and downstream, over a common path. Preliminary experiments, conducted from ~20 to 150 kHz in a 25 cm x 25 cm duct at Mach 0.15, together with the analysis of signal/noise ratio and other factors, support the conclusion that the selected 50 kHz synchronous detection, modulated cw system should provide the required accuracy and response time, in the PWT or similar facilities.

UNCLASSIFIED

## PREFACE

This report was prepared by Panametrics, Inc., Waltham, Massachusetts, under U. S. Air Force Contract No. F40600-73-C-0011. This contract was initiated under Air Force Program Element 65802F. The work was sponsored by the Arnold Engineering Development Center, Air Force Systems Command, with Captain Melvin L. Guiou, Technical Representative.

This report covers work performed during the period July to December 1973. The manuscript used in the reproduction of this report was supplied by the authors and was released for publication in March 1974.

The authors would like to acknowledge Thomas Donaghue, Ralph Fisher and Warren Rea for performing measurements. The authors are grateful to Dr. Edmund H. Carnevale for helpful comments during the program.

## TABLE OF CONTENTS

	<u>Page</u>
INTRODUCTION	9
Statement of the Problem	10
Background	12
Direct-Connect Engine Testing	12
Typical Airplane Model with Flow Through Duct	12
Supersonic and Hypersonic Flow	13
Approach	14
ULTRASONIC FLOWMETER MEASUREMENT APPROACHES	15
Ultrasonic Principles Underlying $v$ Determination	15
Transmission	16
Reflection/Doppler Scatter	17
Beam Drift	18
Correlation	19
Noise	21
Vortex-Shedding	24
Principles Underlying Density Determination	25
Ultrasonic $\rho$ or $\rho c$ Determinations	25
Nuclear Measurement of Air Density Profile	26
SIGNAL-TO-NOISE RATIO	30
Small Signal Considerations	30
Thermal Absorption	31
Relaxation-Humidity	32
Turbulent Scattering	32
Harmonic Generation	37
Diffraction-Beam Spread (Near Field, Far Field, Steered Beam)	37
Noise	41
Source of Noise	41
Noise in Ducts Versus Mach Number	47
Small Signal-To-Noise Ratio	50

## TABLE OF CONTENTS (cont'd)

	<u>Page</u>
OTHER ANALYTIC OR DESIGN CONSIDERATIONS	52
Gas Pressure Effects on Signal Losses	52
Comparison of Ultrasonic Flowmeters for Gases Versus Liquids	52
Electrostatic Transducers	54
Transducer Mounting - Design Configurations	54
Piezoelectric Crystals and Ceramics	58
Magnetostrictive Metals	59
Electromagnetic Transduction	60
Precision, Bias, Stability and Response Time	60
Installation, Operation and Maintainability	61
Calibration	61
Data Acquisition and Recording	62
EXPERIMENTAL RESULTS	63
OPTIMUM DESIGN FOR FUTURE TESTS IN PWT FACILITIES AT AEDC	78
CONCLUSIONS AND RECOMMENDATIONS	83
REFERENCES	84
APPENDIX A - Acoustic Transmission Across 25 cm Duct at Mach 0.15	89
APPENDIX B - Reprint: Ultrasonic Mass Flowmeter	110
APPENDIX C - Reprint: Nonintrusive Dynamic Flowmeter	114
APPENDIX D - Reprint: Nonintrusive Ultrasonic Measurement of Flow Velocity and Mass Flow Rate	118
LIST OF SYMBOLS	126

## LIST OF ILLUSTRATIONS

Figure No.

1a	Typical configuration - mode conversion transducers for upstream-downstream propagation, over the same path.	16
1b	Typical configuration - traveling wave tube mode transmission for upstream-downstream transmission, over different paths.	16

## LIST OF ILLUSTRATIONS (cont'd)

<u>Figure No.</u>		<u>Page</u>
2	Typical scattering transducer configuration.	17
3	Typical beam drift transducer configuration.	18
4a	Typical correlation transducer configuration for a model.	19
4b	Typical correlation pulse-echo configuration for a duct.	19
4c	Typical correlation through-transmission configuration for a duct.	19
5a	Direction distribution of the far field sound radiation for turbulent jets of three different speeds.	23
5b	Noise power versus Mach number.	23
5c	Sound power versus freestream flow velocity for various classes of jets.	23
6	Vortex-shedding ultrasonic flowmeter.	24
7	Geometry for determination of density profiles by nuclear radiation scattering.	28
8	Thermal sound attenuation and amplitude ratios in air at several frequencies, versus path length L.	33
9	Total absorption of sound in air as a function of frequency.	34
10	Attenuation in air due to turbulence and amplitude ratio, versus path length.	38
11	Multiplier for attenuation due to harmonic generation.	39
12	Beam characteristics of circular piston. Dimensions shown are approximations suitable for estimating purposes.	40



## LIST OF ILLUSTRATIONS (cont'd)

<u>Figure No.</u>		<u>Page</u>
13	Schematic of pulse trajectory and wave fronts in a real flow.	42
14	Normalized rms pressure per hertz versus normalized frequency.	45
15	Spatial filtering factor for finite transducers of diameter (d).	48
16	Turbulent rms noise pressure/hertz for a fully developed pipe flow in a 25 cm duct with a 2.5 cm diameter transducer.	49
17	Signal-to-noise ratio in a 25 cm duct with a 2.5 cm diameter transducer.	51
18	Calculated losses due to acoustic impedance mismatch.	53
19	Electrostatic realization of arrays.	56
20	Nonrotated small signal plane wave methods.	57
21	Magnetostrictive transducer used with all-metal seal, with nonmetal gasket, and in direct coupling to duct.	59
22	Wind tunnel for bench tests.	64
23a	Low cutoff frequency large diameter electrostatic transducer.	68
23b	High cutoff frequency small diameter electrostatic transducer.	68
24	Coherent detection system for bench tests.	70
25	Downstream transmitted signals across a 25.4 cm duct with $M = 0.15$ .	72
26	Upstream transmitted signals across a 25.4 cm duct with $M = 0.15$ .	73

## LIST OF ILLUSTRATIONS (cont'd)

<u>Figure No.</u>		<u>Page</u>
27	Measured signal-to-noise versus frequency.	75
28	Oscillogram showing transmission at 0.5 MHz rf burst across a 60 cm static air path.	77
29	Timing diagram.	80
30	Block diagram of ultrasonic flowmeter design for gases, using synchronous detection and demodulation.	81
A1	Transducer mounting relative to flow direction and transducer size.	90
A2	2.54 cm transducers - transmitter upstream by 7.62 cm from receiver (10 kHz).	92
A3	2.54 cm transducers - transmitter upstream by 7.62 cm from receiver (20 kHz).	93
A4	2.54 cm transducers - transmitter upstream by 7.62 cm from receiver (40 kHz).	94
A5	2.54 cm transducers - transmitter upstream by 7.62 cm from receiver (80 kHz).	95
A6	2.54 cm transducers - transmitter downstream by 7.62 cm from receiver (10 kHz).	96
A7	2.54 cm transducers - transmitter downstream by 7.62 cm from receiver (20 kHz).	97
A8	2.54 cm transducers - transmitter downstream by 7.62 cm from receiver (40 kHz).	98
A9	2.54 cm transducers - transmitter downstream by 7.62 cm from receiver (80 kHz).	99
A10	6.35 cm transducers - transmitter upstream by 2.54 cm from receiver (10 kHz).	100
A11	6.35 cm transducers - transmitter upstream by 2.54 cm from receiver (20 kHz).	101

## LIST OF ILLUSTRATIONS (cont'd)

<u>Figure No.</u>		<u>Page</u>
A12	6.25 cm transducers - transmitter upstream by 2.54 cm from receiver (50 kHz).	102
A13	6.25 cm transducers - transmitter upstream by 2.54 cm from receiver (82.2 kHz).	103
A14	6.25 cm transducers - transmitter upstream by 2.54 cm from receiver (99.4 kHz).	104
A15	6.25 cm transducers - transmitter downstream by 2.54 cm from receiver (10 kHz).	105
A16	6.25 cm transducers - transmitter downstream by 2.54 cm from receiver (20 kHz).	106
A17	6.25 cm transducers - transmitter downstream by 2.54 cm from receiver (50 kHz).	107
A18	6.25 cm transducers - transmitter downstream by 2.54 cm from receiver (82.1 kHz).	108
A19	6.25 cm transducers - transmitter downstream by 2.54 cm from receiver (99.4 kHz).	109

## LIST OF TABLES

<u>Table No.</u>		
1	Location in report of analytical considerations.	10
2	Maximum pressure at transmitter (atm) for small signal transmission (1 atm, 300°K).	31
3	Maximum percent of dynamic head which appears as wall pressure fluctuations in various flow situations.	43
4	Comparison of typical parameters, relative to ultrasonic flowmetry.	55
5	Propagation parameters for a 25.4 cm path in wind tunnel.	65

## INTRODUCTION

This report describes the results of a six-month analytic effort, and some bench tests and experiments, conducted to determine the areas of applicability, and the limitations of, nonintrusive (noninterfering) ultrasonic techniques to measure gas mass flow rates.

In this introductory section we will first state the problem in terms of AEDC's requirements. Then we will identify a simple duct as a starting point for analysis and experiments. We will then indicate one possible extension of measurements on a single duct, to measurements on a number of adjacent ducts, analogous to a venturi plate, but with minimal pressure drop. Lastly, we will mention some other applications of interest. The introductory section will conclude with a table that tells where in the report the analyses of the eleven contractually-specified items are to be found (see page 10).

The rest of the report itself is organized into principal sections (see also, Table of Contents) covering these topics:

Ultrasonic Flowmeter Measurement Approaches

Signal, Noise, Response Time and Accuracy

Transducers

Other Analytic Considerations

Experimental Results

Ultrasonic Mass Flowmeter Design for Duct or Pipe,  
~250- to 500-mm Diameter, Mach No.  $\leq 0.5$

Conclusions

Recommendations

Acknowledgments

References

It will be shown that, as a result of the above analysis and experiments, we are able to adapt one of our ultrasonic liquid flowmetering designs to gas flow, suitable for tests in the existing Propulsion Wind Tunnel (PWT) facilities at AEDC.

Table 1. Location in report of analytic considerations.

<u>Item</u>	<u>Page</u>
1. Precision and bias (uncertainty $\leq 0.5\%$ ).	54, 55, 60
2. Response $\leq 1$ sec.	29, 43, 60, 44
3. Stability: system must continuously conform to a particular set of specifications for at least 24 hours.	60, 78-82
4. Ease of installation and operation.	54-61, 66
5. Maintainability.	61
6. Calibration.	61
7. Correct averaging over velocity and mass flow profile.	14, 25-29
8. Duct material and precision requirements.	44
9. Subsonic, supersonic and hypersonic velocities.	9-109
10. Effects on performance caused by:	
a. Noise and vibration environment as experienced in normal wind tunnels.	30-51
b. Particulate scatterers (e. g. , dust in normal wind tunnels).	17, 32
c. Humidity.	32
11. Data acquisition and recording.	62

Let us now state the problem, in language essentially the same as in Annex "A" of the contract.

## I. STATEMENT OF THE PROBLEM

In day-to-day aerodynamic and engine testing in ground test facilities one of the most common requirements is for the determination of gas velocity and mass flow rates in ducts. Conventional methods of adequate accuracy, e. g. , venturi or orifice plates, total and static pressure surveys

or rakes, hot wire or hot filament probes, etc. , have been developed and are presently used. However, these conventional methods have disadvantages in certain applications which at present are accepted because of lack of a better solution. To list a few:

1. Venturi and orifice plates cause a sizable pressure loss in the flow, and require undisturbed inflow conditions and space which may not always be available.
2. Total and static pressure surveys by a movable single probe are impractical for routine development testing. Total and static fixed pressure rakes (multiple probes) disturb the flow, normally to an unknown degree.
3. Movable hot wire or filament probe surveys are too cumbersome and time consuming for development testing in large facilities.

In recent years ultrasonic methods have been introduced as measuring techniques for liquids and gases. Nonintrusive methods have been described for the measurement of volume and mass flow rate, temperatures, speed of sound and density. Flowmeters have been developed for liquids, e. g. , water or fuel flow and natural gas in large supply lines. Although there has been progress and success in applying the ultrasonic technique to measure flow parameters, these developments and applications have been limited and actual potential of acoustic diagnostics methods in aerodynamics testing in comparison to conventional procedures has not been fully established.

Some of the expected basic advantages of ultrasonic methods are as follows:

1. No interference with flow (transducers recessed or on outside wall).
2. Ease of installation and operation.
3. Fast response.
4. Inherent independence of gas type or composition.
5. Minimum space requirement.
6. Potential of combining measurements of several flow parameters such as: density, temperature, speed of sound, and volume or mass flow rate.

The purpose of the present effort was to assess the feasibility, potential practicability and performance of ultrasonic techniques to measure velocity and mass flow rates and related parameters of gases for typical applications at AEDC.

## II. BACKGROUND

Testing in the Arnold Engineering Development Center's numerous facilities requires in many instances and under different conditions determination of gas mass flow rates. Present techniques, installations and requirements vary considerably over large ranges of mass flows to be measured at permanently installed measuring stations or at individually designed stations inside or outside a test model for specific investigations.

Examples of such requirements are:

### 1. Direct-Connect Engine Testing

Duct Mach number:	0.1 to 0.3
Duct static pressure:	0.5 to 400 psia
Temperature:	-75 to 750°F
Mass flow rate:	200 to 2200 lbs/sec
Response time:	1 sec
Duct diameter:	5 to 30 ft
Typical duct length:	30 ft
Accuracy desired:	0.5%
Present technique:	single or multiple venturi or orifice

### 2. Typical Airplane Model with Flow Through Duct

Duct Mach number:	0.2 to 0.9
Duct static pressure:	1.5 to 15 psia
Temperature:	100 to 130°F

Response time:	1 sec
Duct diameter:	2 to 20 inches
Length of duct:	5 to 20 diameters
Accuracy desired:	0.5%
Present technique:	Total and static pressure rates

3. Supersonic and Hypersonic Flow: Other needs are to measure supersonic and hypersonic velocities without disturbing the flow in test facilities up to approximately 20,000 feet per second. Conventional probing techniques in continuous and impulse facilities are extremely difficult for these conditions. Not all these conditions will occur simultaneously and are given below only to indicate the range of conditions:

Mach number:	1.5 to 20
Velocity:	1500 to 20,000 fps
Temperature:	500 to 10,000 °R
Pressure:	0.1 to 15 psia
Present technique:	Total and static pressure rates

These are only examples and general application at AEDC will require other conditions of velocity, temperature, pressure, duct Mach number, etc., therefore, these are not presented as limits to the region of interest. The limitations of the method were a subject of the study.

Application of ultrasonic measurements for conditions approximately described in II. 2 was of immediate interest and had the higher priority, since presently no completely satisfactory method is available. Requirements similar to those described in II. 1 may develop in the future under conditions where venturis or orifices may no longer be acceptable (because of pressure loss).

It was, therefore, the intent of the proposed effort to concentrate on conditions encompassing the requirements of II. 2.



### III. APPROACH

The contractor was to analytically evaluate the potential and performance of different nonintrusive (noninterfering) ultrasonic techniques to measure gas velocity and mass flow rates and related parameters within the envelope of II. 2. This evaluation could extend beyond the described envelope to determine the actual boundaries within which the essential requirements can be fulfilled. The initial studies were to be based on simple straight ducts of circular or square cross section.

Panametrics was to describe the different approaches studied, presenting advantages and disadvantages of each and recommend the best system for possible experimental verification.

The analysis was to cover, but not be limited, to, the items in Table 1. During the analytical phase we decided to conduct certain small scale bench tests of system components as required to supplement and support the analytical study.

If in the analysis a system was defined which could be expected to meet the requirements in II. 2, the contractor was to briefly explore the possible extension of such system to the more severe conditions in II. 1 and II. 3. Regarding this cited Requirement 2, it was agreed early in the program, during a visit to AEDC, to conduct "bench tests" on a simple duct under these conditions including as much as possible of the ranges in Requirement 2. This turned out to involve design, construction and testing in a square duct ~25 cm x 25 cm, operated essentially at atmospheric temperature and pressure, at a Mach No. of ~0.15.

During this same visit to AEDC, it was emphasized by AEDC and ARO personnel, that the pressure drop associated with existing venturi plates was undesirable from both technical and energy-consumption points of view, especially in large-diameter ducts. Some of these ducts are several meters in diameter, which may be too large to reliably propagate across, with adequate signal/noise to achieve the desired accuracy of 1/2%. For such large ducts, we suggested inserting an assembly of short tubes, or a honeycomb, to divide the area into cells of diameter small enough to be measured ultrasonically. The cell walls could be rather thin, ~1 mm, plus some allowance for transducer bodies and cabling. It would therefore appear that even a large number of cells, ~100, might be installed, and yet avoid pressure drops larger than a few percent. Admittedly, this "ultrasonic honeycomb" concept is not nonintrusive. But it appears to offer a profiling and/or averaging capability, with minimal penalty due to pressure drop. It also offers the prospect of applying a design which can be tested and verified in a small flow facility, to much larger ducts, simply by connecting additional cells, to map out the full duct area of interest.

## ULTRASONIC FLOWMETER MEASUREMENT APPROACHES

Determination of the total mass flow rate  $\dot{M}$  through a duct generally involves integrating the local  $\rho v$  products. Let us first consider ultrasonic principles related to measuring  $v$ , and then ultrasonic and other principles related to  $\rho$ .

### ULTRASONIC PRINCIPLES UNDERLYING $v$ DETERMINATION

We may distinguish six (6) different ways of ultrasonically sensing or interacting with a flowing gas:

	<u>Principle Summarized in Equation Form</u>
• Transmission	$\Delta f \sim v; \Delta t \sim v/c^2; \Delta t / \Sigma t \sim v/c$
• Reflection/Doppler Scatter	$f_D \sim v/c$
• Beam Drift	$x/D = v/c$
• Correlation	$x/r = v$
• Noise	$n \sim v^p, p \approx 3 \text{ to } 8, \text{ depending on } v$
• Vortex Shedding	$f \sim v$

Nonintrusive aspects of the first four of these have been discussed in the paper (Lynnworth et al. , 1971) presented in May 1971 at the ISA Symposium on Flow, Noninvasive Ultrasonic Measurement of Flow Velocity and Mass Flow Rate. With the permission of the ISA, a copy of this paper is appended.

The principle of passively "listening" to the flow rate is the basis for at least one commercially available ultrasonic flowmeter (abstract 349, p. 26, in Dowden, 1972). The principle of measuring ultrasonically, the frequency at which vortices are shed by a strut, is the basis for other commercially available ultrasonic flowmeters for liquids and gases. However, the intrusiveness of the strut generally puts vortex shedding devices beyond the scope of extensive consideration in this report. Likewise, the intrusiveness of fluidic flowmeters (abstracts 1672-1676, p. 140, in Dowden) rule out further consideration of this type flowmeter in this report, even though the fluidic oscillator frequency may lie in the ultrasonic range.

For general background and historical perspectives, interesting reviews of sound propagation in air are given by Allen et al. (1950) and later by Nyborg and Mintzer (1955). Sonic anemometry was reviewed briefly by Foxx, 1968. Let us now briefly identify the six above-listed approaches. We will then concentrate on those principles most relevant to AEDC's Requirements.

## Transmission

**Principle:** Sound travels faster with the wind than against it.

**Typical Configurations:**

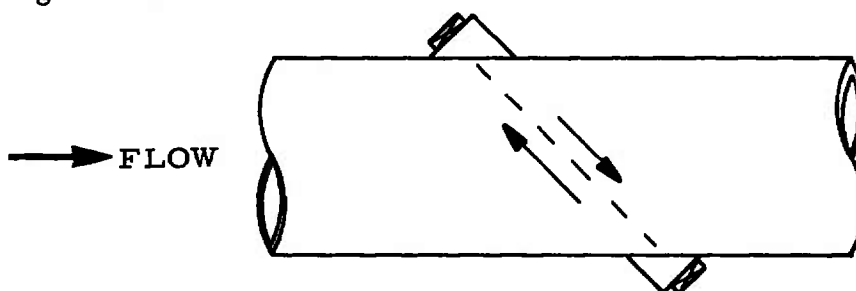


Fig. 1a. Transmission approach wherein upstream and downstream waves propagate over the same path.

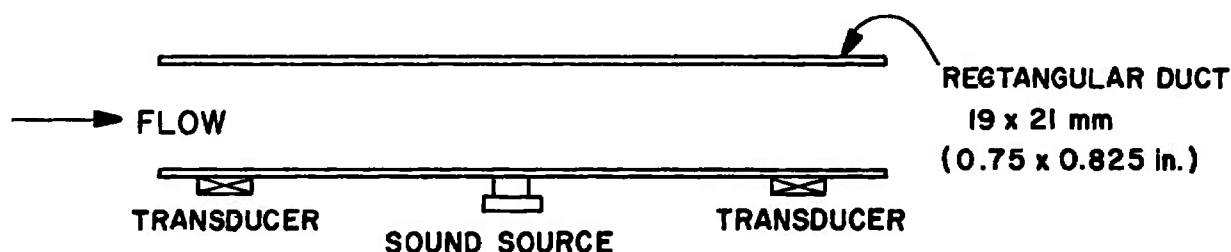


Fig. 1b. Transmission approach wherein a single sound source launches upstream and downstream waves which propagate over different paths (Ingaard and Singhal, 1973).

**Mathematics:** If time intervals  $t_1$  and  $t_2$  are measured upstream and downstream, their difference is  $\Delta t = 2l v/c^2$ . A similar relation holds, if phase shifts are measured. If reciprocals of time or phase are measured, their difference  $\Delta f$  is directly proportional to  $v$ , independent of  $c$ . See Figs. 1a, 1b.

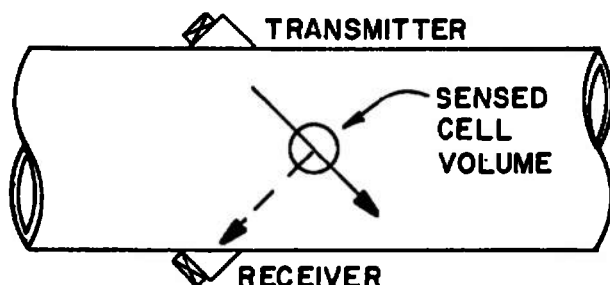
**Panametrics' Application in Liquids:** Aviation fuel mass flow rate  $\dot{M}$  (Eustis Directorate programs; reference: Lynnworth et al., 1972);  $v$  in water and cryogenic liquids (NASA-Langley programs; reference: Pedersen et al., 1972, 1973). Summaries of these transmission approaches are appended. Technique is widely used in commercial ultrasonic flowmeters for liquids and gases, as seen in ultrasonic flowmeters currently manufactured by NUSonics, Saratoga Systems, Scarpa Laboratories, and Westinghouse. This principle, used at MIT to a Mach No. of  $\sim 0.5$ , in a small duct, was reported recently, and is sketched in Fig. 1b (Ingaard and Singhal, 1973). In this MIT work, the sound source and receiving transducers were isolated from the duct wall, and were coupled directly to the air flowing in the duct.

## Reflection/Doppler Scattering

**Principle:** The frequency of a wave is shifted when the wave is reflected from a moving scatterer.

**Typical Configuration:**

Fig. 2. In doppler flowmeters, the transmitted and scattered beams of interest may be orthogonal, as shown here, or oblique, or parallel to one another. As long as at least one of the beams propagates not normal to the flow vector, the scattered wave will be doppler-shifted.



**Mathematics:** The difference  $f_d$  between the transmitted frequency  $f_0$  and the received frequency  $f_1$ , is proportional to  $v/c$ . The "constant" of proportionality depends partly on geometry. It ranges between 0 and  $2 f_0$ .

This approach is mainly used in biomedical studies of blood flow and tissue movement (Ultrasonics 11 (2), 52-53, March, 1973). In industrial applications, this approach has been considered when the fluid already contains scatterers. Examples include contaminants in aviation fuel, vapor bubbles in prepolymers, and the as-yet-undetermined scatterers in relatively pure liquid metals (Fowles, 1973).<sup>\*</sup> The doppler method offers a theoretical immunity to the acoustic short circuit problem which besets most transmission approaches. However, it suffers from phase shifts due to temperature gradients. It provides correct area-averaging only under conditions of uniform intensity and uniform distribution of scatterers, which conditions would be rather difficult to maintain in flowing gases. Lastly, in order to equate the motion of scatterers with the motion of the gas, one must solve the dilemma of having a particle small enough to travel precisely with the gas, yet large enough to scatter efficiently. Such particles generally are not to be naturally expected in a flow facility, nor is their injection into the gas considered welcome or practical. Hence, we terminate consideration of the doppler approach.

<sup>\*</sup>Lynnworth has suggested that strong velocity gradients, or turbulence might be a source of backscattering in an otherwise homogeneous uniform-density liquid. Apart from the well-known ray-bending or forward-scattering mechanisms, small vortices might cause local, perhaps short-term departures from  $c$ , in the effective sound propagation speed. Thus, backscattering could result due to local  $\rho c$  mismatch. This is somewhat analogous to backscattering from anisotropic grains in a polycrystalline solid. (Earlier (February 1973) Pedersen identified the short-term radial components of vortices as having a significant effect on dynamic, fast-response ultrasonic flow measurements where the acoustic path includes a radial component of the eddies.) See also: D. W. Beran et al., J. Acoust. Soc. Amer. 55, 2, 334-338 (Feb. 1974).

## Beam Drift

Principle: Sound beam is carried downstream by wind.

Typical Configuration:

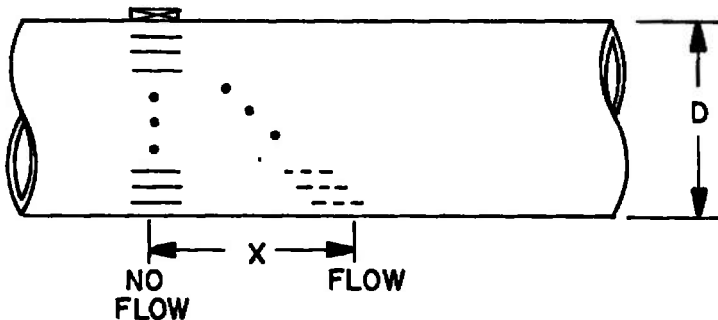


Fig. 3. The beam drift approach to measuring gas flow velocity is probably the simplest ultrasonic flowmetering method in use. It is applicable, depending on geometry, to flows below Mach No. 0.1, up to Mach 1 and beyond. Not unexpectedly, however, the advantages of simplicity and rangeability are offset by accuracy limitations, estimated as  $\sim 5\%$ , in one of the latest systems under evaluation.

Mathematics: If the normal to the wave fronts is orthogonal to the flow vector, the drift angle  $\theta$  is given by  $\tan \theta = v/c$ . The downstream drift  $x$  amounts to  $D v/c$ . The amplitude and phase of the wave at a particular receiving point will depend on  $v/c$  over the path.

Application in Air: National Physical Laboratory, England. Reported in journal *Ultrasonics*, pp. 197-199, September 1972. Flow was measured at 1 MHz in ducts up to 1 ft diameter. Panametrics used a beam drift method to measure the Mach No. of combustor exhaust gas ( $M \approx .25$ ) in a program conducted for GE-Evendale, Ohio (jet engine turbine inlet simulator). We have learned from G. G. Twidle at NPL, that in the beam drift approach under investigation in England's National Physical Laboratory (NPL), the present NPL system uses discrete transducers, not a continuous transducer. The discrete transducers would be expected to yield accuracy of  $\sim 5\%$ , based on processing of amplitude information only, as a measure of the beam drift, and hence a measure of the Mach No. The NPL system does not process phase information, which if used, could in principle improve the accuracy. Delivery of the final components for the NPL Flowmeter was scheduled to be completed in 1973. At the present time, no test results have been made available to us. At the present time, therefore, we have no evidence that this technique, as practiced, can yield accuracy better than 5%. Whether an order-of-magnitude improvement is possible based on phase measurements instead of or in addition to amplitude measurements, is not yet known.

## Correlation

**Principle:** Tags "attached" to the flowing air will successively modulate two interrogating beams or two recordings from spaced microphones at a time interval  $T$  inversely proportional to  $v$ , and essentially independent of  $c$ .

Typical Configurations:

Fig. 4a.

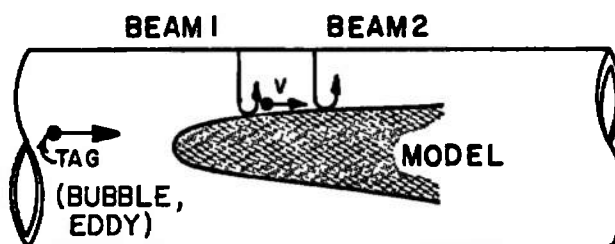
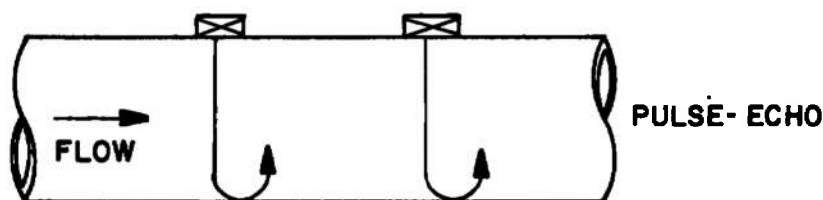


Fig. 4b.



OPTION: CIRCUMFERENTIAL TRANSDUCER NONINTRUSIVELY GENERATES HOT TAG NEAR AXIS WHEN ENERGIZED.

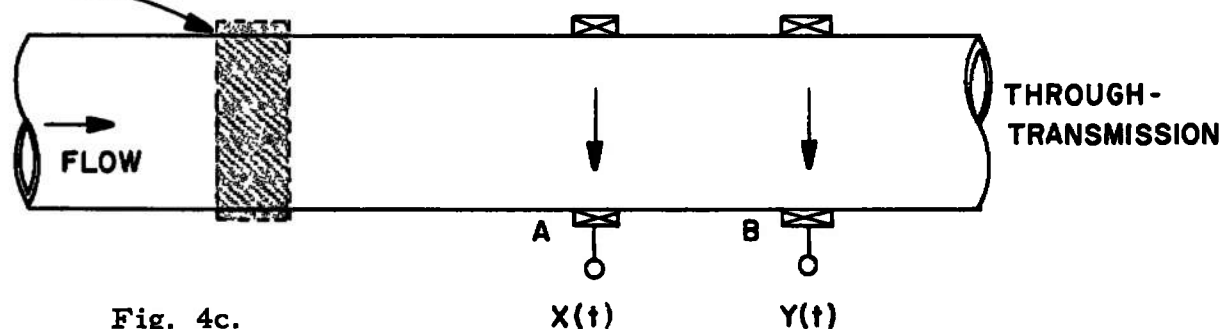


Fig. 4c.

Fig. 4. Correlation approach to measuring gas flow velocity. In (a) a tag, which may be a naturally-occurring eddy, or an introduced bubble, is indicated as a possible means of providing information on flow velocity  $v$  along the surface of a model. In (b) a pulse-echo version is shown, otherwise similar to the through-transmission version practiced by Coulthard (1972) and shown in the right-half of (c). At the left-half of (c) we also show an optional ultrasonic source of pulsed high-intensity waves, to introduce a tag nonintrusively.

**Mathematics:** The correlation time  $\tau = x/v$  where  $x$  = distance between beams.

**Application:** Normally-occurring thermal "tags" have been exploited in order to measure flow velocity profile in liquid metals by Wheelock et al. of the Liquid Metals Engineering Center in California. Thermocouple rakes detected the thermal inhomogeneities. We and others, have suggested using nonintrusive ultrasonic beams to perform an analogous ultrasonic measurement (Fig. 4).

In Fig. 4a we sketch a possible method for remotely determining the value of  $v$  next to a model surface. In Fig. 4b an average flow is sensed. Neglecting attenuation, it is interesting to note that if the transducers in Fig. 4b are applied circumferentially so as to interrogate the entire area within the (assumed) circular duct or pipe, a measure of the area-averaged flow velocity could be obtained, independent of flow profile. On the contrary, the same transducer configuration, utilized in a transmission measurement, would not generally yield the area-average, but the diameter-average.\*

Figure 4c represents a cross-correlation flowmeter developed at Teesside Polytechnic in England (Coulthard, 1973). Consider a disturbance detected at A and then later at B. If the signal recorded at point A is  $x(t)$  whose value is directly related to the instantaneous flow at point B, then the cross-correlation function expressing  $x(t)$  and  $y(t)$  in terms of a time variable  $\tau$  is given by the expression

$$\psi_{xy}(\tau) = \lim_{T \rightarrow \infty} \frac{1}{T} \int_0^T x(t) y(t + \tau) dt.$$

If all components of the flow can be assumed to move at a velocity  $v$ , then, for a transducer spacing  $x$  the flow velocity  $v$  is given by the expression

$$v = \frac{x}{\tau_m}$$

where  $\tau_m$  is the value of  $\tau$  corresponding to the peak value of  $\psi_{xy}(\tau)$ .

It may be argued that the value of  $\tau$  corresponding to the center of gravity of the cross-correlation peak should be taken as a measure of

\*Optionally, an upstream circumferential transducer periodically could be energized impulsively to yield a brief, high-intensity beam directed radially inward (Fig. 4c). This would nonintrusively produce a thermal pulse or tag in the gas. As the tag was carried downstream, its velocity could be measured (see also Fig. 6, p. 24).

the time of flight of the fluid between A and B, particularly if the peak exhibits any degree of asymmetry. Coulthard, however, took the peak value of  $\psi_{xy}(T)$  as the measure of flow since this lends itself more readily to electronic detection in a practical flowmeter. Departures from linearity achieved in initial trials were reported to be  $\sim 5\%$ , for these experimental conditions: air path, 150 mm (6 in.); downstream separation between transducers, 250 mm (10 in.);  $v = 10$  to 35 m/s. Further consideration of the correlation flowmeter is postponed until such time as theory predicts or experiments confirm an accuracy of  $\sim 0.5$  to 1%.

### Noise

In a technical historical paper on advances in aero-acoustics (Powell, 1965), it was shown that several methods of expressing aerodynamically generated sound, in the absence of solid surfaces, yielded the "eighth power law," i. e., the sound power varies as the eighth power of some characteristic flow velocity, on corresponding assumptions of similarity. In this program, it is recognized that the existence of a law for sound power might provide a basis for measuring flow velocity. Initially, however, the principal subject for application of such a theory was the noise caused by the exhaust flow of jet engines. The eighth power relationship was found, but the sound field was heavily biased at an acute angle to the jet direction, Fig. 5a. A transformation to moving axes explained how convection effects produced a bias of the observed type, but this simultaneously caused the power to increase more rapidly than according to the aforementioned eighth power law relationship and markedly so near a convection speed approaching the speed of sound in the atmosphere. It is noted that experimental data showed that this relationship held remarkably well to beyond such a speed, as respectively indicated in the uppermost and lowest curves of Fig. 5b, in which the convection velocity is supposed to be well represented by half the jet exit velocity.

As Powell explains, if one accepted the well-established fact that the simple dimensional analysis was consistent with experimental data so far as the total sound power is concerned (and took the view that the convection effects were yet to be fully explained), then it seemed plausible that various given volumes of the jet would, more or less, also follow the relationships of the simple similarity. Thus by assuming the flow characteristics to be similar in various slices of the jet, e. g., that the Strouhal numbers of the turbulence spectral peaks were all the same, then one could discuss the acoustic power produced per unit length of the jet. Like a boundary layer, the acoustic power was determined to depend only on the area of the constant-shear layer, because as the mixing region increases in thickness, the lesser gradient of the shear and the lesser frequency



turn out to be just compensated by the larger eddy size and thickness of the mixing region occupied by them. However, further downstream, where the mean velocity on the jet axis falls off rather rapidly, the assumed corresponding reduction in turbulent velocity and frequency fluctuations completely overwhelm all other factors, so that the sound power generated per unit length then falls off with the seventh power of the distance from the orifice.

Continuing, Powell traces the later improvement of the convection transformation itself. There were two quite independent approaches which yielded very similar forms of results. These show how the eighth power law ultimately gives way to a lower one at supersonic speeds, as indeed it must sooner or later since the total acoustic power can never exceed the total jet power, in practice being about one percent or so of it. No convection limitations (and consequently no diffractive effects) are incorporated in these theories, and this possibly goes towards accounting for the fact that the theoretical curve still rises appreciably beyond the simple law, as the middle curve of Fig. 5b suggests. At high speeds the theories suggest a third power law, if the effects of the change in jet structure and density are neglected (Fig. 5c).

These later developments have gone far to provide explanations of the various features of jet noise, about which much of the interest in aerodynamic noise has been.

At present, one type of acoustic noise flowmeter is available commercially, manufactured by Scarpa Laboratories, for nonintrusive use on pipes in which a liquid is flowing. Accuracy is claimed to be 2%. However, to relate noise due to a flowing gas, to the flow velocity, independent of the local solid surfaces, appears to be a rather formidable task.\*

Consideration of a noise flowmeter for gases appears to be of academic interest, and perhaps of limited experimental interest, where, for gas flow,  $v$  estimates only somewhat better than order-of-magnitude would be adequate. The possibility of measuring  $v$  to  $\sim 1\%$  appears remote, based on the nature of the variables, as summarized by Powell. Accordingly, the noise flowmeter approach will not be pursued further.

---

\*See, however, abstract 349, p. 26, in Dowden, 1972. It was reported in 1969 that the power level of the ultrasonic noise was directly proportional to the volume flow rate of the moving gas, liquid, slurry or powder (New Scientist 44 (679), 558, December 11, 1969). Theoretically, of course, it is clear that "direct proportionality" could be expected as an approximation only over a limited flow range. A flow/no flow acoustic noise sensor, model SF-14A, is manufactured by Sensor Technology Company of Seattle.

Source:  
Powell, 1965

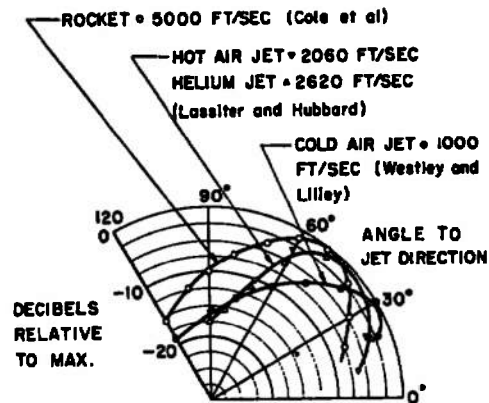


Fig. 5a. Direction distribution of the far field sound radiation for turbulent jets of three different speeds.

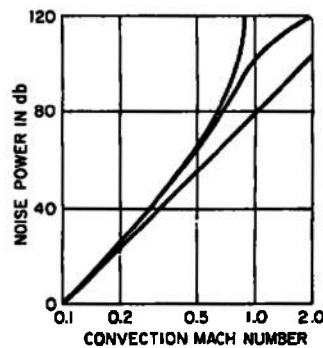


Fig. 5b. The straight line is for the "eighth power law". The highest curve is that when the original convection theory was applied, middle curve being for the improved convection theory. The convection curves are approximations only, based upon the average effect for various types of quadrupoles.

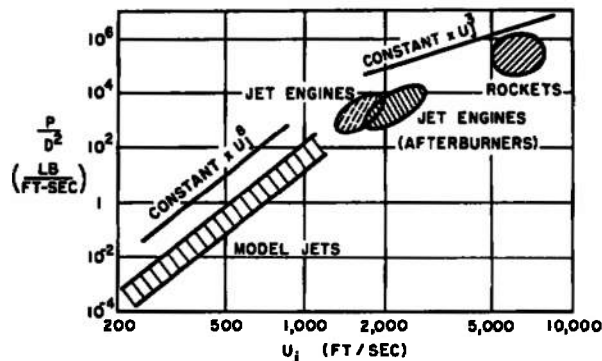


Fig. 5c. The sound power "P" of various classes of jets after the effect of the diameter "D" has been allowed.

## Vortex-Shedding

**Principle:** The rate or frequency at which vortices or eddies are shed from a body effectively depends, in the simplest case, on flow velocity  $v$ . The shed vortices can modulate an ultrasonic beam aimed across the wake.

**Typical Configuration:**

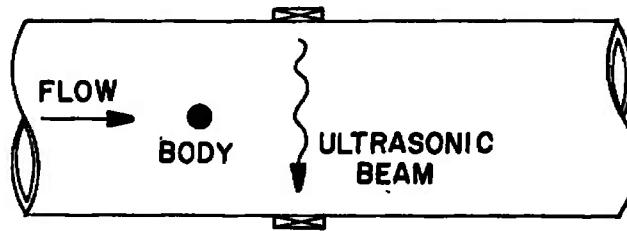


Fig. 6. Vortex-shedding ultrasonic flowmeter.

**Mathematics:**  $f \sim v$ . The mathematics is more complicated for non-circular bodies (Mujumdar et al., 1970) for turbulent flow and for flow gradients.

**Application:** Airspeed, angle of attack measurements. These and other applications are being developed by J-Tec Associates (Klass, 1972). The basic technique is described in U. S. Patent No. 3,680,375. Accuracy is 1% of full-scale.

**Comment:** This principle is considered generally not applicable to the present requirements, because:

- Body which sheds vortices is inherently intrusive (exception: shedding, off parts of model in duct).
- Shedding frequency depends on average Reynolds number, or average  $v$ , over an extended region. However, a strut of nonuniform diameter, or a group of parallel struts, might be used to obtain profile information.

## PRINCIPLES UNDERLYING DENSITY DETERMINATION

### Ultrasonic $\rho$ or $\rho c$ Determinations

There are several ultrasonic approaches to measuring fluid density or impedance:

- Measure resonant frequency of vane (November, 1972); commercially available from ITT-Barton. Yields  $\rho$  near vane.
- Measure electrical input impedance of transducer (e. g. , quartz), radiating into fluid (Kritz, 1955). Yields  $\rho c$  near transducer.
- Compare reflection from rod whose end is in contact with fluid, to reflection from another portion of rod, or from another similar rod, which is not radiating into the fluid (Lynnworth et al. , 1971, 1972). Yields  $\rho c$  at rod end.
- Measure sound speed in fluid. Yields average  $c$  or  $c$  profile across duct.
- Measure signal amplitude after transmission across duct or across other sampled volume. Result depends on  $\rho c$  and attenuation, not just  $\rho$ .

If the gas density is uniform or of predictable profile, nonultrasonic methods are probably easiest to use. If the profile is not predictable, then the resonant vane is ruled out by virtue of the intrusiveness required to determine the profile, and the next two "loading" methods are ruled out because they sample only the fluid close to the loaded or radiating surface. Although they appear to be moderately ( $\sim 0.3\%$ ) sensitive for detecting liquid  $\rho c$ , they would be essentially insensitive to changes in gas  $\rho c$  over the conditions of this program. The last method is not likely to provide high accuracy because of amplitude fluctuations due to turbulence and attenuation. Thus, the only nonintrusive ultrasonic densitometry approach holding potential merit is based on measuring the speed of sound  $c$  in the gas.

One application of  $c$  to  $\rho$  profile determination is as follows. To the extent that the gas is isobaric, the density profile is determined by the temperature profile, and a knowledge of the static pressure at one point, say, at the wall. Now the temperature ( $T$ ) profile can be determined from multipath measurements of  $c$  (which yield the  $c$  profile). That is, when  $p = \text{constant}$ ,  $c \longrightarrow T \longrightarrow \rho$ .

A check on the isobaric state may be obtainable by using a momentum equation. This would utilize the  $v$  profile, possibly measured with the same transducers used to get the  $c$  profile.

It should be noted that ultrasonic impedance-sensing probes, which yield  $\rho c$ , rather than  $\rho$  alone, are not necessarily undesirable for that reason. For it is possible to combine transmission measurements upstream and downstream, or across the stream and oblique or along the stream, to obtain the Mach No.  $v/c$ , which, when multiplied by  $\rho c$ , results in a product proportional to  $\dot{M}$ , the mass flow rate.

Given the nonintrusive constraint, the only instrumentation\* (for  $\rho$ ) techniques in common use today involve nuclear measurements. Recognizing that objections have been raised in the past about this approach, and following AEDC's recommendation not to pursue this approach within the present contract, we have no new results to report in this area. However, to provide some perspective on the present work, and to provide a basis for discussion concerning possible future requirements for densitometry not adequately covered by existing nonnuclear technologies, we include next, a brief discussion of nuclear measurements of air density profile, prepared by F. B. Sellers.

## NUCLEAR MEASUREMENT OF AIR DENSITY PROFILE

### a. Two Dimensional Flow

The measurement of density profiles in the vicinity of an object, such as a wing section, which produces essentially a two dimensional flow pattern is straightforward. In such instances the symmetry of the flow allows measurement of the attenuation of a beam of nuclear radiation ( $\alpha$  or beta rays for densities of interest here) to define the localized density. The quantity measured in this type gage is the integral of the density  $\rho$  ( $\text{g/cm}^3$ ) along the radiation path  $x$ (cm)

$$d(\text{g/cm}^2) = \int_0^l \rho(x) dx \quad (1)$$

from the source location at  $x = 0$  to the detector location at  $l$ . The average density is then

$$\bar{\rho} = \frac{d}{l} = \frac{1}{l} \int_0^l \rho(x) dx \quad (2)$$

If  $\rho(x)$  is constant, independent of  $x$ , then  $\bar{\rho} = \rho$ , which is the case for two dimensional flow. This is because the beam can be directed such

---

\*Various electromagnetic techniques, which are based on index or dielectric constant changes with  $\rho$ , are not considered in this report.

that it is perpendicular to the flow pattern at any desired location in the pattern, and the density at every point within the beam path is the same.

Individual measurements with a density accuracy of better than 1% with a time constant on the order of a second are achievable for the attenuation method.

#### b. Three Dimensional Flow

Three dimensional flow patterns present a more difficult problem, because the nuclear radiation beam cannot normally be directed such that the density at all points along its path is the same. An attenuation measurement can still be employed usefully in those instances in which only the total mass per unit area  $d(g/cm^2)$  along the path of the radiation is of interest, but in this case the average density  $\bar{\rho}$  defined from (2) is not equal to the actual density along the radiation path (except by chance). However, measurement of the density within an arbitrary localized volume is not possible by attenuation.

In such a case it is possible to use a scattering technique, which is illustrated by the simple drawing in Fig. 7. Here a collimated radiation source produces a beam of radiation which passes through the skin (or a small aperture) of the body to be measured, and a detector is collimated in such a manner that it only observes radiation scattered from a particular, "sensed", volume. In this case the detector output depends on the density within the localized, or sensed, volume. If the radiation is such that it is attenuated along the path to and from the volume, then the detector output also depends on the quantity  $d$  defined in (1). But if the density profile is measured starting at a point sufficiently close to the body, then the values of density needed for measurements made far from the body are available.

While the source and detector are shown inside the body in Fig. 7, they can also be located outside if measurements are to be made far from the body, or if the body is too small to contain them. In any case, it is clearly necessary to move either the source, detector, or both simultaneously to complete a scan to determine a density profile.

A technique that may be of some use for this method is introduction into the flow pattern of powdered particles of materials (such as metals) whose scattering cross section is larger than that of air.\* Provided the density ratio of added material to air is independent of position

---

\*The above mentioned objection to seeding still would need to be resolved.

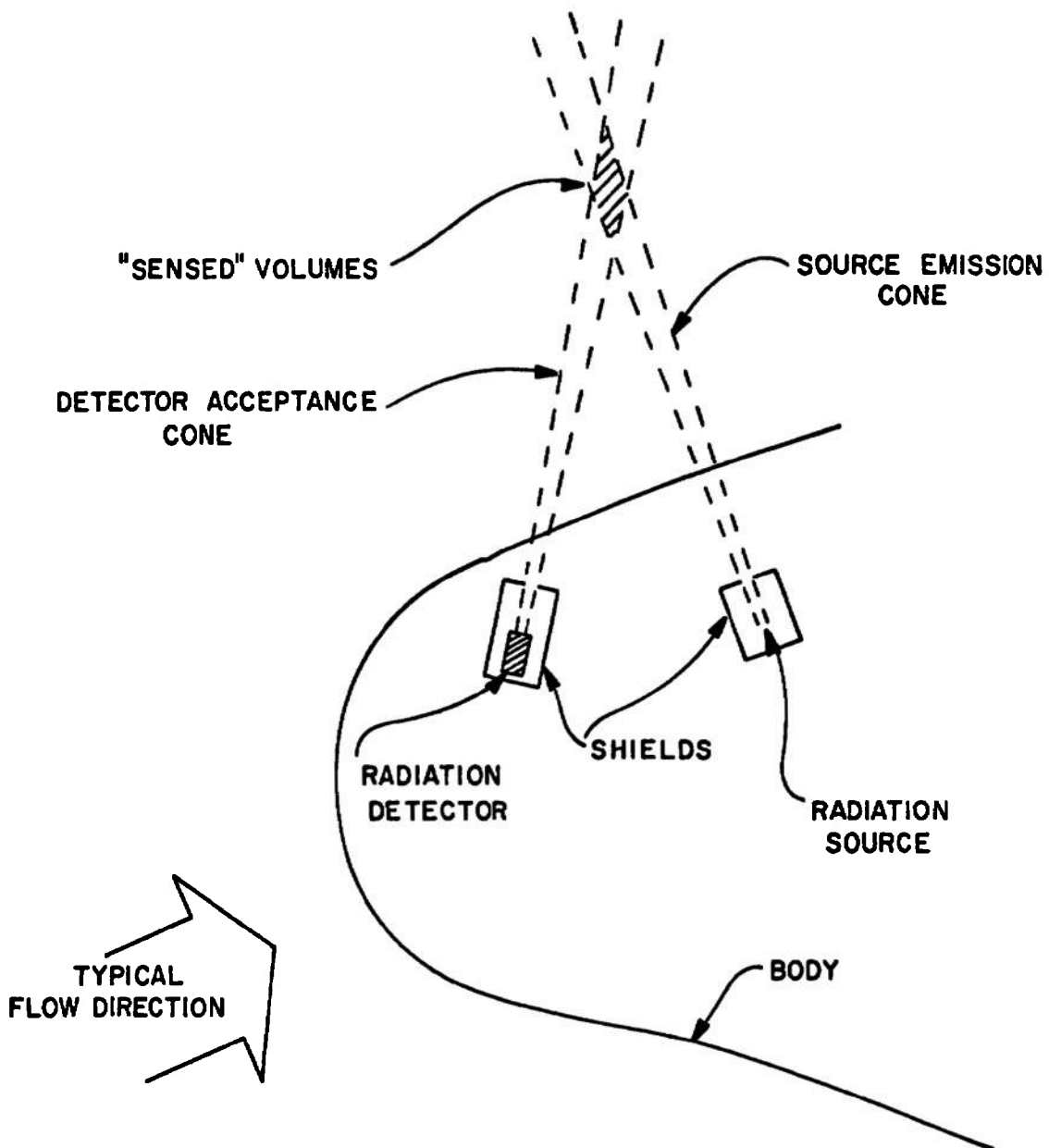


Fig. 7. Geometry for determination of density profiles by nuclear radiation scattering.

within the flow pattern, this can be of significant aid in increasing the detector response for a given radiation source. The detector response could also be enhanced if the material chosen were such that its fluorescent x-ray were excited by the source. This would be the case, for instance, if a Cd-109 22 keV x-ray source were used and molybdenum, whose K absorption edge is at 20 keV, were used as the powdered addition.

It would be necessary during any program to consider the maximum radioactivity source that could be used under these conditions. However, provided the source is sufficiently intense it is possible that accuracy better than 1% can be achieved with spatial resolution of less than 1 cm<sup>3</sup> with time constants of a few seconds. Theoretically, the number of counts that must be recorded in a gage of this type to obtain 1% statistical accuracy is 10,000, and the number for 1/2% is 40,000. Thus, it would be easier to obtain a given accuracy with a longer counting time, for example, 10 sec, since then the counting rate need not be too high.

#### c. Radiation Source Types

Due to the atmospheric densities expected (~.15 to 15 psi) it will be necessary to use x or beta sources rather than alpha sources. Useful x-ray sources would be Cd-109 (22 keV), Am-241 (60 keV) and Co-57 (~100 keV). Useful beta sources would be Pm-147 (~225 keV max.) and Sr-Y-90 (~2 MeV max.). All of these have half lives greater than one year and are readily obtainable.

#### d. Parameters

While estimates of the expected accuracy have been given above, it will be necessary to consider the actual accuracy achievable by considering the following parameters during a particular program:

- source types
- source strength
- allowed geometrical configurations
- time constants
- dimensions of sensed volume

The tradeoff between these various parameters will be determined to define the optimum system and accuracy for the required models.



## SIGNAL-TO-NOISE RATIO

### SMALL SIGNAL CONSIDERATIONS

Usually the type of wave energy used for probing a medium is chosen to make the medium as transparent as possible (radar, sonar) to the waves. Sound is more sensitive to flow than light is, because the interaction of sound and flow is strong. The strong interaction of sound and flow also makes ultrasonic flow measuring devices sensitive to flow noise and leads to larger attenuation. Therefore, the range over which a successful flow measurement can be made is determined by the signal-to-noise ratio which can be obtained. The maximum signal strength one can transmit through the gas in acoustics is limited in principle by non-linear distortion of the signal. In fact, the peak power one can obtain from a transducer which fits the other system requirements is more often the limit. The signal undergoes considerable distortion and is difficult to interpret (in terms of flow, for instance) at power limits below the maximum power one can transmit. The problems encountered using the maximum transmitted power are briefly discussed in a later section. The maximum power consistent with linear propagation will be considered in the small signal section.

Small signal is defined here as the maximum power which can be transmitted across the required gap ( $l$ ) without shock formation. The pressure level  $p_{\max}$  corresponding to this power level is (Beyer, 1965)

$$p_{\max} = \frac{2 c^2}{(\gamma + 1) \omega l} \rho c \quad (3)$$

where  $\omega$  is the angular frequency,  $\gamma$  the specific heat ratio,  $c$  the sound speed, and  $\rho$  the density. The longer the path and the higher the frequency, the lower the maximum pressure level becomes.

The pressure levels for small signal operation at various frequencies and pathlengths are given in Table 2. It should be noted that a cw ultrasonic wave with a pressure amplitude  $10^{-1}$  atm puts 10 watts/cm<sup>2</sup> into the gas. While the power level is acceptable on a peak pulse basis, power levels of 0.1 watts/cm<sup>2</sup> ( $p_{\max} \sim 10^{-2}$  atm) are more realistic for cw operation. Note the maximum small signal pressure drops directly as the gas pressure.

The first part of the present section is devoted to calculation of the attenuation of small acoustic signals in the gas path. This includes losses due to thermal absorption, turbulent scattering, refraction due to large scale flows, and beam shape factors. The turbulent noise

pressure will then be discussed. The final section will be devoted to putting the signal-to-noise information together to obtain response time versus accuracy for applications of interest.

Table 2. Maximum pressure at transmitter (atm) for small signal transmission (1 atm, 300°K).

Frequency, kHz	10	50	100	500
$l = 5 \text{ cm}$	$1.31 \times 10^{-1}$	$2.61 \times 10^{-2}$	$1.31 \times 10^{-2}$	$2.61 \times 10^{-3}$
$l = 25 \text{ cm}$	$2.62 \times 10^{-2}$	$5.24 \times 10^{-2}$	$2.62 \times 10^{-3}$	$5.24 \times 10^{-4}$
$l = 50 \text{ cm}$	$1.31 \times 10^{-2}$	$2.61 \times 10^{-3}$	$1.31 \times 10^{-3}$	$2.61 \times 10^{-4}$

### Thermal Absorption

Thermal absorption includes losses of sound energy to heat by viscosity, thermal conductivity and relaxation (rotational and vibrational relaxation). Thermal conduction, viscous dissipation and rotational relaxation dominate the true sound absorption in dry air under the temperature-pressure conditions contemplated here. The sound absorption due to thermal conductivity and viscosity is given by

$$\alpha_c = \frac{2\pi^2 f}{\rho c^3} \eta \left[ 1 + \frac{\gamma-1}{P_r} \right]. \quad (4)$$

Here  $f$  is the ultrasonic frequency,  $c$  the sound speed,  $\rho$  the density,  $\gamma$  the specific heat ratio, and  $P_r$  the Prandtl number. The total loss including rotation relaxation (Zmuda, 1951) is

$$\alpha = \alpha_c (1 + 0.067 Z_R). \quad (5)$$

The rotational collision number ( $Z_R$ ) for air is close to that for nitrogen and oxygen (Carnevale, 1967; Brau, 1970; Lordi, 1970). The value of  $Z_R$  at 300°K in air is  $Z_R \sim 3.8$  collisions and increases slowly with temperature.

\*Below  $\sim 100 \text{ atm}$   $\rho c^2 = \gamma p$  is a useful simplification.

The attenuation times the pathlength is plotted versus pathlength in Fig. 8 for air at 300°K, 1 atm for frequencies of 50, 100, 200 and 400 kHz. The ratio of received amplitude to transmitted amplitude is also plotted on the same graph. Note that there is very little  $\left(\frac{A}{A_o} > 0.9\right)$  absorption in a 20 cm path at 100 kHz and below due to thermal effects. The attenuation at any temperature and pressure can be scaled from the results in Fig. 8 using the relation

$$\alpha L(T, p, f) = \left[ \frac{T^{1/4} f^2}{p} \right] \quad (6)$$

where  $f$  is the operating frequency in kHz,  $T$  the temperature in °K, and  $p$  the pressure in atm.

Vibrational relaxation also occurs in air. However, at the temperatures and pressures of interest here, in dry air, the relaxation frequency and the relaxation strength are both too small to cause any effect. The addition of water vapor increases the efficiency of collisional transfer in  $N_2$  and  $O_2$ .

#### Relaxation-Humidity

Relaxation of air is very complex (Bass, 1972) due to the many molecules which make it up. Water vapor has catalytic effects on the vibrational relaxation of oxygen, nitrogen and  $CO_2$ . The addition of water vapor can shift the relaxation time of 20°C air from less than 100 Hz to just over  $10^5$  Hz at 100% humidity (Evans, 1974). The absorption triples at 50 kHz as the relative humidity of the air goes from 0-100%. This multiplier may be used on the results in Fig. 8 to include the effects of relaxations at high relative humidities. A plot of total absorption for different relative humidities taken from Evans, 1974, is given in Fig. 9. There is also a small effect on the sound speed. An analytic expression for sound speed and absorption is given in Bass, 1972. As pointed out by the authors, the lack of good relaxation times prevents accurate calculations of sound absorption beyond about 3° of 20°C. These problems do not affect the flow measurement since sound speed is measured, not calculated, in the flowmeter designs contemplated in the present work.

#### Turbulent Scattering

Scattering of sound by the turbulent flow fields can cause significant signal attenuation in many flows of aerodynamic interest. Theories for scattering of sound by isotropic turbulence have been developed and tested

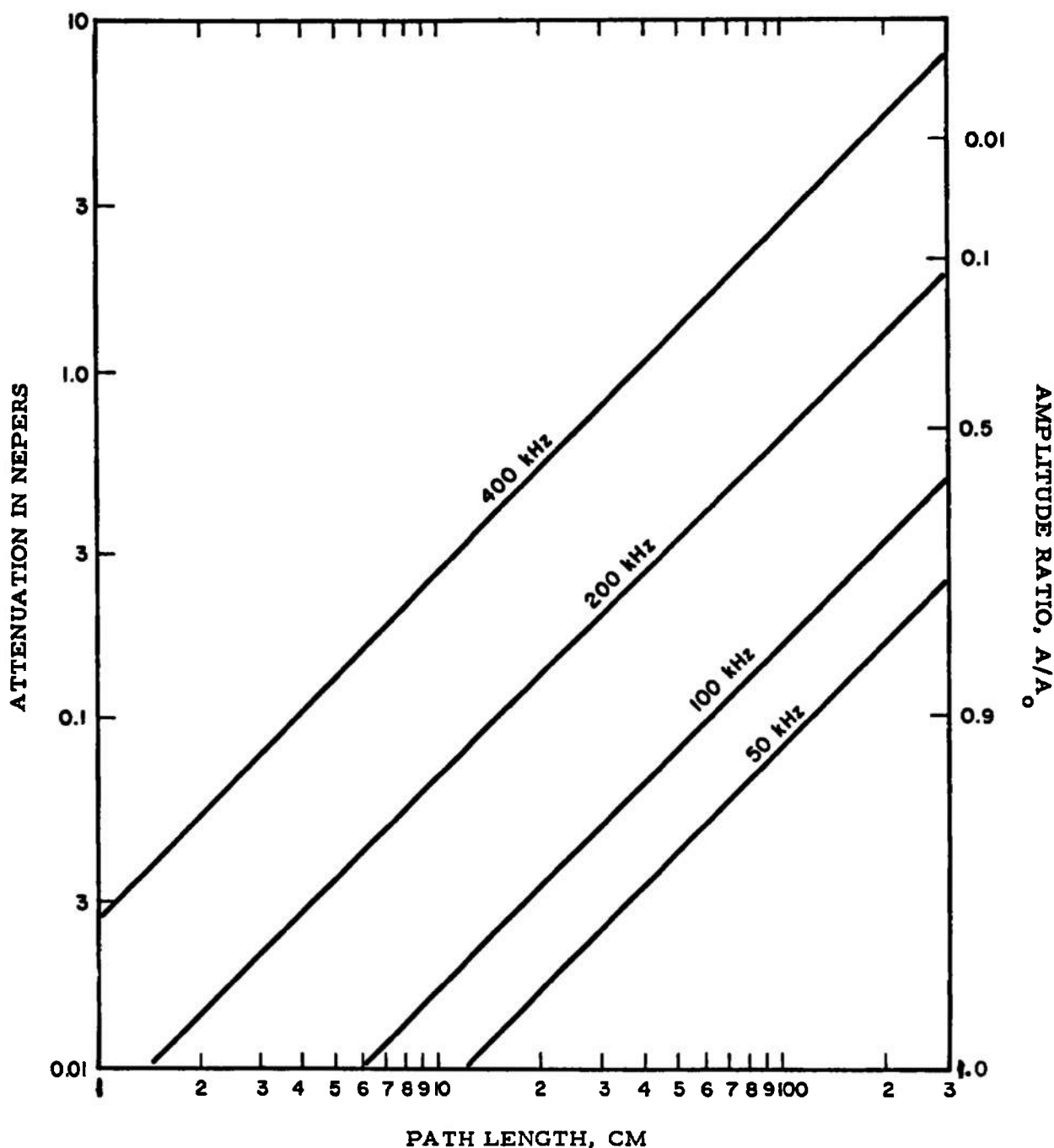


Fig. 8. Thermal sound attenuation, in nepers, and amplitude ratios in air at several frequencies, versus path length  $L$ . Knowing  $L$  and  $f$ , one uses this graph to find  $\alpha L$  and  $A/A_0$ .

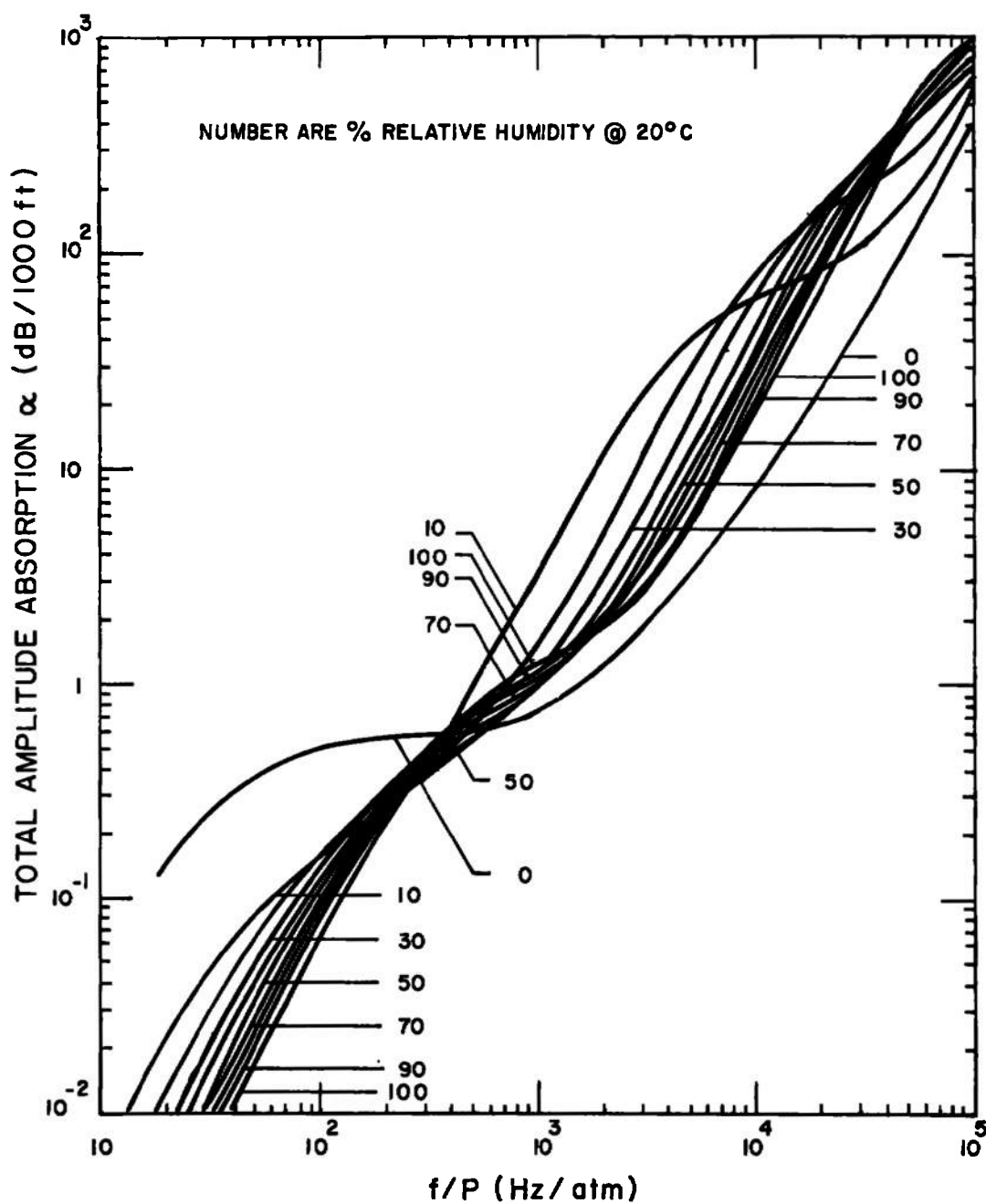


Fig. 9. Total absorption of sound in air as a function of frequency (after Evans, 1974).

for oceanic and atmospheric sounding. However, for nonisotropic turbulence such as is the case for boundary layer and pipe flow, the best one can do is appeal to the notion of locally isotropic turbulence (Tatarsky, 1961, pp. 66-70). Even when one is willing to assume local isotropy the required correlation functions for turbulent temperature and flow velocity fluctuation fields are not usually available for the flows of interest. Below, the scattering due to turbulence is calculated in terms of quantities that are readily available in standard texts on turbulent flow.

The attenuation of sound from turbulence is much less than that due to viscous and thermal losses when the wavelength is much longer than the scale of the turbulence. The reason for the small scattering in the long wavelength region can be seen by considering the size of the terms in the absorption expressions one finds in the literature, i. e., (Chernov, 1960, p. 55)

$$\alpha \approx \overline{\mu^2} k^4 a^3 \quad (7)$$

where  $\overline{\mu^2}$  is the mean square Mach number fluctuation. The mean square Mach number fluctuation  $\overline{\mu^2}$  is typically  $10^{-3}$ . Since the wave number turbulent scale product ( $ka$ ) is less than 1, the absorption never reaches 0.01 neper/cm.

The scattering for  $ka \gg 1$  can easily be greater than the thermal absorption. However, the magnitude of the calculated absorption can vary by factors of 4, depending on the assumptions made about the structure of the turbulence. The calculation below is based on formulas given by (Tatarsky, 1961) and corrected by (Monin, 1962). Assuming that the correlation functions are exponential

$$B_{rr} = \frac{1}{3} V_o^2 \exp - \left( \frac{|r|}{a} \right) \left[ 1 + \left( \frac{r}{a} \right)^2 \right]^{-1} \quad (8)$$

for velocity, and

$$B_T = T_o^2 \exp - \left( \frac{|r|}{a} \right) \left[ 1 + \left( \frac{r}{a} \right)^2 \right]^{-1} \quad (9)$$

for thermal fluctuations the absorption due to turbulence is given by

$$\alpha = \left[ \frac{3\pi}{8a} \frac{\overline{\Delta u^2}}{c^2} + \frac{2}{a} \frac{\overline{\Delta T^2}}{T^2} \right] k^2 a^2. \quad (10)$$

The correlation length ( $a$ ), the mean square velocity ( $\overline{\Delta u^2}$ ), and temperature ( $\overline{\Delta T^2}$ ) fluctuations must be known to use Eq. (10). The sound speed  $c$ , the mean temperature ( $T$ ), and the ultrasonic wave number ( $k$ ) are all known.

The correlation length was taken to be the mixing length (Schlichting, 1960, p. 510) in the absence of measured correlation lengths. The mixing length for a pipe varies from zero at the wall to about 14% of the pipe radius at the centerline. The mixing length for a turbulent boundary layer (Rotta, 1972, p. 350) rises from zero to 10% of the displacement thickness ( $\delta^*$ ) at  $\frac{x}{\delta^*} \sim 0.2$  and remains

constant almost to  $\delta^*$ . The turbulent intensity  $\frac{\sqrt{\overline{\Delta u^2}}}{U}$  is taken as constant and equal to 0.05 for both pipe flows and boundary layer flows.

Temperature changes in turbulent flow will usually vary about the mean temperature by the same fractional amount as the flow variations

$$\frac{\overline{\Delta T^2}}{T^2} \sim \frac{\overline{\Delta u^2}}{c^2} = \frac{\overline{\Delta u^2}}{U^2} M^2. \quad (11)$$

Thus, for order of magnitude calculations such as are contemplated here, Eq. (10) becomes

$$\alpha = 2.59 \times 10^{-2} \frac{M^2}{a} (k a)^2. \quad (12)$$

It should be noted that where aerodynamic heating or cooling are involved

$\frac{\overline{\Delta T^2}}{T^2}$  can easily be greater than  $\frac{\overline{\Delta u^2}}{c^2}$  especially at low Mach numbers.

For instance, if a turbulent pipe flow with a  $3^\circ\text{C}$  temperature difference between the walls and the free stream flows in a pipe with a bend, the resulting secondary flows convect 1% temperature differences to the cooler walls. At  $M = 0.1$ ,  $\frac{\overline{\Delta T^2}}{T^2}$  is  $\sim 10^{-4}$  while  $\frac{\overline{\Delta u^2}}{c^2} \sim 10^{-6}$ . Thus, at low

Mach numbers Eq. (12) may underestimate the absorption due to turbulent scattering.

Absorption due to turbulence according to Eq. (12) has been plotted in Fig. 10 as a function of pathlength and frequency for a  $M = 0.5$  fully developed pipe flow. The absorption due to turbulence is greater than the thermal absorption (Fig. 8) under the conditions calculated. Numbers can be scaled from Fig. 10 using Eq. (12). Note that the absorption due to turbulence does not depend on pressure. Thus, at sufficiently low pressures thermal absorption dominates while at elevated pressures turbulent losses dominate.

### Harmonic Generation

One might expect that the signal attenuation due to turbulence and thermal loss can be added to give a total loss in the path. However, we defined the small signal power level so that the path is one discontinuity distance (p. 22). There is considerable loss at these power levels to harmonics generated by the nonlinear mixing of the signal with itself (Beyer, 1965). The effective attenuation, including losses to harmonic generation, are as much as four times the absorption calculated from Figs. 8 and 10. A plot of the effective attenuation divided by thermal and turbulent absorption ( $\alpha_0$ ) versus normalized pathlength, is given in Fig. 11. Notice the multiplier on attenuation is largest for the lowest path loss. This is because the signal strength and therefore the nonlinear losses are great over more of the path than is the case for a large  $\alpha_0$ . Nonlinear mixing leads to diminishing returns on increasing driver amplitude.

### Diffraction-Beam Spread (Near Field, Far Field, Steered Beam)

A major source of signal loss is due to beam spreading and misalignment of transmitter and receiver. The general shape of the field of a piston radiator is shown in Fig. 12. The beam is highly collimated in the near field zone between  $Z = 0$  and  $Z = \frac{1}{4} \frac{d^2}{\lambda}$ . Here,  $d$  is the diameter of the transducer,  $\lambda$  the wavelength of sound, and  $Z$  the distance from the transducer face. The length of the near field increases as the frequency of the ultrasonic wave is increased ( $\lambda$  decreased), and as the diameter of the transducer is increased the near field extends further from the transmitter.

The near field transducer with its wave fronts perpendicular to the flow reaches the receiver with a minimum loss. The advantage of the beam drift\* configuration is that it minimizes alignment losses. A near field

---

\*The transducers positioned so that the receiver is just downstream enough to catch the drift of the beam due to flow is called the beam drift configuration.



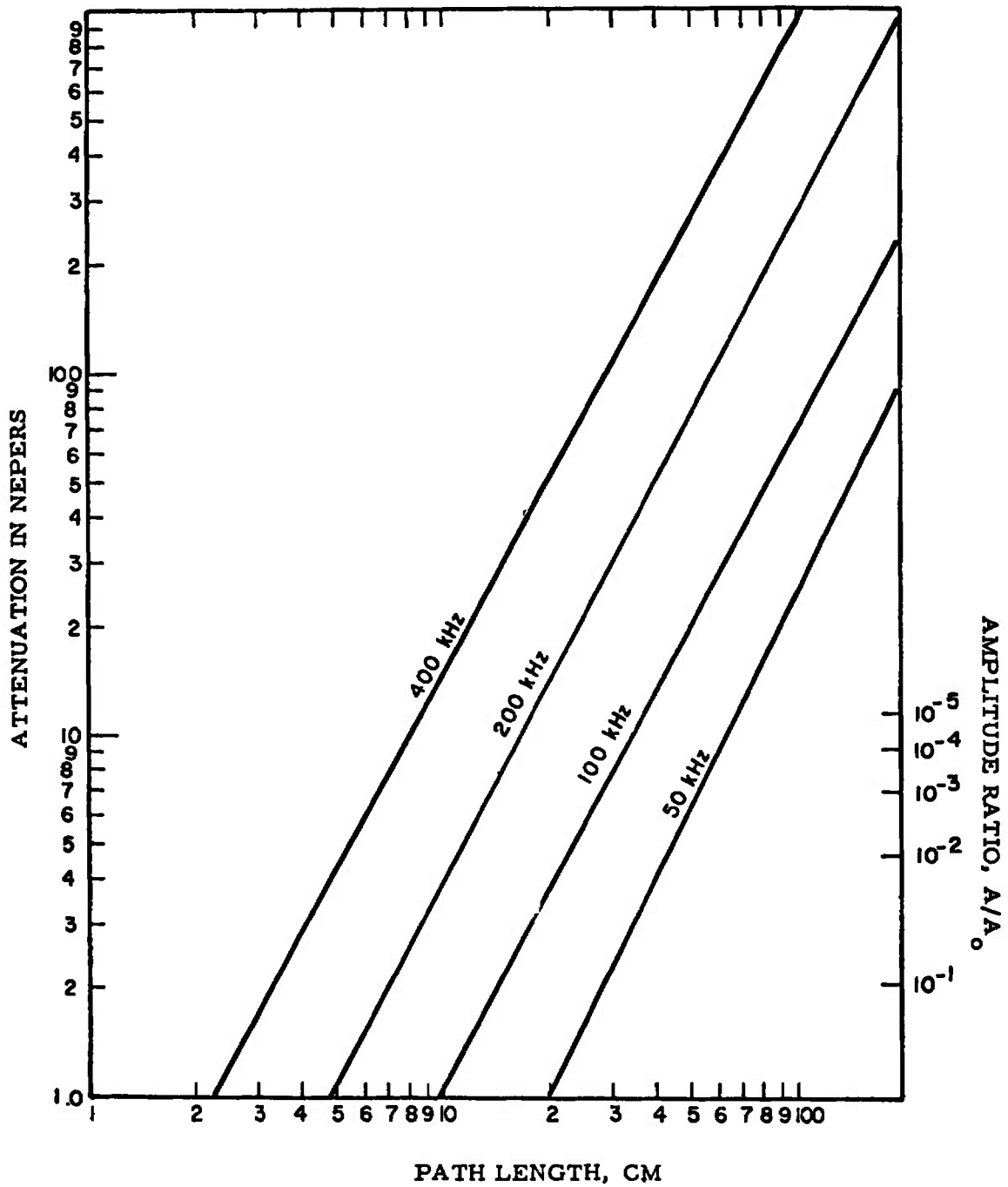


Fig. 10. Attenuation in air due to turbulence, in nepers, and amplitude ratio, versus path length.

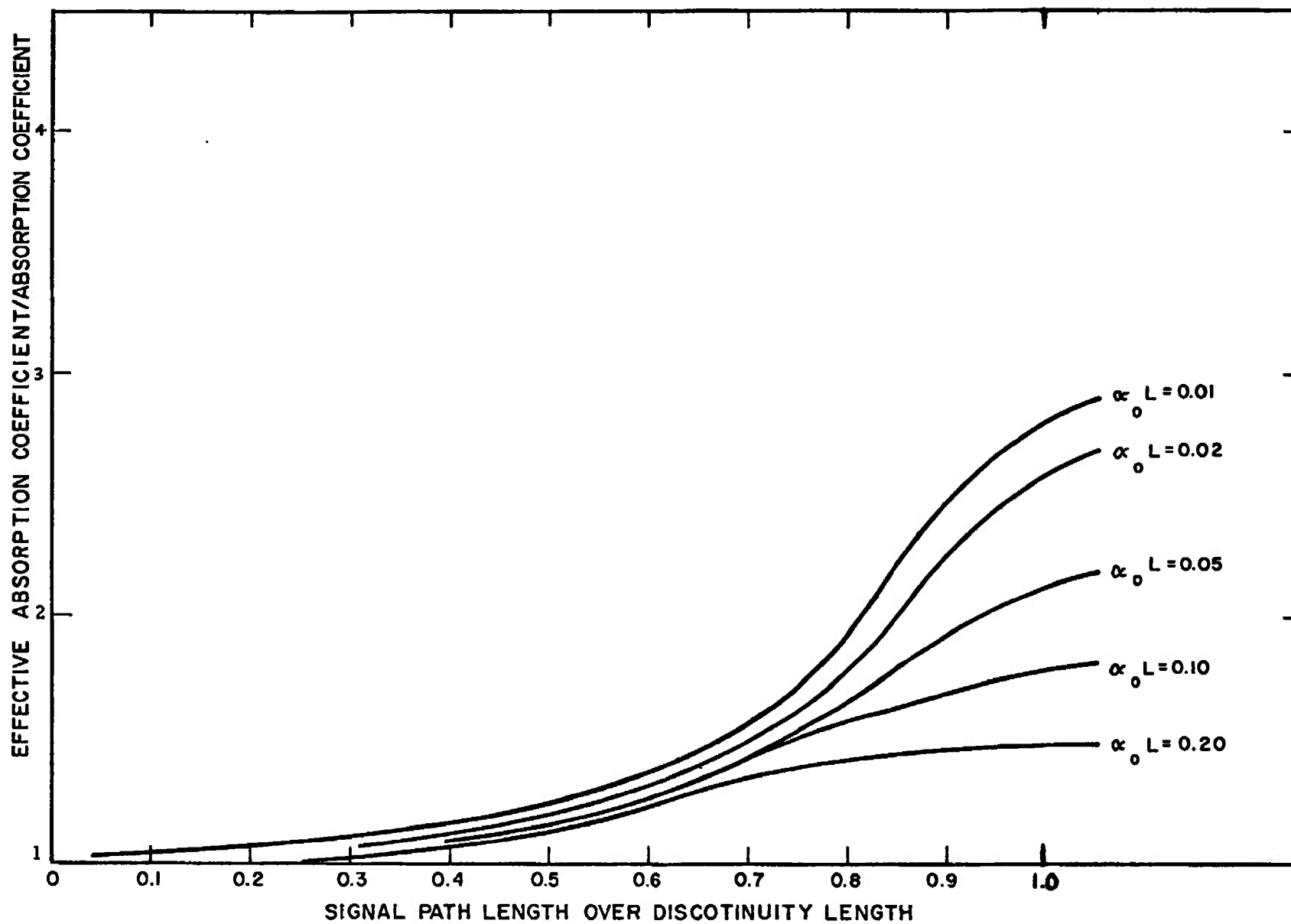


Fig. 11. Multiplier for attenuation due to harmonic generation.

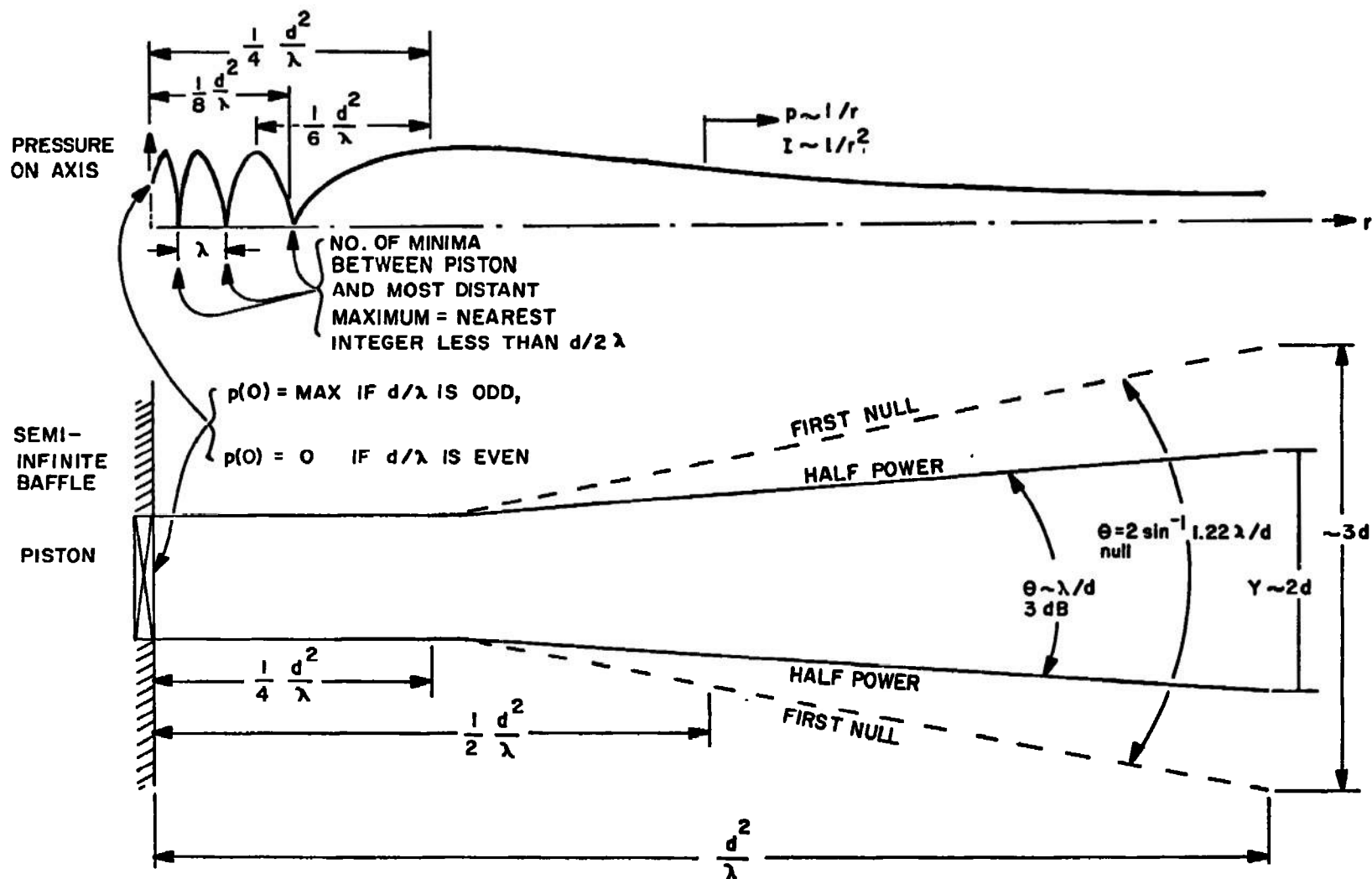


Fig. 12. Beam characteristics of circular piston. Dimensions shown are approximations suitable for estimating purposes.

transducer is very sensitive to tilt in the wave front. To maintain a near field out to 50 cm at 100 kHz, requires a transducer with a diameter of about 24 wavelengths (8 cm). A misalignment of  $\sim 0.13$  radians causes a substantial phase shift across the receiving transducer face, resulting in large phase jitter. However, the average amplitude is preserved.

The other extreme is in the wide beam transducer. Referring again to Fig. 11, a wide beam is obtained by decreasing  $d$ . Any practical phase measuring system for ultrasonic flow measurement requires upstream and downstream signal paths. A 50 kHz system suitable for measuring flows between  $M = 0.2$  and  $M = 0.7$  must have a beam width of  $45^\circ$  and a transducer diameter roughly equal to one wavelength ( $\lambda$ ) is  $\sim 0.66$  cm. Only a small solid angle of the signal is subtended by the receiver at each flow Mach number. Thus, the pressure loss due to spherical spreading in a 25 cm path is a factor of 400 or -63 dB. In fact, the loss will be about 12 dB greater due to the angle between the signal wave fronts and the receive transducer.

Finally, there is the loss of signal due to spreading of the ray trajectories for a realistic flow as indicated in Fig. 12. Note that three sound sources are required to obtain an upstream and a downstream ray in many cases. When the flow velocity gradients are sufficiently sharp a downstream ray will return to the wall due to refraction. This phenomenon called shadow zone propagation is aggravated by flows with a hot free stream. A set of typical rays is shown in Fig. 13 for various launch angles,  $\alpha_0$ . In addition, Fig. 13 shows downstream rays are spread apart leading to an effective attenuation which depends on the flow and temperature gradients. Ray spreading can lead to an additional 20 dB loss for downstream rays.

## NOISE

### Source of Noise

Acoustic noise generated by the flow itself may be the limiting factor on the accuracy or feasibility of many acoustic measurements. The pressure fluctuations on the face of the transducer  $p_n$  and the signal  $p_s$  enter the detection system together. Thus, there is nothing that can be done to improve the signal-to-noise ratio by electrical or acoustic nonresonance impedance matching on the receive side. However, increasing the transducer size, increasing operating frequency and narrow band filtering, discriminate against the turbulent noise. The most noise reduction one can expect from transducer size is a factor of  $10^3$ . Any attempt to broaden

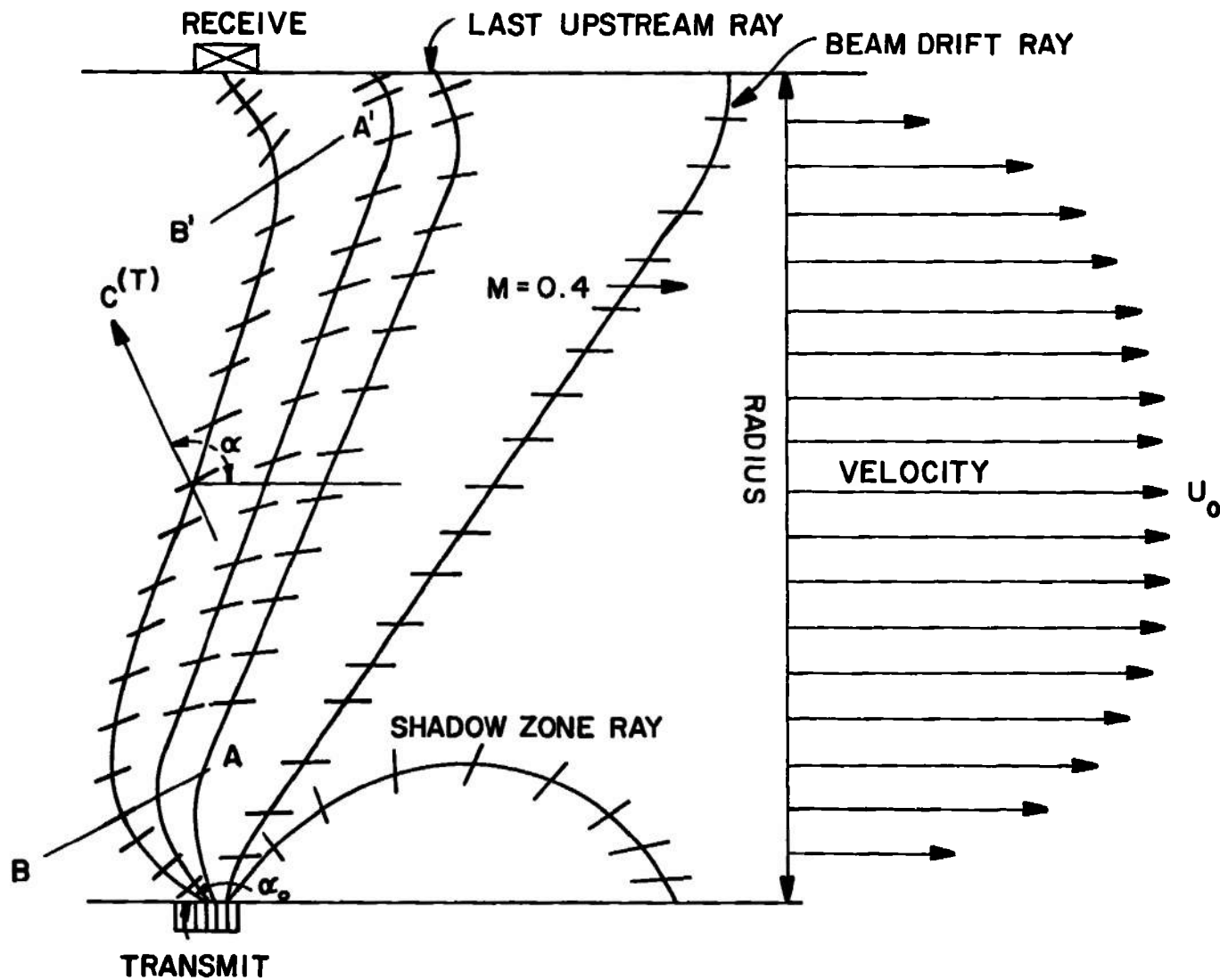


Fig. 13. Schematic of pulse trajectory and wave fronts in a real flow.

or steer the beam forces the use of smaller transducers, thus increasing the noise. A narrow band system can reduce the noise at the expense of response time. As discussed below, there are practical limits to how much the bandwidth reductions can improve the signal-to-noise ratio. However, a factor of  $10^4$  relative to the total wide band noise pressure fluctuation can probably be obtained with cw acoustic transmission. Under turbulent flow conditions in air at  $M_g = 0.5$ , the turbulent wall pressure noise ranges between  $1.78 \times 10^2$  dyne/cm<sup>2</sup> to  $\sim 3.46 \times 10^4$  dyne/cm<sup>2</sup>. Using optimum filtering and transducer size an equivalent acoustic pressure of  $1.78 \times 10^{-5}$ - $8.46 \times 10^{-1}$  dyne/cm<sup>2</sup> enters the transducer with the signal.\*

The noise generated by turbulence depends to a large extent on the type of flow involved (Sidden, 1973). The fraction of the dynamic head ( $\rho U^2/2$ ) converted into noise pressure fluctuations in different types of flow varies over a three order of magnitude range as shown in Table 3. True sound radiated from distant turbulent sources makes only a small contribution to the total flow noise. The true sound level is representative of the noise level one should expect from a transducer mounted on a boundary layer stripper or on a model in a low turbulence tunnel.

Table 3. Maximum percent of dynamic head which appears as wall pressure fluctuations in various flow situations.

True Acoustic Radiation	Pseudo-Sound Under Turbulent Boundary Layer	Separated Flow Near Reattachment Zone	Lift and Drag Fluctuations Due To Freestream Turbulence Over Thin Boundary Layer
0.01	0.6	6	10

The noise under a thick ( $\sim 0.5''$ ) turbulent boundary layer or in fully developed pipe flow is due to pressure fluctuations on the wall itself (Haddle, 1969 and 1960). The rms pressure fluctuations are typically 0.6% of the dynamic pressure. Separation (Frick, 1968, 1970, and Siddon, 1973) of the boundary layer leads to a factor of ten increase in the wall pressure near reattachment.

\*This should be compared with the signal levels of  $10^{-2}$ - $10^{-9}$  dyne/cm<sup>2</sup> which are likely to be received in practice as indicated in the previous section.

The fluctuating lift and drag forces due to a turbulent free-stream can cause very large pressure fluctuations up to 20% of the dynamic pressure. Lift and drag pressures are important sources of noise on models (Siddon, 1973) near leading edges where the boundary layers are thin. Transducers which are immersed into the flowing stings or acoustic wave guides develop large drag noise signals. In general, the acoustic wave guides and transducers must be carefully isolated from those portions of wall which protrude into the flow.

The order of magnitude of the acoustic noise and some general constraints on the acoustic flowmeter system can be determined from the general information given above. Probes which protrude or are recessed from the duct walls will result in a factor of 30 increase in turbulent noise over that due to the turbulent boundary layer. Thus, flush-mounted transducers are advisable.\* Similarly, the noise levels on models in a turbulent freestream may be larger than the noise on the duct walls by a similar factor. Once the expected wide band noise levels are calculated for the type of flow involved, the dynamic head, and the factor in Table 3, the bandwidth and transducer factors can be used to obtain a first estimate of the final signal-to-noise level. Typically, for a 1 second response time a  $10^7$  reduction in flow noise can be expected with cw operation. This improvement is reduced by the duty cycle for pulse operation. See also: Camp et al., 1970.

More exact noise information shows that the flow noise drops off as some high ( $\sim 3$ ) power of frequency. In addition, a more exact calculation of spatial filtering due to transducer size allows the noise penalty for small transducers to be calculated (Corcos, 1967; Racine, 1971; Petrovskii, 1973; Smolyakov, 1970). Many methods for obtaining rays over a wide solid angle requires the use of small transducers. Therefore, the remainder of this section is devoted to more detailed calculation of turbulent noise.

The most intense source of noise is due to the boundary layer flow near the wall. The noise from turbulent boundary layers has been exhaustively studied by aerodynamicists and sonar specialists. However, emphasis has been on the low frequency end of the noise spectra. Fortunately, in the megahertz range the noise spectrum is dominated by the balance of energy transfer to the higher frequencies via nonlinear mixing (Ellison, 1962; Kuznetsov, 1970). The turbulent energy is

---

\*With the exception of low turbulence freestreams where boundary layer strippers are advisable to avoid the boundary layer.

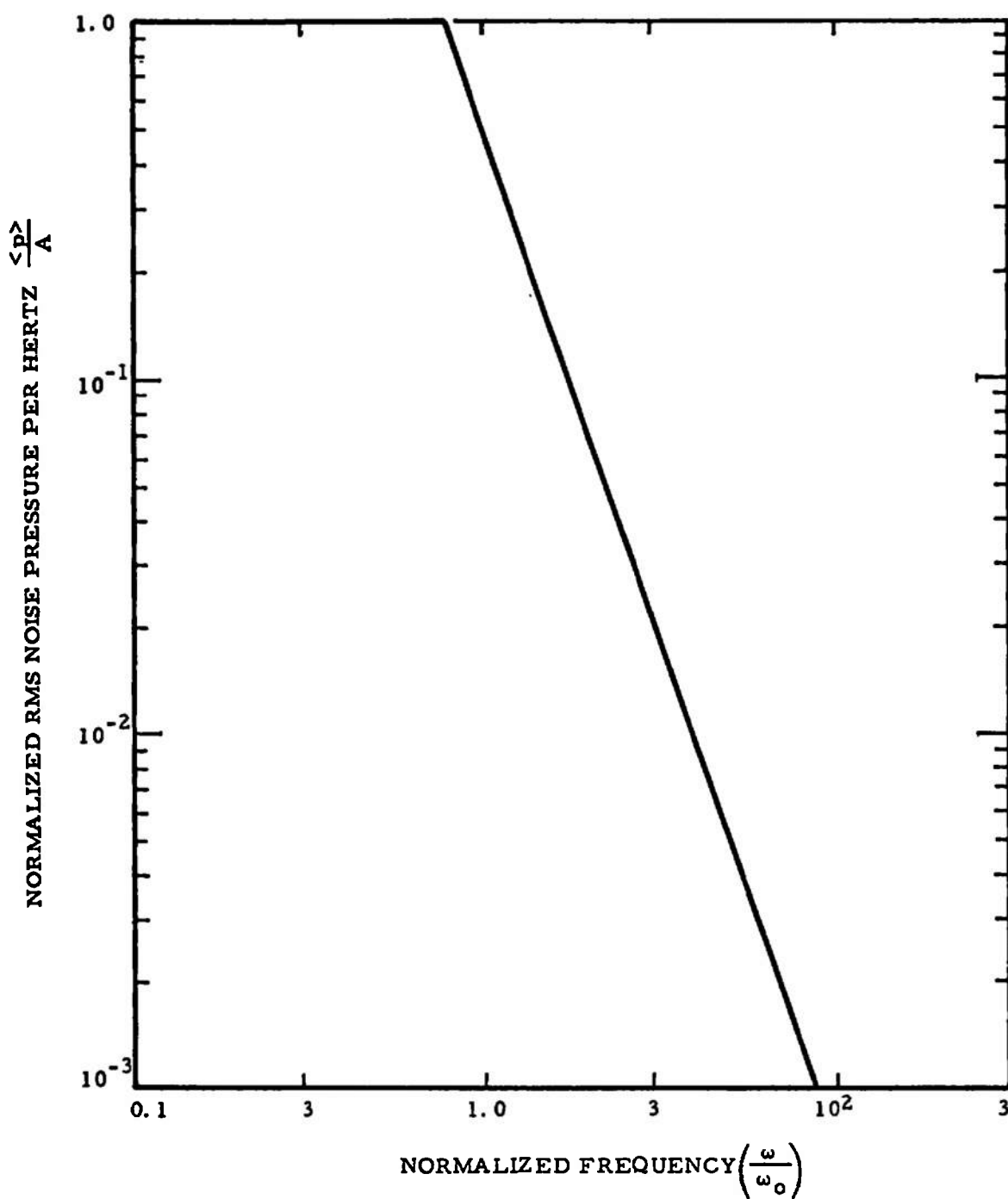


Fig. 14. Normalized rms pressure per hertz versus normalized frequency.



introduced to the flow at low frequencies near the wall. Therefore, the high frequency noise power universally falls off as  $f^{-3}$ .

A convenient analytic form for normalized mean square pressure/unit frequency (power spectral density at frequency  $\omega$ ) vs normalized frequency was taken from Strawderman, 1968. The normalization used in Fig. 14 correlates boundary layer noise from many extremely different types of flows in liquids and gases. This graph is based on the analytical expression for mean square pressure given by

$$\langle p^2 \rangle = \begin{cases} A, & \omega \leq 1.256 \omega_o \\ 2A \left( \frac{\omega_o}{\omega} \right)^3, & \omega > 1.256 \omega_o \end{cases} \quad (13)$$

$$A = 0.75 \times 10^{-5} \frac{\alpha^2 \rho_f^2 U_o^4}{\omega_o} \quad (14)$$

and  $\rho_f$  is the fluid density,  $\delta^*$  the boundary layer displacement thickness, or the pipe radius for fully developed pipe flow, and  $\alpha$  a dimensionless quantity:

$$\alpha = 1.0 \text{ (for air)} \quad (15)$$

$$\alpha = 3.0 \text{ (for water)} \quad (16)$$

and  $U_o$  is the freestream flow velocity. The convection frequency  $\omega_o$  is

$$\omega_o = \frac{U_o}{\delta^*}.$$

The pressure fluctuations on an arbitrarily small transducer are constant out to a frequency  $\omega = 1.256 \omega_o$ . The noise pressure then falls off as  $\omega^{-1.5}$ . Thus, it is advantageous to operate with a carrier frequency which is as high as the attenuation will allow. The normalized rms pressure amplitude versus frequency is shown in Fig. 14. This graph is universal. The noise pressure on the crystal face can be calculated from the displacement thickness (or pipe radius,  $R$ ), centerline flow velocity  $U_o$  and dynamic head ( $\rho U_o^2/2$ ) for any frequency.

The noise pressure is not coherent across the face of the transducer. Thus, the noise which enters the transducer is reduced by phase

cancellation over the transducer face (Corcos, 1967, 1960). The cancellation effect is improved somewhat when the transducer diameter is larger than the displacement thickness (Smolyakov, 1970). Cancellation is less complete when transducer sensitivity is not constant over the transducer face (Petrovskii, 1973). The signal is more coherent than the noise over the transducer face and does not suffer as much attenuation due to spatial filtering.

A spatial filtering factor was taken from Recine, 1971, and is given in Fig. 15. The existing measurements end at  $\frac{\omega A^{1/2}}{U_0} = 15$ . The data were extrapolated to  $\frac{\omega A^{1/2}}{U_0} = 200$  for Fig. 15. The correlation

of pressure fluctuations across the transducer face and the spatial variation of transducer sensitivity must be known to determine the effect of transducer size exactly. However, the product of the noise pressure from Fig. 14 times the spatial factor from Fig. 15 gives an order of magnitude of the noise to be expected from typical transducers subject to turbulent boundary layers. The percentage factors in Table 3 should be applied to the turbulent boundary layer predictions to arrive at the frequency dependent flow noise in the other types of flow enumerated in Table 3.

### NOISE IN DUCTS VERSUS MACH NUMBER

The noise in a 25 cm diameter duct with a fully developed pipe flow is of specific interest for the tests in the PWT facilities. The rms noise pressure appearing at the electrical terminals of a 2.5 cm transducer in the 25 cm duct is shown in Fig. 16. This transducer is the size that would be used in a transmission (upstream-downstream) measurement. The frequency at which the noise falls off varies from 654 Hz at  $M_s = 0.2$  to 2800 Hz at  $M_s = 0.8$ . The rms noise pressure decreases as the cube of the flow velocity above this frequency. Suppose we wish to receive a signal after processing which is 10 to 100 times the pressure level generated by turbulence at the highest Mach number of interest. This means that a system designed to operate up to Mach 0.8 with a bandwidth of 10 Hz at  $\sim 100$  kHz must receive a signal level of  $10^{-2}$ - $10^{-1}$  dynes/cm<sup>2</sup>. The conditions under which this signal level can be achieved are deduced from the signal level discussion on p. 41.

The noise pressure in other duct diameters can be scaled from the values in Fig. 16 using Eq. (17). Thus, the rms noise pressure  $p_d$

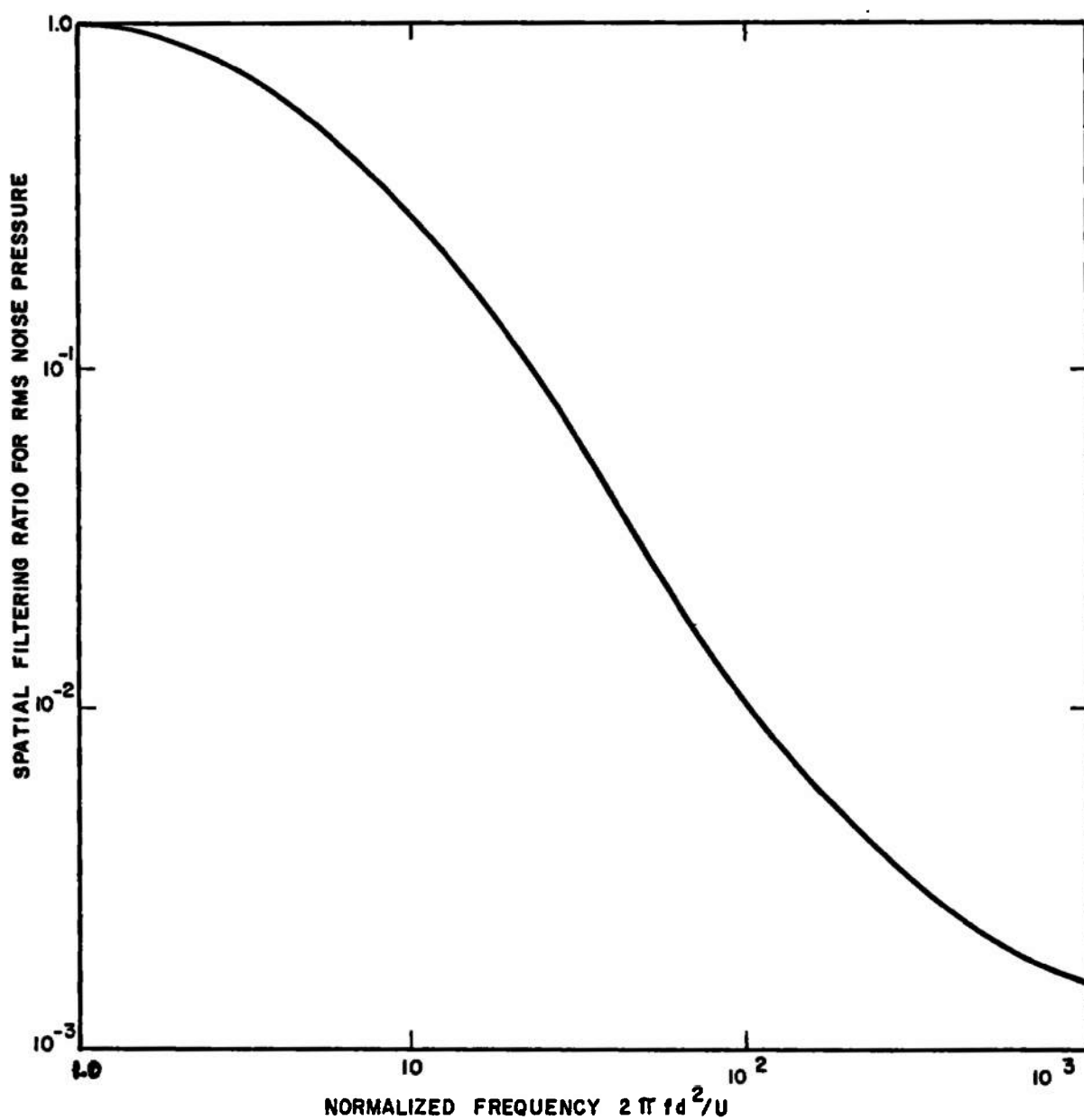


Fig. 15. Spatial filtering factor for finite transducers of diameter (d).

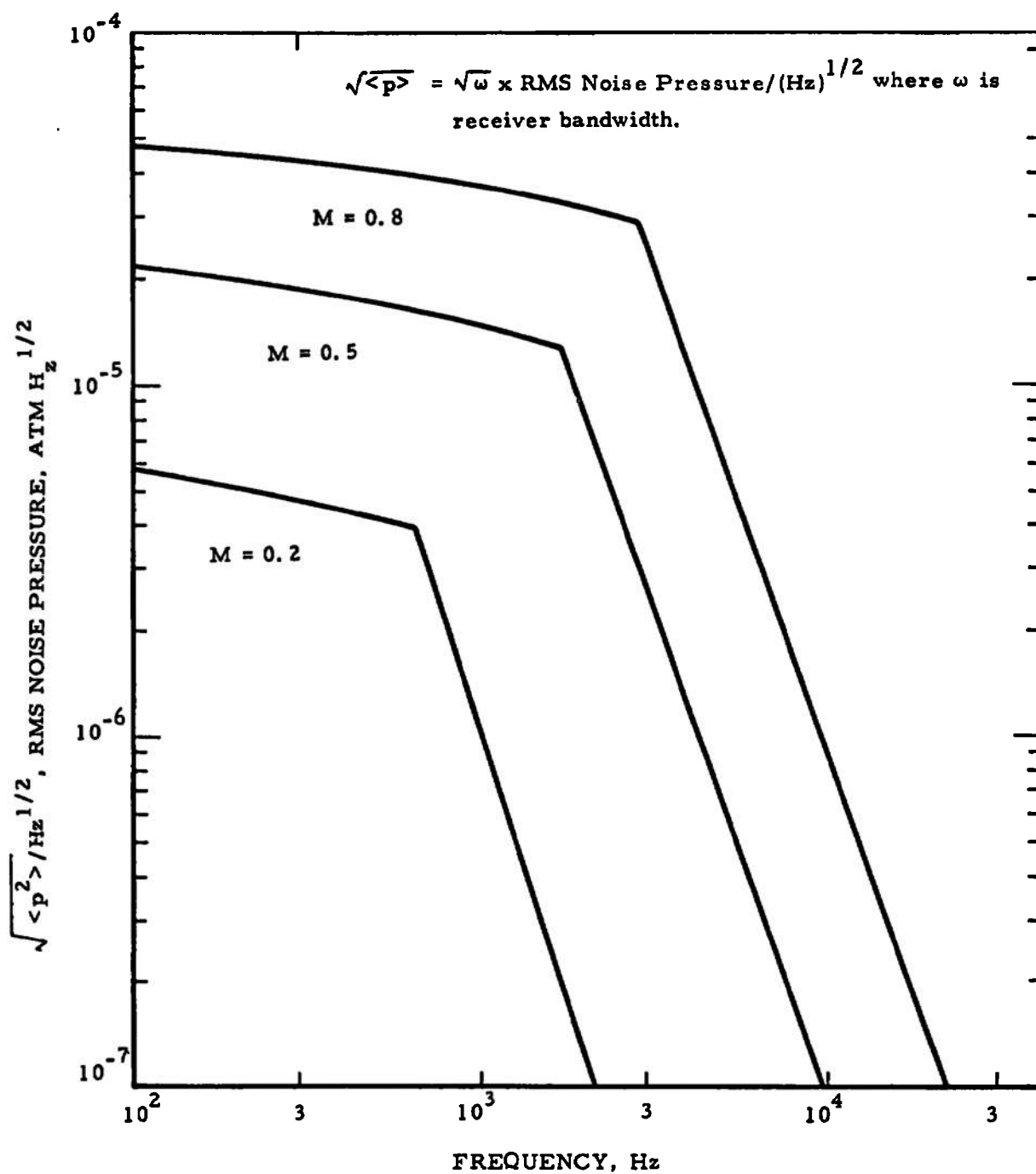


Fig. 16. Turbulent RMS noise pressure/(Hz)<sup>1/2</sup>, calculated for empirical data for a fully developed pipe flow in a 25 cm diameter duct with a 2.54 cm diameter transducer.

in a fully developed pipe flow in a duct of diameter D is

$$p_d = p_o \left( \frac{50.8}{D} \right)^2 \quad (17)$$

Here  $p_o$  is the noise pressure from Fig. 16.

Similarly, to obtain the noise in ducts where the flow is not fully developed the displacement thickness  $2\delta^*$  is put into Eq. (17) in place of the duct diameter D. Noise pressures for the small diameter ~5 cm ducts in the "ultrasonic venturi" would be determined by the displacement thickness of the ducts. It is important in the "ultrasonic venturi" application that the ultrasonic transducers be located at least 5 cm downstream from the leading edge of the duct to avoid lift and drag noise. In addition, the operating frequency can proportionately be increased in smaller ducts. For instance, if 50 kHz is appropriate for a 25 cm duct, 250 kHz can be used in a 5 cm duct. Looking at the noise fall-off with frequency in Fig. 16, a factor of 25 noise reduction is obtained by increasing the frequency of the ultrasonic wave by this factor of 5. This makes the ultrasonic venturi a very attractive prospect.

#### SMALL SIGNAL-TO-NOISE RATIO

The signal and noise can now be put together to see if sufficient signal-to-noise ratio can be achieved to perform the desired measurement. The case of fully developed pipe flow in a 25 cm duct with 0.6 cm spherical radiators operating at several frequencies were calculated. The signal-to-noise ratios are shown as a function of Mach number in Fig. 17 for a beam drift trajectory. The signal-to-noise ratio is optimum at 100 kHz. However, sufficient signal-to-noise level is obtained at 50 kHz to do the measurement. It is more convenient to generate a 50 kHz sound wave at the small signal maximum pressure than it is at 100 kHz.

The response time required to make a measurement to a given precision in the presence of uncorrelated noise decreases with the signal-to-noise ratio. The exact relation between response time, precision, and signal-to-noise ratio depends on details on the quantity being measured and the measurement system. However, the typical precision one should expect is one minus the amplitude signal-to-noise ratio. The response time required to make the measurement to this precision is the one over the bandwidth of the receiver. Figure 17 is calculated for a constant bandwidth of 10 Hz. Thus, the greatest precision we should expect from a 0.1 second response time system at the frequencies and Mach numbers given in Fig. 17 is % precision =  $\left(1 - \frac{S}{N}\right)$  where  $\frac{S}{N}$  is the signal-to-noise from Fig. 17.

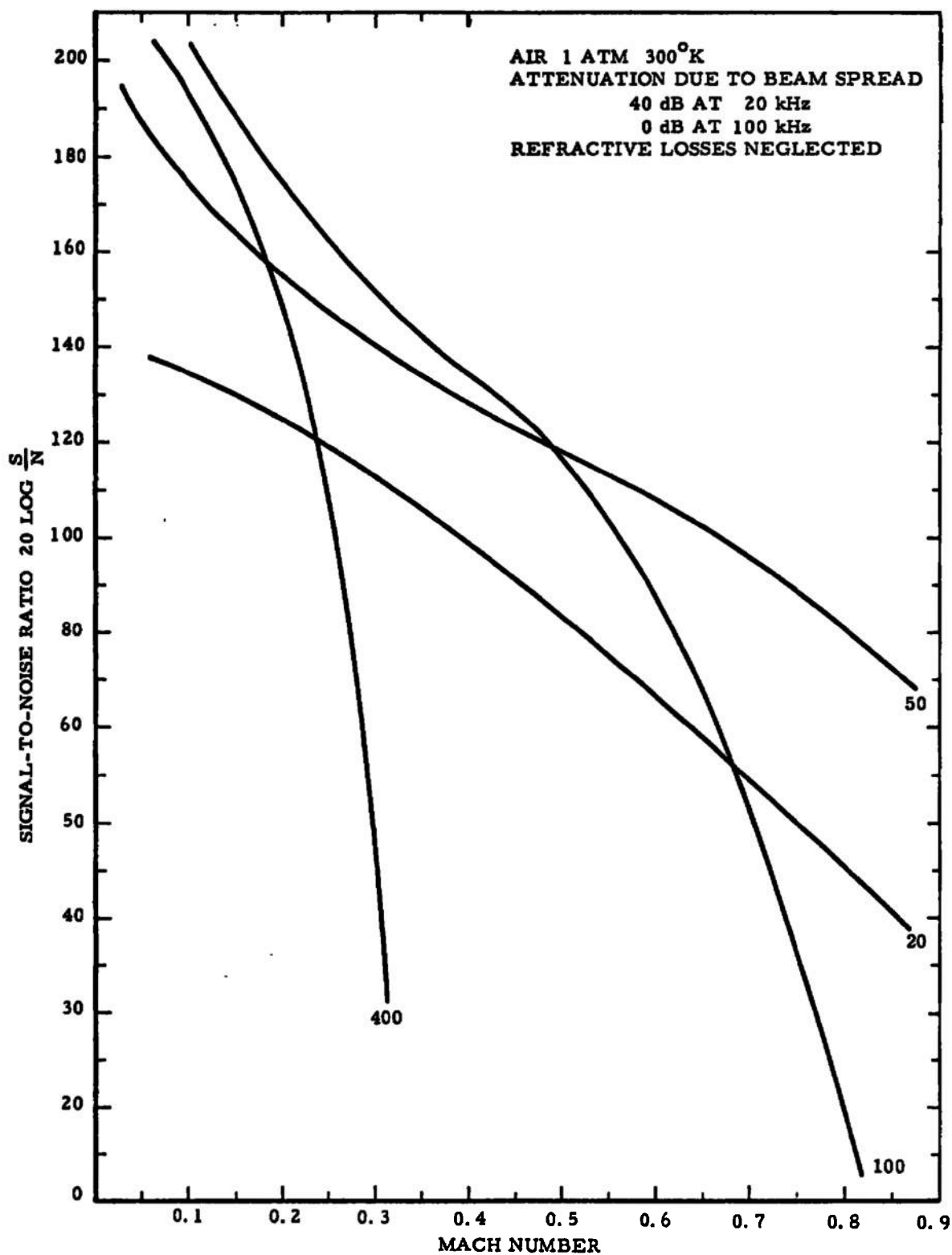


Fig. 17. Signal-to-noise ratio in a 25 cm duct with a 2.5 cm diameter transducer.

## OTHER ANALYTIC OR DESIGN CONSIDERATIONS

GAS PRESSURE EFFECTS ON SIGNAL LOSSES

The gas pressure  $p$  has two principal effects on classical sound propagation:

- (1) The sound energy transmission coefficient increases as  $p$  increases, as the probe/gas mismatch is lessened;
- (2) The classical absorption coefficient decreases as  $p$  increases.

Other effects of  $p$ , relative to maximum signal intensities that to not yet introduce nonlinear or "finite amplitude" effects, and relative to noise, are not considered here. The effect of temperature  $T$  is to increase slightly, the losses  $L_z$  and  $L_\alpha$ , as shown in "Table II", p. 719, of the cited paper on ultrasonic temperature measurement (Lynnworth and Carnevale, 1972).

To graphically show the two principal effects listed above, in Fig. 18 we have plotted lines of constant loss due to classical absorption,  $L_\alpha$ , and a line of loss  $2L_z$  due to impedance mismatches at transmitter and receiver sides.  $L_z$  is independent of pathlength and frequency.  $L_\alpha$  increases in proportion to pathlength and in proportion to frequency squared. The graph shows that for most conditions of interest in Requirement 2,  $L_\alpha$  is very large at 1 MHz, but reasonably smaller, by a factor of 100, at 0.1 MHz. (Losses due to turbulence have not been calculated.)

The additional diffraction (beam spread) loss at 0.1 and 1 MHz is readily calculated, for an assumed transducer diameter  $2a = 3$  cm, a sound speed in the gas of  $c = 300$  m/s, and a path  $z = 30$  cm ( $\approx 1$  ft). The dimensionless Seki parameter  $S = z\lambda/a^2 = zc/a^2f = 4$  at 0.1 MHz, and 0.4 at 1 MHz. The corresponding diffraction losses are 3.85 dB and 1.2 dB. These values are negligibly small relative to  $L_z$ , suggesting that low frequencies ( $\sim 0.1$  MHz) can be used, without significant penalty due to beam spread losses.

COMPARISON OF ULTRASONIC FLOWMETERS FOR GASES VERSUS LIQUIDS

On page 15 we identified six (6) basic types of ultrasonic flowmeters. All but the correlation type have been manufactured as commercial instruments for application in gases and liquids. Based on data in the literature,

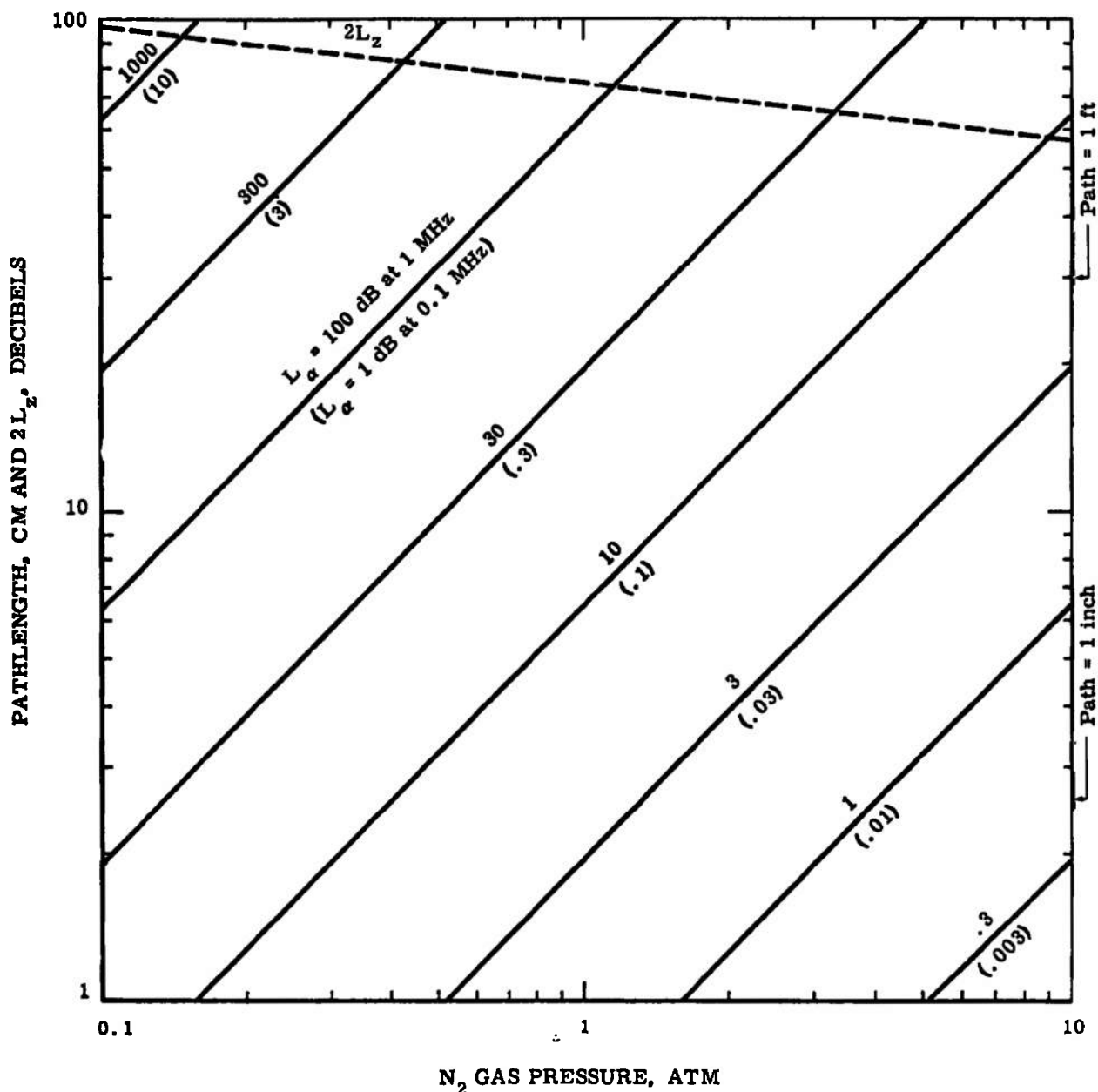


Fig. 18. Calculated losses due to acoustic impedance mismatch,  $2L_z$  and classical absorption,  $L_\alpha$ , at 1 MHz (and at 0.1 MHz) in nitrogen at 300K, as functions of pathlength and gas pressure. Calculations assume a solid buffer impedance of  $1.3 \text{ g/cm}^2\text{-}\mu\text{s}$ , and neglect beam spread.



and manufacturer' product information sheets, and our analysis, we can compare some general characteristics of ultrasonic flowmeters. The purpose of Table 4, p. 55, is to afford some perspective on approaches and on the practicality of these devices, and provide an estimate of accuracy.

## ELECTROSTATIC TRANSDUCERS

Several transducers using flexure to match intense acoustic signals to air in the tens of kHz range (Barone, 1971; Massa, 1965), have been used. Renewed interest in electrostatic transducers for this purpose has come into use recently (Kuhl, 1954; Legros and Lewiner, 1973).\*

The electrostatic transducer has additional advantages for ease of installation and operation. An electrostatic transducer schematic is shown in Fig. 19. The transducer is made of inert flexible films which can easily be installed flush on curved surfaces. In addition, the stiffness of the transducer is the air cushion behind the plastic films. Thus, the impedance match is better than is obtained with other transducers.

The initial design for the flow transducer is a simple broad beam radiator. However, a phased array offers the possibility of recovering most of the 80 dB signal loss due to spherical spreading. Two such electrostatic arrays are shown in Fig. 19. The array in Fig. 19 shows slots in the transducer backup plate which vary across the transducer face. The first groove is cut to  $\lambda/4$  at 50 kHz,  $\lambda/4 \sim 0.17$  cm. The other grooves vary in even steps down to 0.03 cm deep. The  $\lambda/4$  groove will cause resonant phase shift ( $90^\circ$ ) in the motion of the portion of the membrane just above it (Kuhl, 1954). The phase shift of each succeeding portion of membrane will drop off towards  $45^\circ$ . Thus, the transducer when driven at the frequency for which the first groove is  $\lambda/4$  will radiate a pencil beam at  $45^\circ$ . For lower frequencies the array will sweep its beam towards the normal. A focused transducer realization is shown in Fig. 19 which operates on the small principle.

## TRANSDUCER MOUNTING - DESIGN CONFIGURATIONS

The schematics in Fig. 20 illustrate nonrotated, small signal plane wave methods for interrogating on a gas path along the three directions which, relative to the duct axis, are: parallel, oblique and orthogonal. In one of the oblique beam drift cases, the triangular transducer mosaic is shown connected differentially to yield an output proportional to the Mach No.  $v/c$ . This mosaic is an "analog" or continuous version of the "digital" or discrete transducer arrangement indicated in the British NPL work.

\*Electret transducers subject to large electrode displacements are analyzed by G. M. Sessler, J. Acoust. Soc. Amer. 55, 2, 345-349 (Feb. 1974).

Table 4. Comparison of typical parameters, relative to ultrasonic flowmetry.

<u>Parameter</u>	<u>Gas</u>	<u>Liquid</u>
Usual approach	1, 3*	1, 2
Common path up and down	Along axis, $M < 1$ , or oblique, $M \ll 1$	Yes, since $M \ll 1$
Sound speed $c$ , m/s	$\sim 300$	$\sim 1000$
Density, $\text{g/cm}^3$	$10^{-4}$ at NTP	1
Transmission loss, dB	$\geq 100$	$\sim 20$
Mach No. $M$	$\sim 10^{-2}$ to $\sim 10^1$	$\sim 10^{-3}$
Gradients	Large	Small
Interaction of sound beam and fluid	Large	Small
Focusing by circular pipe	On-axis	Off-axis
Fluctuations in $\Delta c/c$ vs those in $\Delta v/v$	Small	Large
Ratio of $c_{\text{solid}}/c_{\text{fluid}}$	20:1	5:1
Response time required, seconds	$10^{-1}$ to $10^4$	$10^{-2}$ to $10^2$
Rangeability required	0 to hypersonic	100:1
Accuracy, % of range, standard models	0.5%	0.5%

\*(1) Upstream minus downstream; (2) Doppler shift off scatterers; (3) Beam drift; (4) Correlation; (5) Noise; (6) Vortex shedder.

$$\begin{aligned}
 50 \text{ kHz } \frac{\lambda}{4} &= 0.15 \text{ cm} \\
 100 \text{ kHz } \frac{\lambda}{4} &= 0.30 \text{ cm} \\
 500 \text{ kHz } \frac{\lambda}{4} &= 0.06 \text{ cm} \\
 1 \text{ MHz } \frac{\lambda}{4} &= 0.03 \text{ cm}
 \end{aligned}$$

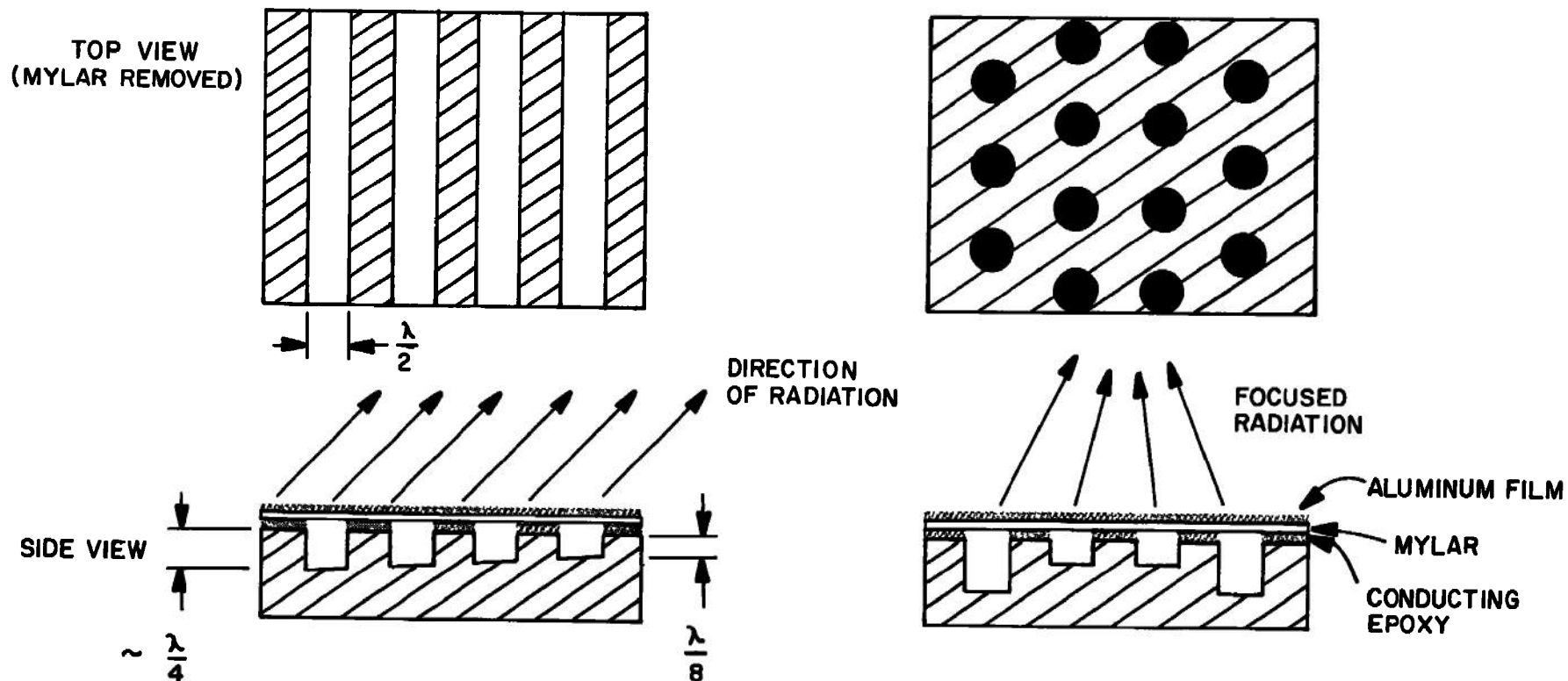


Fig. 19. Electrostatic realization of arrays.

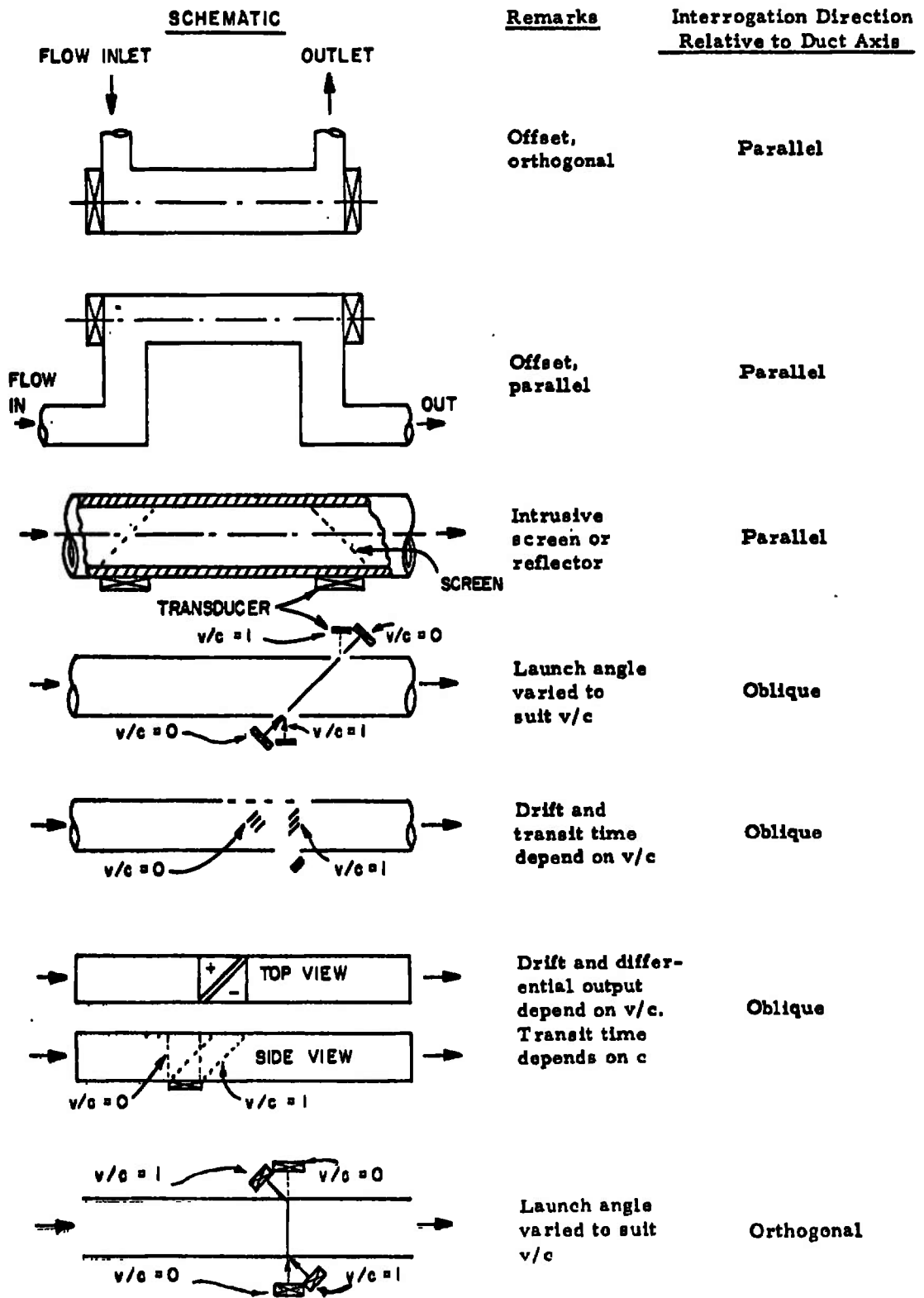


Fig. 20. Nonrotated small signal plane wave methods.

PIEZOELECTRIC CRYSTALS AND CERAMICS

Since several books have been devoted to this topic (Mason, 1950; Mattiat, 1970) we will only summarize a few important considerations. The choice of piezoelectric material depends on what characteristics are most important. For example, the short list below could be used to select a piezoelectric material to emphasize activity, linearity, high temperature or broadband characteristics:

<u>MATERIAL SELECTED</u>	<u>TO EMPHASIZE</u>
PZT	Activity
Quartz	Linearity
Lithium Niobate	High Temperature
Lead Metaniobate	Broadband

Practical applications will usually involve optimizing the response to a number of different requirements. These may typically include, in addition to the characteristics listed, electrical and acoustical impedance, mode purity,  $Q_{\text{mech}}$ ,  $Q_{\text{elec}}$ , temperature coefficients, sensitivity, size, aging, availability, compatibility with environmental factors other than temperature, such as humidity, vibration, pressure, and, occasionally, nuclear radiation.

As far as we are aware, all present commercial ultrasonic flow-meters employ transducers of the piezoelectric type. To illustrate their use, we obtained several oscillograms of transmission across stationary (no-flow) air, up to 1500 psig, room temperature and at slightly elevated temperature, and a pathlength of 69 cm (27 in. ). These transducers were designed to have low  $Q_{\text{mech}}$  and were operated under spike and also rf excitation at 0.5 MHz. Figure 28, p. 77, showing one bench test result with these piezoelectric transducers is contained in the section on Experimental Results. We have also made extensive use of piezoelectric transducers in ultrasonic measurements in shock tubes and in other high temperature sources.

As the operating frequency is reduced below  $\sim 1$  MHz, however, say, to the decades 10-100 kHz or 100-1000 kHz, magnetostrictive and electromagnetic transduction become increasingly effective. This is because the field of the exciting wave can penetrate deeper and more efficiently into the transducer material ( $\text{skin depth} = 1/\sqrt{\pi f \mu \sigma}$ ) as frequency  $f$  decreases. On the other hand, the capacitive reactance  $X_C = 1/2 \pi f C$  of a piezoelectric transducer increases as  $f$  decreases,

which can aggravate matching and cable loading problems. Therefore, we briefly examine magnetostrictive and electromagnetic transducers, in the following paragraphs.

### MAGNETOSTRICTIVE METALS

A variety of metals are commonly used as magnetostrictive transducers (Kikuchi, pp. 44, 45, in: Mattiat, 1970). We have mainly used remendur, an alloy principally of 48% Co, 48% Fe, 4% Va. This alloy has relatively high coupling and high curie point, nearly  $1000^{\circ}\text{C}$ . We have conducted bench tests on several disc resonators, excited axially, using a rod of remendur, 1.4 mm (0.056 in.) diameter by  $\geq 15$  mm long, to propagate across paths several hundred mm long, at  $f \lesssim 100$  kHz. The discs may be excited at their center by one remendur rod, or at a number of points essentially along or near a nodal path such as a mid-radius circle. The beam patterns thereby generated have been analyzed to some degree, for the discs themselves (Barone and Juarez, 1972). The patterns may be controlled to peak at preferred off-axis directions such as  $45^{\circ}$ , for example. Thus, they may be useful in beam steering. They may also be installed in a manner that hardly perturbs a given duct. Installation can even take advantage of an all-metal seal, since the energizing field is of low enough frequency to penetrate a tubular sheath such as stainless steel, of wall thickness  $\sim 0.2$ - $0.5$  mm thick. This construction is illustrated below, and has been found useful, at least as far as sealing and transduction is concerned, in nuclear thermometry applications (Lynnworth, 1971).

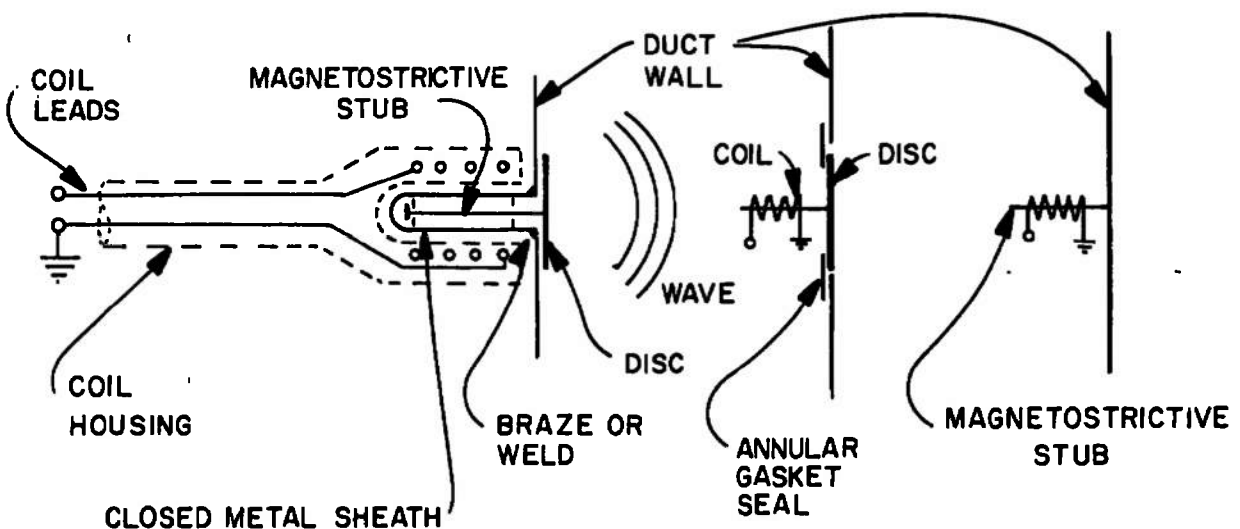


Fig. 21. Magnetostrictive transducer used with all-metal seal, with nonmetal gasket, and in direct coupling to duct.

## ELECTROMAGNETIC TRANSDUCTION

Thorough accounts of this type of transduction are now available in the literature (Gordon, 1969; Thompson, 1973; Dobbs, pp. 127-191, in Mason and Thurston, 1973). Briefly, in electrically conductive materials, through the Lorentz force, ultrasonic waves can be generated or detected through the interaction of the ultrasonic-frequency oscillation and a dc biasing magnetic field.

The effect is generally much weaker than for piezoelectric or magnetostrictive transduction, and so it has seen little industrial use so far. However, through improved signal processing, whereby adequate S/N can be achieved, this approach should be considered, because of its several interesting features. These include: the convenient launching of particular modes or polarization, operation unlimited by temperature per se (e. g. , no curie point limit), noncontact, and flexible geometrical constraints. Thompson has shown that the method is well suited for certain measurements of ultrasonic phase and group velocity, and possibly for detecting defects in large steel pipes. These applications represent both laboratory and, ultimately, rugged field tests. If such field applications prove practical, then the extension of this approach to measurements in ducts or other situations may be a worthwhile pursuit.

## PRECISION, BIAS, STABILITY AND RESPONSE TIME

The precision of the electronic phase measurement, if done in a digital manner, is  $\pm 1$  count. This may be  $\pm 0.1^\circ$  out of a range of  $\pm 180^\circ$ . Even finer resolution is obtainable on commercial phase meters, e. g. ,  $\pm 0.01^\circ$ . However, other factors will surely limit precision so that electronic efforts to measure phase to better than  $\sim 0.1\%$  are considered unwarranted, for the anticipated applications.

The bias in the optimum design will probably be dominated by path or propagation differences in the upstream versus downstream directions. To the extent that the paths are noncongruent, and to the extent that the propagation "constant" is not actually constant, even over the brief interrogation interval of  $\sim 1$  ms, there will not be a complete cancellation of the effects of  $c$ . Thus, the  $v$  result will be biased by the uncanceled influence of  $c$ .

Depending on the actual flow and temperature variations encountered in the PWT facilities, appropriate selection of the time constant may average out much of the short-term  $c$  bias. As mentioned elsewhere, the time constant may also determine, to some extent, the influence of modulation noise (phase-jitter) that the measuring system does not suppress.

Since the stated response time in this program is given as  $\leq 1$  second, for Requirement 2, and this is essentially the same as required in the Eustis fuel flow program (0.5 second) it is expected that the same computational times will suffice in the present gas flow metering project.

### INSTALLATION, OPERATION AND MAINTAINABILITY

The optimized electronics proposed for the PWT facilities tests would be maintained the same as other electronic test equipment of similar complexity.

The electrostatic transducers proposed for the PWT facilities tests have survived repeated starts and runs (in some cases over  $\sim 100$  runs) in the wind tunnel duct used in our bench tests. Other electrostatic transducers have passed similar tests (Schmidt and Tilmann, 1969). These type transducers can be repaired in some cases. However, the simplest procedure will probably be their direct replacement, should failure occur. The two main failure modes appear to be: (a) tearing due to shear stresses near the wall; (b) electrical breakdown of the dielectric.

As mentioned elsewhere, in the transducer section, piezoelectric materials have been used over wide pressure ranges, and over some temperature ranges, with negligible maintenance.

Electromagnetic transducers would probably exhibit mechanical problems similar to the electrostatics, and would be sensitive to coil burnout, but relatively insensitive to dielectric breakdown.

Magnetostrictive transducers appear to be the most rugged, and would therefore be the easiest to maintain, in the sense that they would generally require the least maintenance. Such transducers, for example, have been used for thousands of hours in ultrasonic thermometers for nuclear reactors.

### CALIBRATION

Calibration, historically, has often been a difficult area to resolve, for ultrasonic flowmeters. In some cases this is due to the differences between ultrasonic readings and reference readings being attributable to errors in the reference.

For the anticipated PWT facilities tests, we expect to compare the ultrasonic readings with venturi or other standard measures of flow velocity and mass flow rate. Such reference measures are understood to be available at AEDC for use in the PWT facilities tests.



## DATA ACQUISITION AND RECORDING

At present, the 5 MHz liquid fuel "steady state" flow velocimeter system we are developing for the Eustis Directorate provides a digital readout of mass flow rate  $\dot{M}$ . (This system contains several improvements over that described in the appended 1972 publication.) By relatively simple changes in or additions to the basic program, the calculator chip in this system can yield digital computation results for other parameters such as  $c$ ,  $\rho v$ ,  $v/c$ , etc. Totalizing,  $M = \sum \dot{M}(t) \Delta t$ , can also be accomplished, which is convenient for weigh tank calibrations and other purposes. Conversion to analog readout can, of course, be accomplished with D/A modules. The optimized low frequency system, designed to operate at, say, a 50 kHz carrier frequency, could be expected to provide similar outputs, digital and/or analog. The digital response time of the 5 MHz system presently is  $\sim 1$  second. This could be shortened to  $\sim 0.1$  second if required.

In another design developed in our laboratory, unsteady flow has been measured with a dynamic flowmeter having a response time of  $\sim 10$  ms. One form of this system is described in the 1973 appended publication. It is seen that a continuous analog signal is available for recording. For example, in oscillatory flow tests on liquid nitrogen, conducted February 1974, response out to 50 Hz was demonstrated by recording output voltages using a light beam oscillograph, and also using an oscilloscope and camera. Similarly, a chart recorder and oscilloscope and camera were used to record unsteady or transient ultrasonic flow measurements, wherein a column of water, approximately 75 mm diameter x nearly 2 m long, was allowed to drop under the acceleration of gravity, for intervals up to  $\sim 0.5$  seconds.

It is to be understood that gas flowmeters which may be developed for the PWT facilities or other AEDC facilities, could be built so their output would be compatible with the particular recording equipment available at the test site of interest.

## EXPERIMENTAL RESULTS

Limited bench tests were carried out to obtain experimental information on the statistics of signals transmitted across a 25 cm (10 inch) path in turbulent gases. The precision of ultrasonic flow velocity measurements depends on maximizing signal-to-noise, and processing out the phase and amplitude jitter as well as the spectral broadening of the transmitted signal. The effectiveness of coherent detection in improving the precision of such measurements was demonstrated. Finally, electrostatic transducers, particularly suitable to the present work, were tested. The transducers were mounted nonintrusively with minor disturbance to the wind tunnel wall. The resulting transducers have excellent isolation from the wall, can be driven over a broad frequency range, and can match power into the gas more efficiently than other high frequency transducers. Thus, key ideas for an ultrasonic flowmeter have been reduced to practice and serve as a basis for extrapolating to higher Mach number conditions.

A simple wind tunnel (Fig. 22) was constructed to create a path in a turbulent air stream 25.4 cm long, flowing at speeds between  $M_s$  0.1 and 0.2. A standard 15 HP blower was used to take air from outside the building, drive it through 7 feet of 10 inch square cross section wind tunnel duct, and exit the air back into the atmosphere. The test section was mounted at the end of a 3 foot length of 10 inch cross section duct work attached to the blower as shown in Fig. 22. The dynamic pressure and air temperature were determined 6 inches downstream from the test section.

Since the test section is only four duct diameters downstream from the entrance, the boundary layer is only about 1 inch thick and the freestream turbulence is determined by blower turbulence at the duct entrance. It was felt that any attempt to control or measure freestream turbulence was beyond the scope of the limited tests envisioned. However, some speculation on the state of the flow at the duct inlet might be appropriate. The blower is designed to avoid large scale turbulence which causes equipment vibration. However, a considerable volume of turbulent gas is generated by the boundary layer on the blower housing. The outer rim of the blower blade is traveling roughly at  $M$  0.25 relative to the gas. On the 8 ft of blower housing between cutoff and the end of the housing a turbulent boundary layer of about 3 inches is developed. Typically, the velocity profile of such a blower peaks at the upper edge of this boundary layer and drops to 30% of its peak value at the blower wall near the cutoff. The

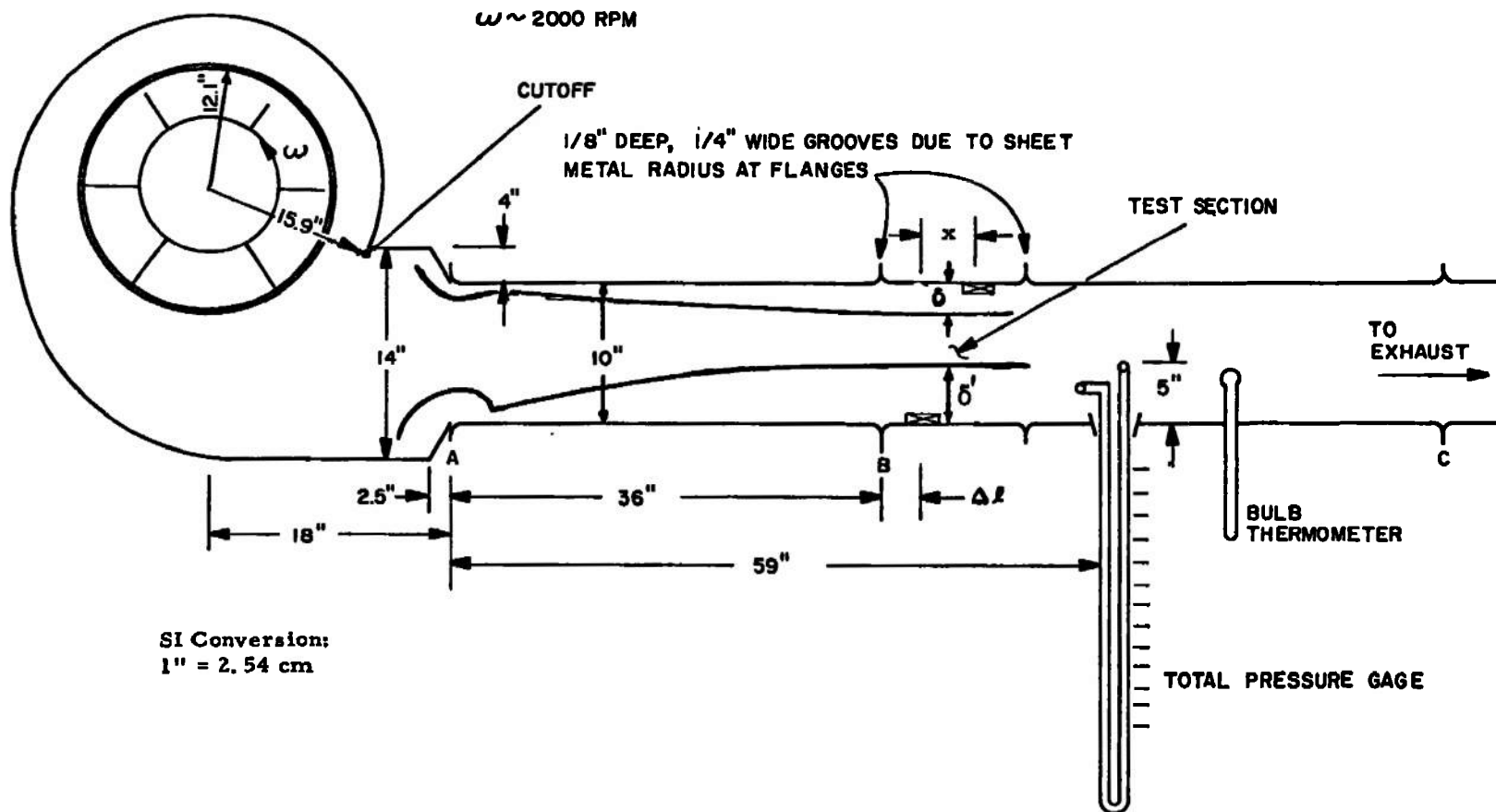


Fig. 22. Wind tunnel for bench tests.

sharp constriction at point A (Fig. 22) displaces this maximum towards the center of the duct and reduces the variation in the mean flow across the duct entrance. The discontinuity at flange A also causes separation of the flow and subsequent thickening of the turbulent boundary layer downstream. Thus, the flow in the duct freestream is highly turbulent. A large cross flow component is present due to the right angle turn at the blower intake. In addition, there is a wake-like periodicity (period  $\sim 1$  sec) in the freestream which is readily observed in the fluctuations of the ultrasonic transmissions and the dynamic head readings. These nearly periodic variations of flow amount to about 5% of the mean flow.\*

The qualitative flow description can be translated into variations of amplitude and phase of the ultrasonic transmissions across the duct. A 5% fluctuation  $\left(\frac{u}{U}\right)$  in a mean flow  $U$  of Mach number  $\frac{U}{c} = 0.1$  is equivalent to a sound speed variation of 0.5%. That is, when the velocity fluctuation  $u$  is in the same direction as the propagation direction, the sound speed is increased from  $c$  to  $c + u$ . Similarly, an opposing velocity fluctuation decreases the sound speed to  $c - u$ . Here  $c$  is the sound speed in a still gas. Assuming the largest vortex to be  $\sim 10$  cm, the magnitude of the phase fluctuations caused by these fluctuating flows can be estimated. The maximum possible phase shift fluctuation can be obtained by multiplying the fluctuation in sound speed times the number wavelengths in the path times  $360^\circ$ . The results are given in Table 5 for room temperature air flow in the present wind tunnel.

Table 5. Propagation parameters for 25.4 cm path in wind tunnel.

Frequency kHz	Number of Wavelengths in 25.4 cm	$\Delta\phi_{\max}$	Wavelength cm
150	114	205	0.233
100	75.8	13.6	0.335
50	37.9	68.2	0.670
10	7.58	13.6	8.35

An additional ( $\sim 0.1\%$ ) index of refraction fluctuation results from the convection of air from the warm boundary layers into the main stream

\*It should be noted here that no periodicity is observed in the noise which is dominated by the shear in the wall boundary layer.

by secondary flows. In fact, the largest phase shift fluctuation observed at 50 kHz was  $30^\circ$ . As can be seen by the oscillogram in Fig. 25a, the average fluctuation was less than  $10^\circ$  at 50 kHz. The measured phase fluctuations can be used to characterize the size and intensity of the free-stream vorticity in some detail (Schmidt and Tilmann, 1969, 1972; G. Witten, 1971; Dinkelacker and Stiewitt, 1971). However, it is sufficient here to note that the amplitude and phase jitter of sound transmitted through the present wind tunnel are largely due to the freestream flow fluctuations discussed above.

The acoustic noise is determined by the shear on the wind tunnel wall. The effects of the wall shear should extend into the flow a distance roughly equal to the equivalent flat plate boundary layer thickness (for a completely turbulent freestream)

$$\delta = 0.37 \ell \left( \frac{U \ell}{\nu} \right)^{1/5}.$$

Taking  $\ell$  to be the distance from the duct entrance to the test section,  $U$  the freestream flow velocity, and  $\nu$  the kinematic viscosity for  $300^\circ\text{K}$  air, the boundary layer thickness is about 5 cm (2 inch). Thus, the boundary layers extend over roughly 40% the total duct cross section. The slope of the noise versus frequency allows the displacement thickness to be estimated. As described below, this was carried out and gave the expected value within  $\sim 2\%$ . This shows that the boundary layer does indeed dominate the flow noise.

Two test sections, with 10 inch square cross sections to match the duct, were made. The test section was joined to the duct as indicated in Fig. 22 by sheet metal flanges. Grooves  $\sim 1/4''$  wide and  $1/8''$  deep were formed on the inside of the duct by the radius of curvature of joint between the flanges and the duct side walls. This disturbance in the duct wall is much smaller than the turbulent boundary layer. In addition, no difference in flow noise level was observed for transducers located different distances from this groove.

Electrostatic transducers were "flush" mounted on the duct walls. A construction was employed which emphasized the adaptability of the electrostatic transducers for model instrumentation. The transducers are completely flexible and can be mounted as easily on curved surfaces as on flat surfaces. The transducers match acoustically into the gas better than into the solid walls. Therefore, no acoustic feedthrough in the walls is observed. The overall height of the transducers above the wind tunnel walls is 0.016" for the one of the design employed and 0.004"

(0.1 mm) for the other. The major perturbation is the coaxial line required to carry the signal. Even this could have been done with strip line construction without broaching the wind tunnel walls.

The detailed construction of the transducers is given in Figs. 23a and b. A large diameter transducer was built with paper spacers to allow operation at low pressures. The displacement required to produce a given pressure  $\tilde{p}$  in the gas is related to the frequency according to





$$\xi = \frac{\tilde{p}}{\rho c \omega}$$

where  $\rho$  and  $c$  are density and sound speed of the gas and  $\omega$  is the angular frequency ( $2\pi f$ ). Thus, a low frequency transducer needs a large amplitude swing to create a given pressure. To maintain a high output  $\tilde{p}$  at low frequencies requires sufficient spacing between the membranes to accommodate  $\xi$ . The paper washers provide the spacing to maintain output down to 9 kHz.

The transducer consists of two aluminized mylar layers. The aluminum coating on the middle layer is the high voltage electrode. A dc voltage (200V) on the high voltage electrode would cause the entire assembly to draw together. Both the aluminum film and the outer mylar film and the wind tunnel wall are grounded. Superposition of an alternating field (50V) on the membrane causes the two mylar films to vibrate and emit an ultrasonic wave. The connections to the aluminum films are accomplished by silver epoxy cement and the paper spacers are bonded to the middle mylar film. The aluminum is removed from the outer 1/4" of the middle mylar to prevent short circuiting. The outer rim of both mylars are bonded with a nonconducting cement to the wind tunnel walls. The active area of the larger transducer is roughly equal to the area of the aluminum film ( $31.6 \text{ cm}^2$ ) on the middle mylar. Referring to Table 5 and Fig. 23c, the ratio of transducer diameter to wavelength  $\left(\frac{d}{\lambda}\right)$  varies between 1 and 30 for the larger transducer.

The small transducer used in the present work does not have any spacers. This transducer operates on the air trapped in surface roughness. The roughness of the wall and the middle mylar aluminum coat is exaggerated to illustrate this point in Fig. 23b. The output of the smaller transducer falls off at about 40 kHz. The active area of this transducer is 2.54 cm (1 inch) giving a  $\left(\frac{d}{\lambda}\right)$  of  $\sim 0.3-10$ . As discussed below, the small  $\left(\frac{d}{\lambda}\right)$  transducer was used to provide acoustic rays over a large angular spread.

## LEGEND:

-  ALUMINUM COATING
-  MYLAR DIELECTRIC
-  PAPER WASHERS
-  SILVER EPOXY

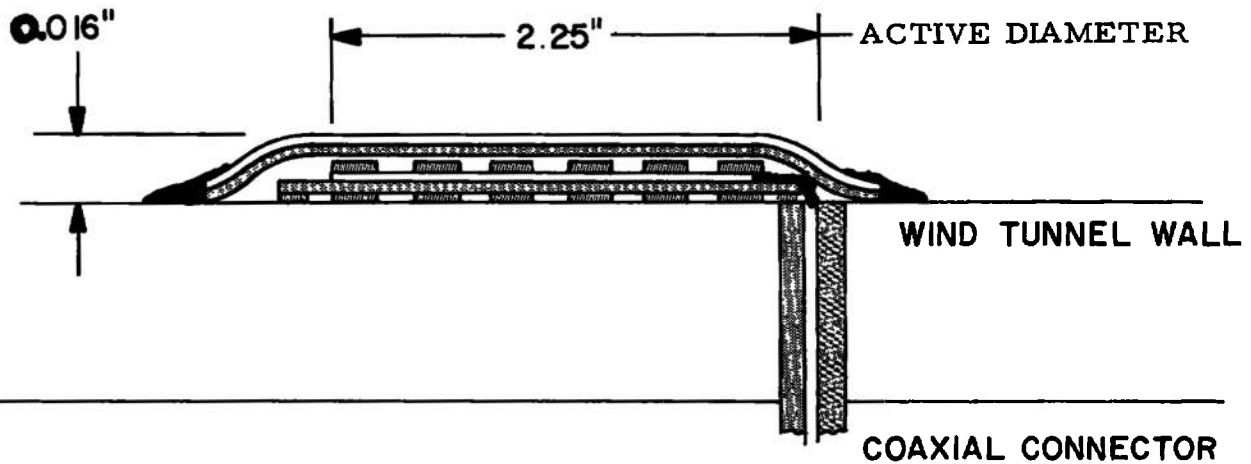


Fig. 23a. Low cutoff frequency large diameter electrostatic transducer.

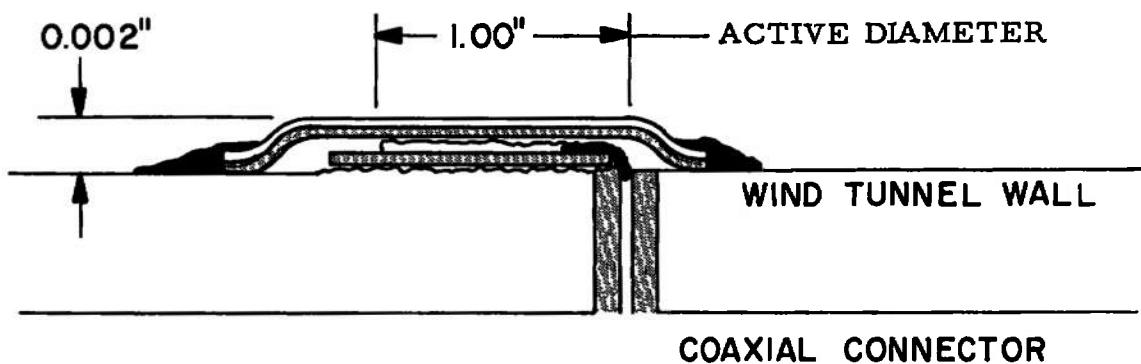


Fig. 23b. High cutoff frequency small diameter electrostatic transducer.

Transducers were mounted on opposing walls as shown in the wind tunnel diagram, Fig. 22. Two sets of large diameter (Fig. 23a) transducers were mounted on the vertical side walls. One pair was mounted on walls directly opposing each other\* ( $x = 0$ ). Thus, when the flow was turned on the signal dropped. A second pair of transducers was mounted with an offset of  $x = 1$  inch. The beam drift in the present wind tunnel flow is roughly one inch (see beam drift above). These transducers provide signal-to-noise information appropriate to a beam drift flow velocity measurement (page 10).

A second set of small (Fig. 23b) transducers was mounted on the horizontal walls with a separation  $x = 3''$ . The  $\left(\frac{d}{\lambda}\right)$  of these transducers was made sufficiently small to assure an upstream ray. The signal-to-noise information obtained with these transducers is representative of transmission (upstream-downstream phase shift) measurement of flow velocity (page 16).

The coherent detection system used for the tests is shown in Fig. 24. The main burden of the bench test electronics is carried by the PAR\*\* phase-lock amplifier Model HR-8. All of the components within the dotted lines of Fig. 24 are contained in the PAR HR-8. A cw sine wave oscillator is amplified and used to drive an electrostatic transducer. The signal was picked up by a similar receive transducer, amplified and fed back into the PAR HR-8 signal channel. The first stage of the HR-8 is a tuned amplifier gang tuned with the cw sine wave generator with a Q of 25. The output of this stage was detected and recorded to give signal amplitude. The phase-lock output was also recorded. This output allowed the product of amplitude and angle to be recorded at various noise bandwidths between 1 kHz and 0.1 Hz with and without flow.

The signal-to-noise was determined by measuring the amplitude and phase-lock outputs with and without a signal on the drive transducer. The signal amplitude to noise amplitude showed a 100:1 improvement when the frequency was raised from 10 kHz to 100 kHz, as expected. The tradeoff between bandwidth and signal-to-noise was dramatically demonstrated using the phase-lock output.

The frequency and flow velocity scaling of the acoustic flow noise and turbulent scattering is well-known from recent work on sonar and atmospheric propagation studies. These scaling laws were used to predict system performance across a 25 cm duct at elevated Mach numbers. The detailed results are presented below.

---

\* $x$  is defined in Fig. 22 as the streamwise distance between the centers of the transducers.

\*\*PAR - Princeton Applied Research, Princeton, New Jersey.



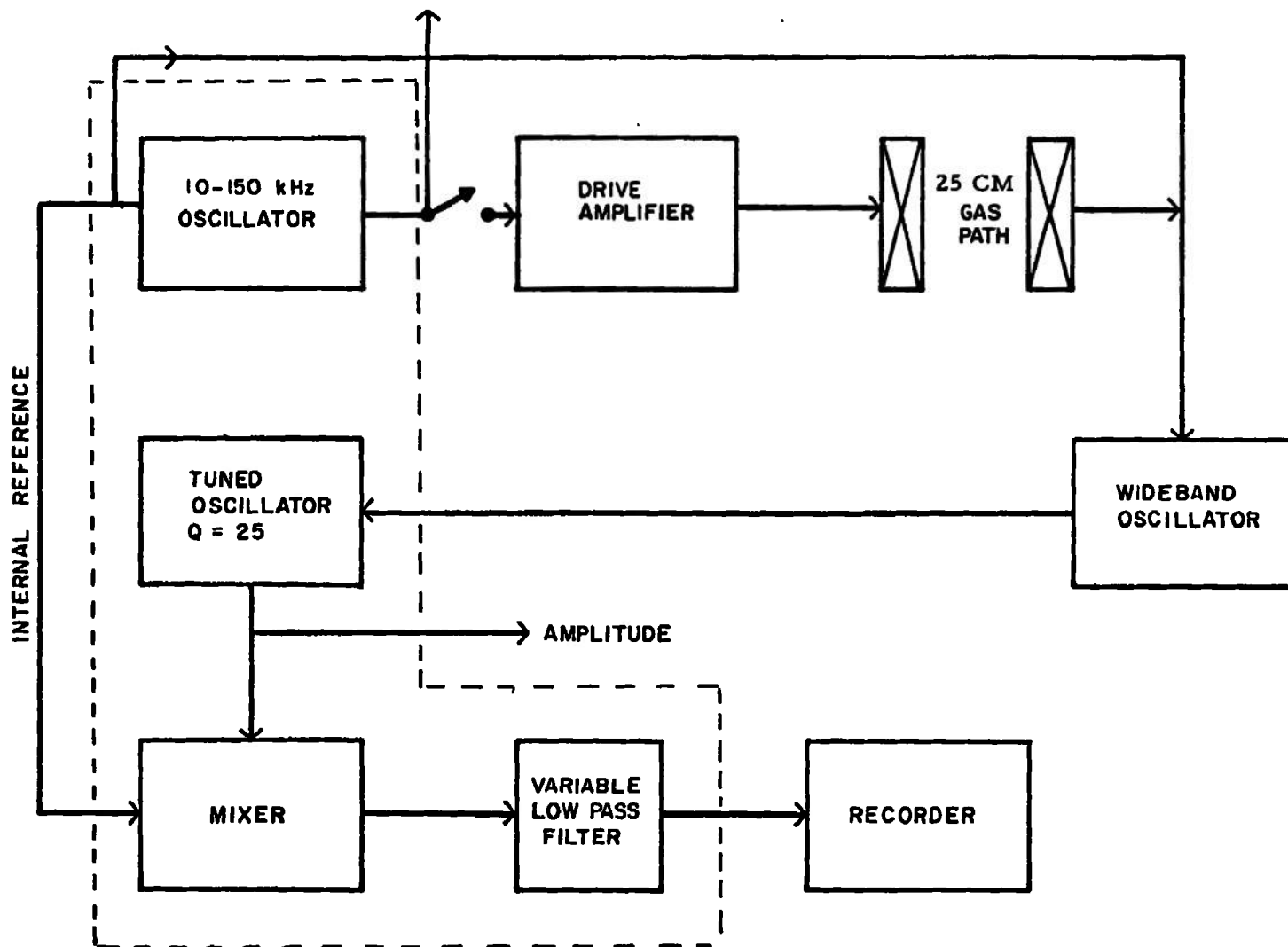


Fig. 24. Coherent detection system for bench tests.

The measured transmission showed maxima and minima every 200 Hz as the frequency was varied. This is due to multiple reflections within the duct. There are only certain modes of sound propagation which can satisfy the boundary conditions. These modes can be thought of as systems of plane waves propagating at small angles with respect to the duct walls (Reschevkin, 1963). The dominant mode is plane wave propagation normal to the duct walls. Other modes reflect back and forth at angles. The observed maxima are very closely spaced at high frequencies, 150 kHz, because there are many low angle modes to reverberate. The modes begin to disappear at about 250 kHz because of absorption and overlap.

There are two techniques for avoiding the amplitude buildup due to the reverberation process described above. First, the system can be pulsed and reverberations gated out. Second, the operating frequency may be chosen sufficiently high to absorb most of the energy (under flow conditions) in one round trip.

The only effect the reverberations had during the present tests was to increase the phase jitter. The flow variations disturbed the resonance of the mode, causing large phase shifts (Mungar, 1969; Eversman, 1972).

The signals transmitted across the gas path for the small transducer at 50 kHz are shown in Figs. 25 and 26. The signal and noise under flow conditions are compared with the no flow signal in Fig. 25 for the case where the transmitter is located upstream. The signal transmitted under no flow is smaller than the signal with the flow on because the small transducers are offset by 7.62 cm. The small transducers are  $\sim 1.90\lambda$  in radius at 50 kHz. Referring to Fig. 14, the angle at which transducer output is reduced by one-half is 0.132 radians. The angle between the centers of the two transducers is 0.253 radians. Thus, under no flow one would expect a signal level reduced by about 0.23 from the maximum. Under flow conditions an upstream ray offset angle equal to the Mach number (0.12 radians) reaches the receive transducer. The signal at 0.12 radians off beam center should be about 0.580 of maximum. Thus, the ratio of the flow to no flow signals\* is

$$R = \left( \frac{0.580}{0.228} \right)^2 = 6.45$$

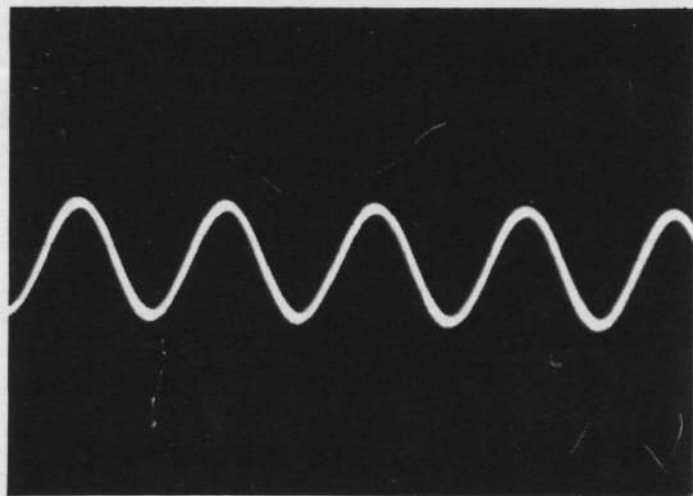
The ratio observed from Fig. 25 is

$$R = 3.66 .$$

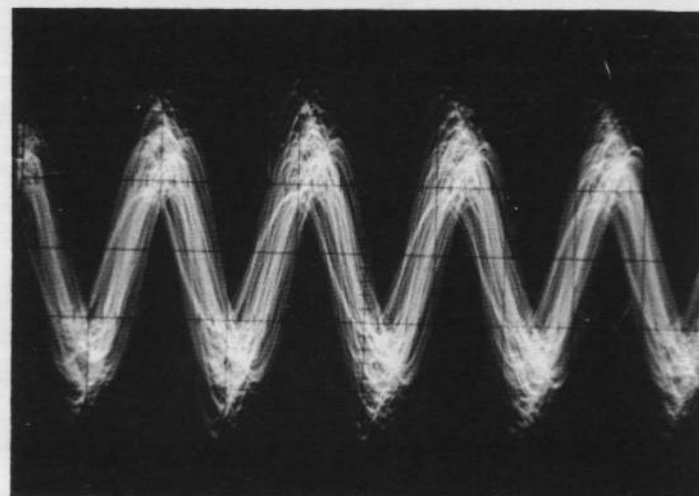
This indicates virtually no attenuation.

---

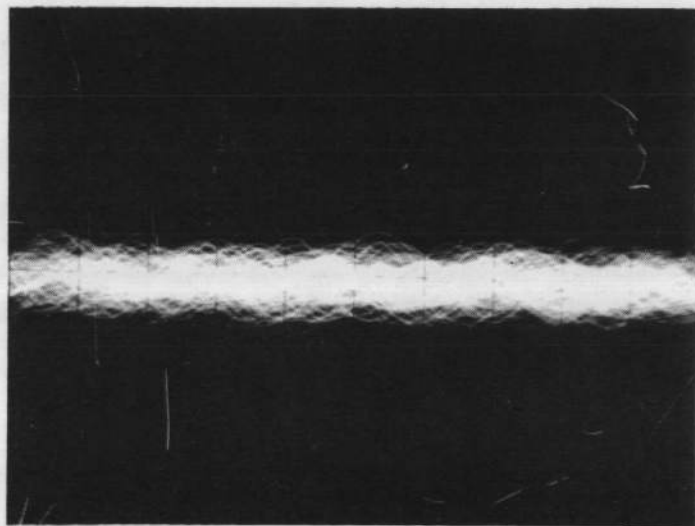
\*The square is due to angle of incidence.



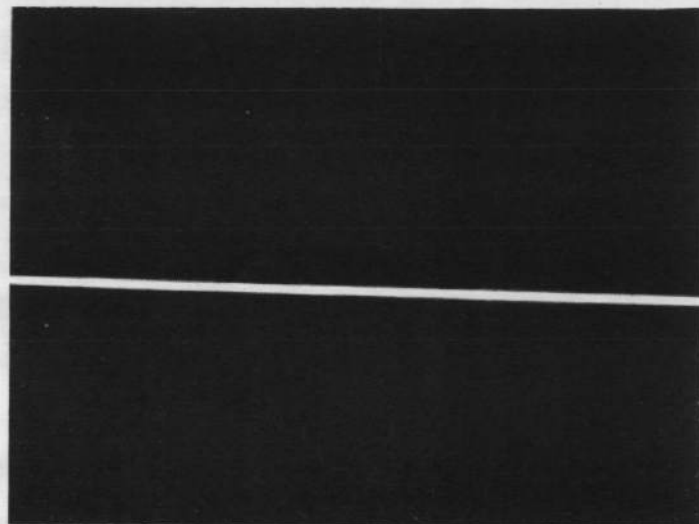
No Flow - Receive Signal - 500  $\mu$ V Sensitivity



Flow Signal - 1 mV Sensitivity

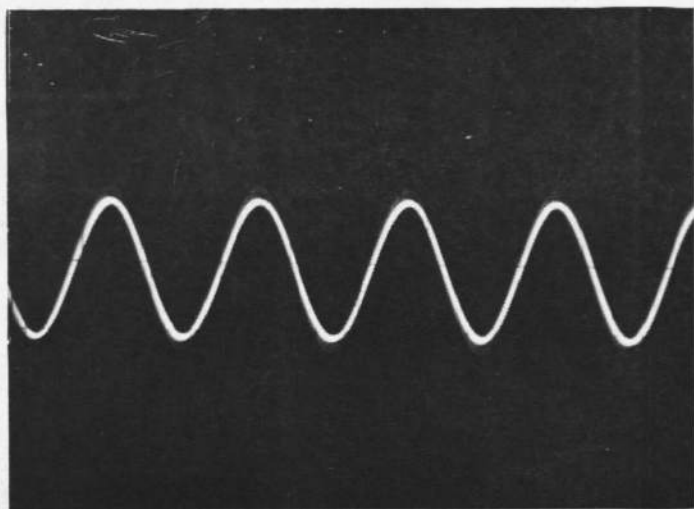


Noise Under Flow - 50  $\mu$ V Sensitivity

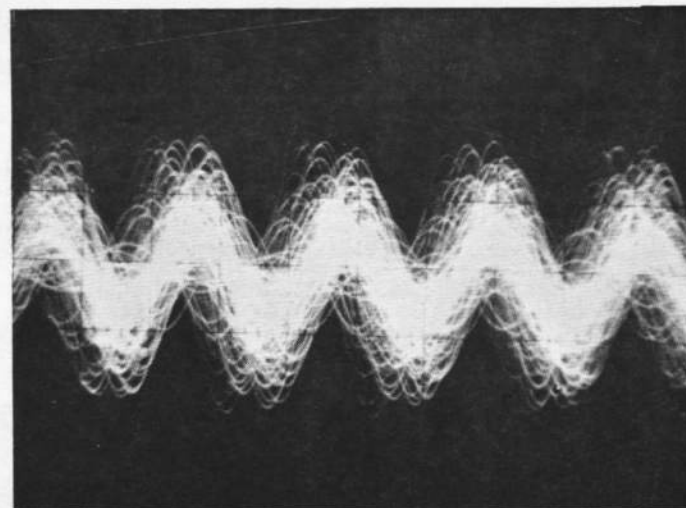


Noise Under Flow - 1 mV Sensitivity

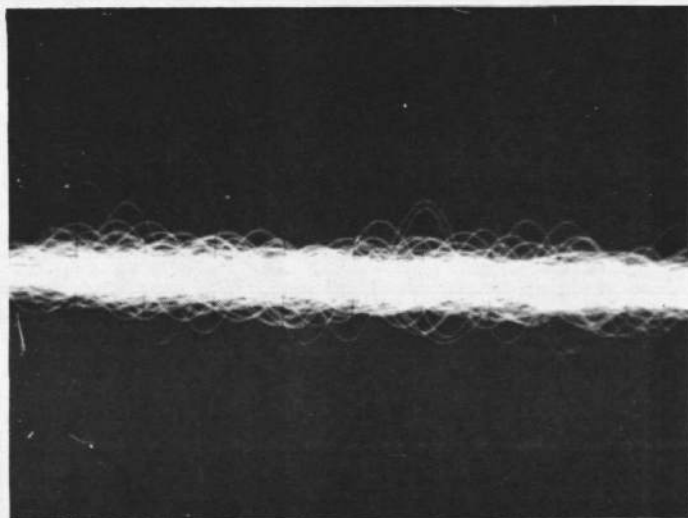
Fig. 25. Transmitted signals across a 25.4 cm duct with  $M = 0.15$ . 2.5 cm transducers, receiver center 7.5 cm downstream from transmitter center.



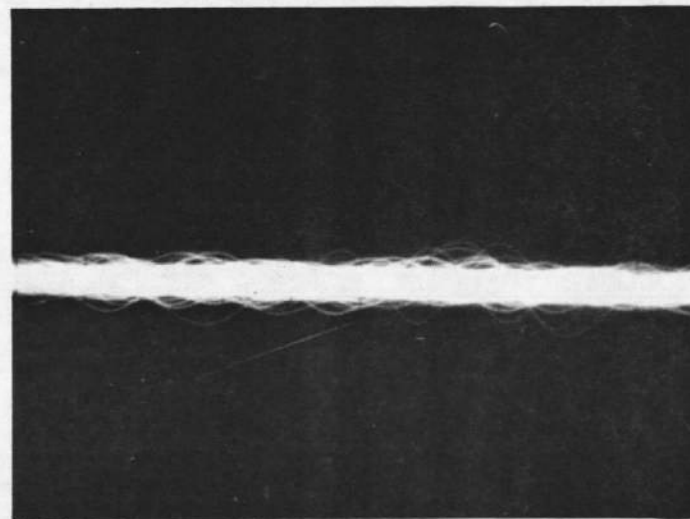
No Flow - Receive Signal - 500  $\mu$  V Sensitivity



Flow Signal - 200  $\mu$  V Sensitivity



Noise Under Flow - 100  $\mu$  V Sensitivity



Noise Under Flow - 200  $\mu$  V Sensitivity

Fig. 26. Transmitted signals across a 25.4 cm duct with  $M = 0.15$ . 2.5 cm transducers, receiver center 7.5 cm upstream from transmitter center.

Similar signals are shown in Fig. 26 for the upstream direction. The signal under no flow is larger in this case than the signal under flow. The ray which reaches the receiver under flow conditions is offset by the 0.253 radians due to transducer location plus 0.15 radians due to Mach number from the beam center. In fact, the ratio of flow to no flow signal from Fig. 26 is 0.400.

The attenuation due to thermal absorption and scattering over the 25 cm pathlength used is negligible. The attenuation is entirely due to beam spread. These losses can be reduced by optimum deployment of transducers. For instance, an array of downstream receivers\* can be used to give temperature. A receiver directly across from the transmitter can be used to receive the upstream ray containing flow information. The "temperature" receivers would be arranged so that one of them would be close to the beam drift position at each Mach number. Thus, the attenuation for these receive positions would be less than observed in the bench tests. The receiver directly across from the transmitter would see a ray between 0.2 and 0.7 radians off the transmitter beam axis for Mach numbers between  $M = 0.2$  and  $M = 0.8$ . Thus, the signal attenuation for any of these transducers would be similar to that obtained in the bench tests reported above.

The signal-to-noise versus frequency was also measured. The noise versus frequency is shown in Fig. 27 for the one inch transducers. The noise falls off as the frequency squared over the entire frequency range 10 kHz-150 kHz. On the other hand, the signal for the transducers falls off much more rapidly as the beam spread becomes too small to provide a ray at the necessary angle. Measurements with the larger transducers (described above, page 68) offset by the beam drift distance, showed a signal-to-noise which increased as  $f^2$  over the entire range.

A signal-to-noise ratio of 40 for the downstream transducer and 8 for the upstream signal at 50 kHz under the  $M = 0.15$  flow was observed in the present bench tests. Proper location of the transducers should allow signals equal to the downstream\* transmission to be obtained at least up to Mach 0.5. Since the noise increases at the Mach number to the sixth power, a signal-to-noise ratio of  $3 \times 10^{-2}$  would be obtained at  $M = 0.5$  in a 25 cm duct at 50 kHz and a bandwidth of 2 kHz ( $Q = 25$ ). A bandwidth of  $\sim 1$  Hz can be obtained in the phase-locked mode, giving a signal-to-noise of 600 to 1 at  $M = 0.5$  in a 25 cm diameter duct.

---

\*Different transducers would provide the signal for different Mach numbers.

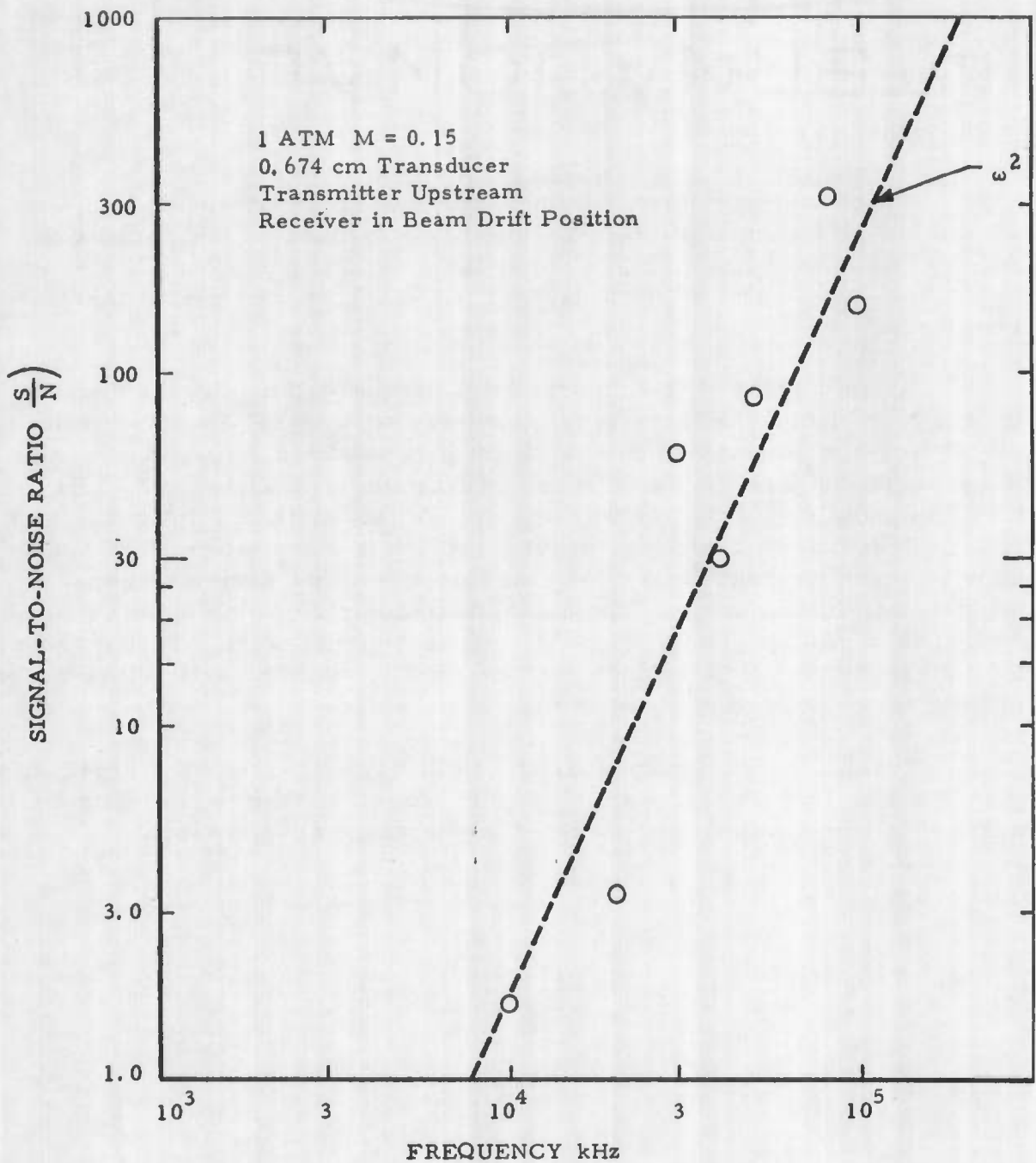


Fig. 27. Measured signal-to-noise versus frequency.

The signal levels used in the present work were  $10^{-4}$  atmospheres. This was done to allow a wide band of frequencies to be used in the present tests. There is a tradeoff between gain and bandwidth. The signal levels can be raised two orders of magnitude (Kuhl, 1954) by redesigning the transmitter. A signal-to-noise level of 200 to 1 could be obtained this way.

Transmissions were obtained over the frequency region between 10 and 500 kHz. Some of these results are summarized in Appendix A. At ~50 kHz, the observed signal-to-noise ratio and phase stability were optimum, and the electrostatic transducer used, worked well at this frequency.

Extrapolation of the experimental results obtained in the present program at higher Mach numbers indicates that a signal-to-noise ratio of 600 to 1 can be obtained over a 25 cm path in  $M = 0.5$  flow at one atm. A series of one inch diameter receive transducers operated at 50 kHz would be suitable for the measurements. A bandwidth of 1 Hz in the phase-locked mode would give about a 600:1 to 1 signal-to-noise ratio.\* This is based on obtaining a  $10^{-2}$  atm output from properly designed electrostatic transducers. The signal-to-noise ratio would be decreased to 35:1 at  $M \sim 0.9$ . Thus, there is sufficient signal amplitude to make a flow measurement in a ten inch duct essentially over the entire flow range of interest as defined by Requirement 2, page 12.

For comparison purposes, and to illustrate the use of a broadband piezoelectric transducer, we include Fig. 28. This shows transmission across a ~60 cm air path at elevated temperature and pressure.

---

\*The limitations of equipment available during the present bench tests, prevented our taking advantage of a bandwidth as narrow as 1 Hz.



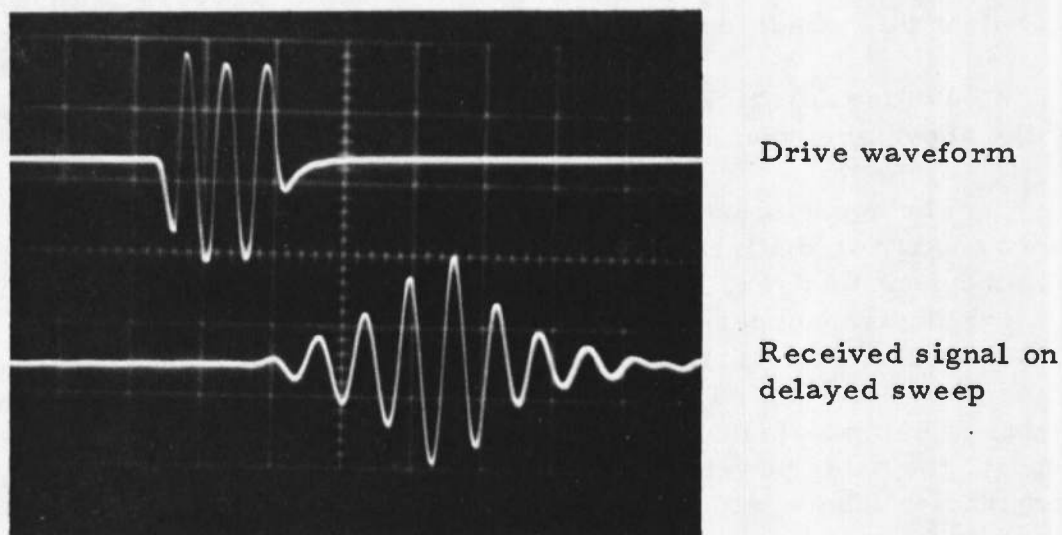


Fig. 28. Oscilloscope showing transmission of 0.5 MHz rf burst across ~60 cm static (no flow) air path, at ~40 atm (585 psig) and slightly elevated temperature (50°C). Measurement utilized a pair of broadband piezoelectric transducers. Transit time = 1.87 ms. Sweep, 5  $\mu$ s/div.



## OPTIMUM DESIGN FOR FUTURE TESTS IN PWT FACILITIES AT AEDC

The flow measuring system to be used in the PWT facilities must provide an overall accuracy in the range 0.5% to 1%. It must be capable of operation in the presence of very high ambient noise levels, Mach numbers between 0.1 and 0.5, and, of course, highly turbulent flow conditions, in which gradients are expected to occur.

Before describing the actual measurement system, the effects of the above environmental factors will be briefly described.

The acoustic noise types to be encountered in the measurement are of two distinct types. These are (1) additive noise, and (2) modulation noise. The additive noise is that which appears at a receiving transducer due to acoustic radiation from within the turbulent gas, and due to frictional effects of the gas flowing by the transducer location. This noise is present whether or not an acoustic signal is being transmitted across the duct. As shown earlier in this report, the noise power per hertz decreases with frequency at high frequencies (above ~20 kHz) and is relatively independent of frequency at lower frequencies.

The second noise type, which we have named modulation noise, results in the spreading of the spectrum of an otherwise narrow band transmitted acoustic wave, and is due to the varying properties (temporal and spatial) of the turbulent medium being probed. Because of these perturbations, multipath effects will give rise to rapid fading (amplitude modulation) of the received signal. In addition, local variations in sound speed and flow velocity will result in phase modulation of the received wave. These modulation effects become more severe as the frequency of the transmitted wave is increased because more acoustic wavelengths must be traversed by the transmitted wave across the duct, which results in increased phase shifts as well as increased multipath interference. If we characterize the medium as being permeated with moving scattering centers (the inhomogeneities), it is easy to visualize how scattering by these centers can result in interference effects due to small-angle forward scattering. Such interference will increase with frequency.

In addition to the above, acoustic reverberation of the transmitted wave within the duct can occur. Such reverberation would not only inherently reduce measurement accuracy, but would also greatly enhance the modulation noise effects discussed above.

From the above discussion, it is clear that, in order to overcome additive noise effects, we should attempt to operate at high frequency, utilizing very narrow bandwidth. Coherent operation would be ideal. However, such high frequency operation would result in unacceptable phase and amplitude modulation of the transmitted wave. Depending on the pathlength, use of high frequencies may also result in excessive attenuation. Thus, there would appear to be impasse. However, the flowmetering situation can be greatly improved if the following features are incorporated in the measuring system:

- (1) Utilize a high frequency carrier wave to provide operation in the spectral region of low additive noise.
- (2) Modulate the above carrier in such a way as to reduce or eliminate the effects due to modulation noise and reverberations.
- (3) Simultaneously transmit both upstream and downstream to eliminate first order errors due to variations in sound speed from the measurement. (It may be necessary to use beam steering to efficiently accomplish this over a common path.)

The measurement technique described below meets the three requirements.

A coherent carrier wave in the range 50 kHz to 100 kHz is amplitude modulated by a rectangular pulse whose time duration is approximately half the transit time across the duct (on the order of half a millisecond for a one foot duct). This waveform is applied simultaneously to both the upstream and the downstream transducers. At an appropriate time ( $\sim 1$  millisecond after transmission begins), the two transducers are connected to separate receivers. The receivers are connected for  $\sim 1$  millisecond. This sequence is repeated after a time sufficiently long ( $\sim 10$  milliseconds) to insure that energy due to reverberations in the duct will not enter the receivers. The modulation waveform (assuming a one foot duct and sound speed  $c \approx 10^3$  ft/sec) is shown in Fig. 29, along with the timing of the receiver gates and the arrivals of the upstream and downstream waveforms at the appropriate receivers. (A block diagram is shown in Fig. 30.)

In the timing scheme of Fig. 29 a modulation period of  $5 \times 10^{-4}$  sec and utilization of a 50 kHz carrier provide 25 complete cycles (not shown in the figure) in each transmission. The total transmitted waveform can be mathematically shown to be the Fourier series of the

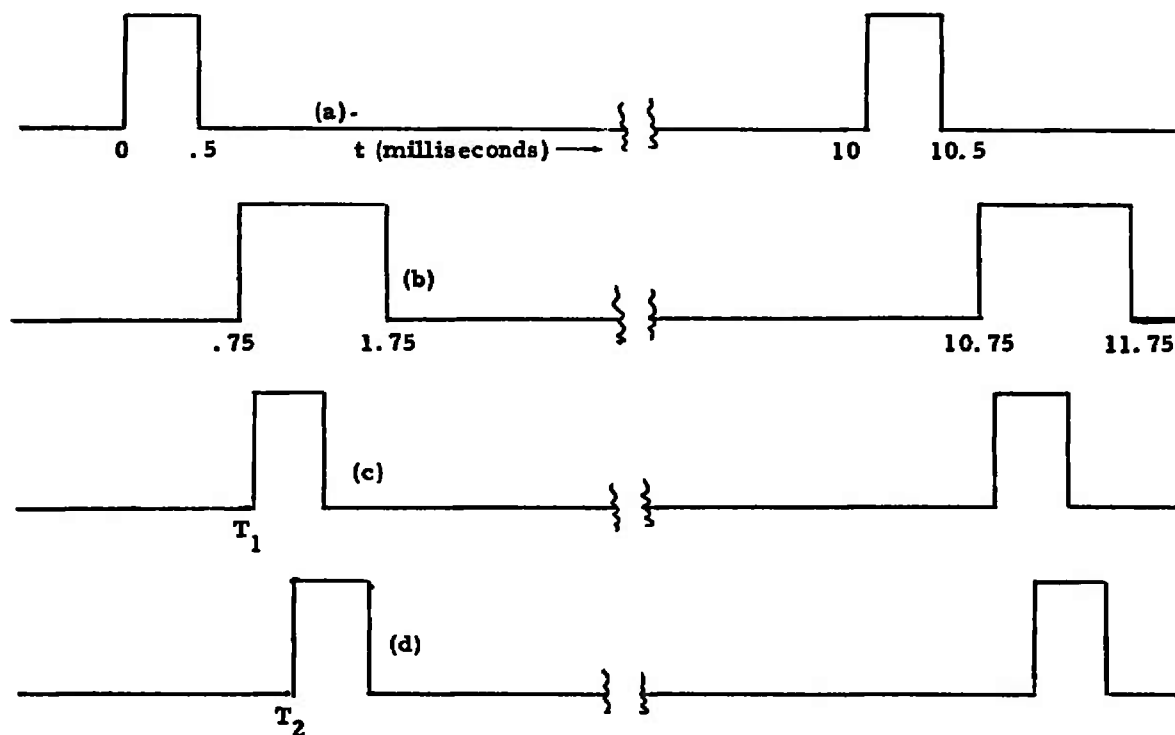


Fig. 29. Timing diagram showing

- (a) Simultaneous upstream/downstream transmission
- (b) Simultaneous enabling of upstream/downstream receivers
- (c) Downstream received signal. Delay =  $T_1$
- (d) Upstream received signal. Delay =  $T_2$

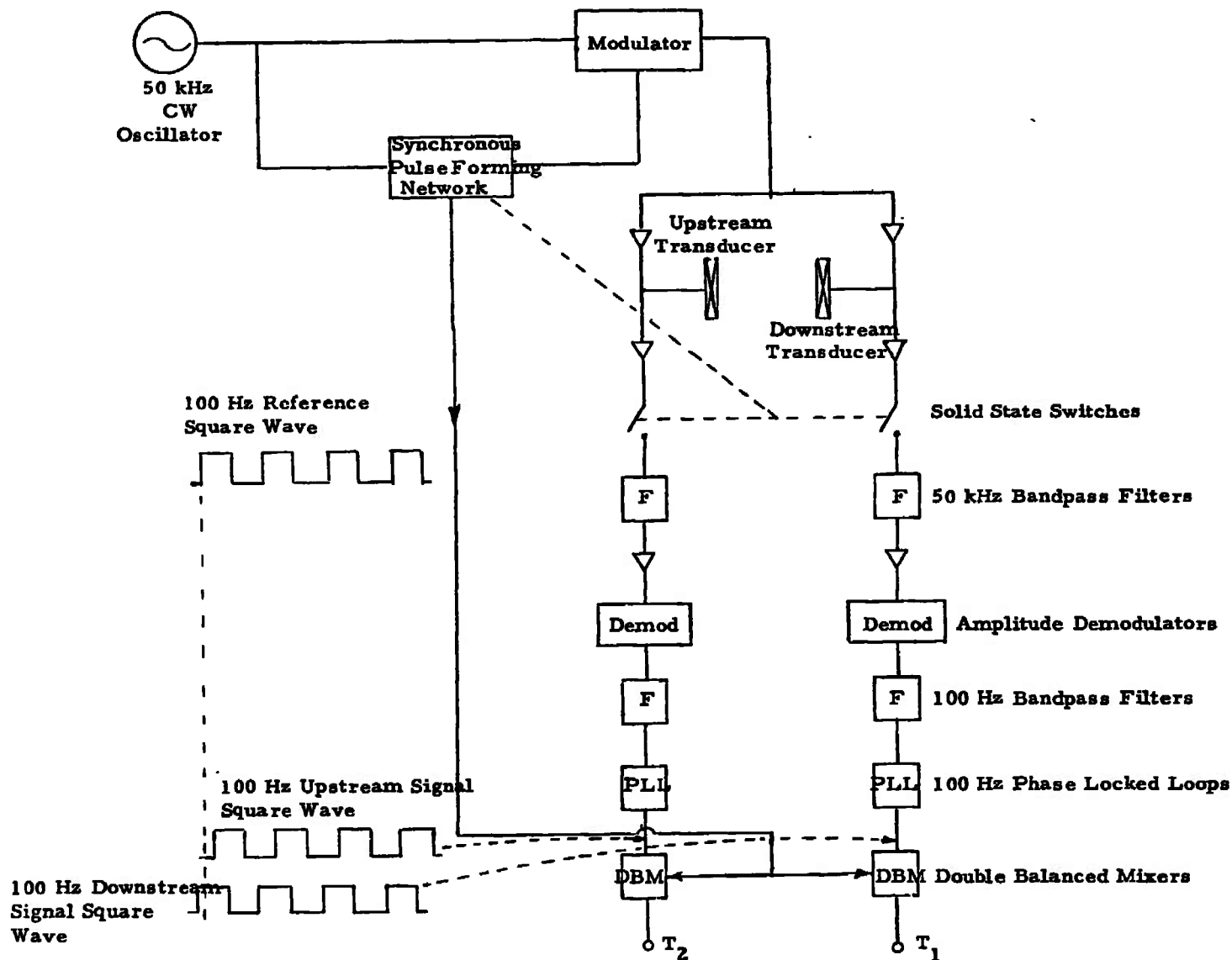


Fig. 30. Block diagram of ultrasonic flowmeter design for gases, using synchronous detection and demodulation.

modulation is just the reciprocal of the repetition rate (100 Hz in the example). This frequency can be recovered in the receivers by means of amplitude demodulation and narrow band filtering. The times  $T_1$  and  $T_2$  (see Fig. 30) can be independently determined by means of separately measuring the phase shift of each of the 100 Hz fundamentals in the upstream and downstream receivers. It can be shown that the flow velocity, averaged over the path, is given by

$$v \sim l \left( \frac{T_2 - T_1}{T_2 T_1} \right) ,$$

where  $l$  = axial distance between transducers. Thus, accurate measurements of both  $T_2$  and  $T_1$  insure an accurate determination of  $v$ .

This measurement system is considered to be the optimum design for meeting those contractually-specified parts of Requirement 2, that can be simulated in the PWT facilities. It is a low-frequency (e. g. , 50 kHz) version of a 5 MHz flow velocimeter that has been built for the Eustis Directorate for use with aviation fuels. Based on preliminary tests with the 5 MHz system, and in view of the analysis and test results in the present phase of this program, it appears that the optimum design will provide a practical solution for the PWT facilities' and similar applications.

## CONCLUSIONS AND RECOMMENDATIONS

In view of Requirement 2 in the Scope of Work, and in particular, with regard to tests anticipated in the PWT facilities at AEDC, it is concluded that the transmission approach presently offers the most promise\* with regard to accuracy and response time, for flows up to at least Mach 0.5, and possibly as high as  $\sim 0.9$ . Theory and experiments indicate that, for a path of  $\sim 25$  cm, a suitable carrier frequency is 50 kHz. Based on the present requirements, and taking note of recent developments using coherent detection of modulated cw transmission across liquids such as aviation fuel, water and liquid nitrogen, it appears reasonable to apply a low-frequency (e. g., 50 kHz) version of that type of flow measuring system to the gas flow-metering situation. Electrostatic transducers offer advantages of impedance matching and small perturbation of the duct, and so may be preferred over the more usual piezoelectric types, or even over the more rugged magnetostrictive types which suffer from lower sensitivity.

It is recommended that the "optimized design" outlined in this report, be fabricated and tested in the PWT facilities at AEDC. The object of such tests would be to determine, under flow conditions of interest, the actual limits of signal/noise ratio, and, correspondingly, the limits on accuracy and response time. It is expected that accuracy of  $\sim 0.5\%$ , and response times of  $\leq 1$  second, can be achieved.

---

\*That is to say, the ultrasonic transmission approach, preferably executed using simultaneous launching of upstream and downstream waves over a common path, is to be preferred over the other ultrasonic approaches considered, namely, reflection/doppler scatter, beam drift, correlation, noise and vortex shedding.

## REFERENCES

- C. J. Ahern, C. S. Longstreet, B. R. Teitelbaum and W. E. Wetts, Ultrasonic Transmission Investigations for Turbine Inlet Gas Temperature Measurement, AFAPL-TR-72-75 (1972).
- C. H. Allen et al. , Atmospheric Physics and Sound Propagation, Final Report for period July 1, 1945 to May 20, 1950, Pennsylvania State College (Sept. 1, 1950).
- A. Barone and J. A. G. Juarez, J. Acoust. Soc. Amer. 51 (3), Part 2, 953-959 (1972).
- H. E. Bass and J. J. Bauer, Atmospheric Absorption of Sound Analytical Expressions, J. Acoust. Soc. Amer. 50, 821-825 (1972).
- R. T. Beyer, Nonlinear Acoustics in: Physical Acoustics, W. P. Mason (ed. ), Vol. 11, Part B, 321 (1968).
- C. A. Brau and R. M. Jonkman, Classical Theory of Rotational Relaxation in Diatomic Gases, J. Chem. Phys. 52, 477-484 (1970).
- L. Camp, R. Stern and B. M. Brown, Underwater Acoustics, 223-272, Wiley-Interscience, New York (1970).
- E. H. Carnevale, C. Carey and G. Larson, Ultrasonic Determination of Rotational Collision Numbers and Vibrational Relaxation Times of Polyatomic Gases at High Temperatures, J. Chem. Phys. 47, 2829-2835 (1967).
- E. H. Carnevale, G. Larson, L. C. Lynnworth, C. Carey, M. Panaro and T. Marshall, Experimental Determination of Transport Properties of High Temperature Gases, NASA CR-789 (1967).
- L. A. Chernov, Wave Propagation in a Turbulent Medium, Dover (1960).
- G. M. Corcos, The Resolution of Turbulent Pressures at the Wall of a Boundary Layer, J. Sound Vib. 6, 59-72 (1967).
- J. Coulthard, Ultrasonics 11 (2), 83-88 (March 1973).
- A. Dinkelacker and H. H. Stiewitt, Modulation von Ultraschall. durch Turbulente Wasser Strömungen (Experimentelle Untersuchungen), Proc. 7th Int. Conf. on Acoustics, Akademia Kiado, Budapest, 449-452 (1971).

## REFERENCES (cont'd)

- E. R. Dobbs, in: Research Techniques in Nondestructive Testing, Vol. 2, Academic Press, New York (Nov. 1973); also in: Physical Acoustics, Principles and Methods, W. P. Mason and R. N. Thurston (ed.), Vol. 10, 127-191, Academic Press, New York (1973).
- R. R. Dowden, Fluid Flow Measurement - A Bibliography, The British Hydromechanics Research Association, 22-26 (1972).
- T. H. Ellison, The Universal Scale Spectrum of Turbulence at High Reynolds Number, in: The Mechanics of Turbulence, Gordon and Breach (1962).
- L. B. Evans, H. E. Bass and L. C. Sutherland, Atmospheric Absorption of Sound Theoretical Predictions, J. Acoust. Soc. Amer. 51, 1565-1573 (1972).
- W. Eversman and R. J. Beckemeyer, Transmission of Sound in Ducts With Thin Shear Layers - Convergence of the Uniform Flow Case, J. Acoust. Soc. Amer. 52, 219-220 (1972).
- W. W. Fowles, Liquid Metal Flow Measurements Using an Ultrasonic Doppler Velocimeter, Nature Phys. Science 242 (242), 12-13 (March 5, 1973).
- H. L. Foxx, Continuous-Wave Three Component Sonic Anemometer, BBN Report No. 1311, AFCRL-68-0180 (15 March 1968).
- F. R. Frick and D. C. Stevenson, Pressure Fluctuations in a Separated Flow Region, J. Acoust. Soc. Amer. 44, 1189-1200 (1968).
- F. R. Frick and D. C. Stevenson, Estimation of Wall-Pressure Fluctuations in a Separated Flow, J. Acoust. Soc. Amer. 50, 985-991 (1970).
- R. A. Gordon, Electromagnetically Excited Acoustic Standing-Wave Resonances in Metals, Ph. D. Thesis, Brown University (1971); Bull. Amer. Phys. Soc. 16, 103, 359 (1971).
- G. P. Haddle and E. J. Skudrzyk, Noise Production in a Turbulent Boundary Layer by Smooth and Rough Surfaces, J. Acoust. Soc. Amer. 32, 19-34 (1960).
- G. P. Haddle and E. J. Skudrzyk, The Physics of Flow Noise, J. Acoust. Soc. Amer. 46, 120-138 (1969).



# REFERENCES (cont'd)

- J. O. Hinze, Turbulence, McGraw-Hill, Chap. 7 (1959).
- U. Ingaard and V. K. Singhal, J. Acoust. Soc. Amer. 54 (5), 1343-1346 (1973).
- P. J. Klass, Aviation Week and Space Techn., 45-47 (Nov. 6, 1972).
- J. Kritz, ISA Proc. 10, Part 2, 55-16-3, pp. 1-6 (1955); Instruments and Automation 28, 1912-1913 (Nov. 1955).
- W. Kuhl, G. R. Schodder and F. K. Schroeder, Acustica 1, 519-532 (1954).
- V. P. Kuznetsov, On the Spectra of High Intensity Noise, Soviet Physics Acoustics 16, 129-130 (1970).
- D. Legros and J. Lewiner, Electrostatic Ultrasonic Transducers and Their Utilization with Foil Electrets, J. Acoust. Soc. Amer. 53 (6), 1663-1672 (1973).
- J. A. Lordi and R. F. Mates, Rotational Relaxation in Non-Polar Diatomic Gases, Phys. Fluids 13, 291-308 (1970).
- L. C. Lynnworth and E. H. Carnevale, pp. 715-732, in: H. Plumb (ed.), Proc. Fifth Symp. on Temperature, Washington, D. C. (1972).
- L. C. Lynnworth and N. E. Pedersen, USAAMRDC Technical Report 72-66, Ultrasonic Mass Flowmeter for Army Aircraft Engine Diagnostics (Jan. 1973).
- L. C. Lynnworth, et al. IEEE Transactions on Nuclear Science, Vol. NS-18 (1) (Feb. 1971).
- L. C. Lynnworth, et al., Flow - Its Measurement and Control in Science and Industry, Vol. 1, ISA, pp. 917-924 (1974).
- W. P. Mason, Piezoelectric Crystals and Their Application to Ultrasonics, Van Nostrand (1950).
- O. E. Mattiat (ed.), Ultrasonic Transducer Materials, Plenum Press, New York (1971).

## REFERENCES (cont'd)

- A. S. Monin, Characteristic of the Scattering of Sound in a Turbulent Atmosphere, *Soviet Phys. Acoustics* 7, 370-373 (1962).
- A. S. Mujumdar and W. J. M. Douglas, *Phys. Fluids* 13 (6), 1635-1637 (June 1970).
- P. Mungar and G. M. L. Gladwell, Acoustic Wave Propagation in a Sheared Fluid Contained in a Duct, *J. Sound Vib.* 9, 28-48 (1969).
- W. L. Nyborg and D. Mintzer, Review of Sound Propagation in the Low Atmosphere, WADC Technical Report 54-602, Brown University, AD 67880 (May 1955).
- M. H. November, *The Oil and Gas Journal* (Feb. 21, 1972).
- N. E. Pedersen and L. C. Lynnworth, NASA CR-112313, Nonintrusive Dynamic Flowmeter (R) (June 1973).
- V. S. Petrovskii, Averaging of Turbulent Pressure Fluctuations by a Distributed-Sensitivity Sound Receiver, *Soviet Phys. Acoust.* 19, 262-265 (1973).
- A. Powell, pp. 231-262, in: D. E. Commins (ed.), Proc. 5<sup>e</sup> Congress International d'Acoustique, Liege, Belgium (1965).
- E. C. Racine, Measured Discrimination of Boundary-Layer Pressure Fluctuations by Round, Square and Rectangular Transducers, *J. Acoust. Soc. Amer.* 51, 369-377 (1972).
- S. N. Reschevkin, The Theory of Sound, Pergamon Press (1963).
- C. Rotta, Turbulente Strömungen, B. G. Feubner (1972).
- H. Schlichting, Boundary Layer Theory, McGraw-Hill (1960).
- D. W. Schmidt and P. M. Tilmann, Experimental Study of Sound-Wave Phase Fluctuations Caused by Turbulent Wakes, *J. Acoust. Soc. Amer.* 47, 1310-1324 (1969).
- D. W. Schmidt and P. M. Tilmann, Über die Zirkulationsentwicklung in Nachläffen Von Rundstäben, *Acustica* 27, 14-22 (1972).

# REFERENCES (cont'd)

- T. E. Siddon, Surface Dipole Strength by Cross Correlation Method, J. Acoust. Soc. Amer. 53, 619-620 (1973).
- A. V. Smolyakov, Cross Spectrum of Low Frequency Pseudosonic Turbulent Pressures, Soviet Phys. Acoust. 16, 241-243 (1970).
- W. A. Strawderman, Turbulence-Induced Plate Vibrations: An Evaluation of Finite and Infinite Plate Models, J. Acoust. Soc. Amer. 46, 1294-1307 (1969).
- V. I. Tartarski, Wave Propagation in a Turbulent Medium, Dover (1961).
- R. B. Thompson, Electromagnetic, Noncontact Transducers, IEEE 1973 Ultrasonics Symposium Proc., IEEE Cat. No. 73 CHO 807-8SU, 385-392.
- S. Uva, Ultrasonic Propagation in High Temperature Gases and Plasmas, Ph. D. Thesis, Boston College (1968).
- G. Witten, Modulation von Ultraschallen durch Turbulente Wasser Strömungen (Theoretische Untersuchungen), Proc. 7th Int. Conf. on Acoustics, Akademia Kiado, Budapest, pp. 445-448 (1971).
- A. J. Zmuda, Dispersion of Velocity and Anomalous Absorption of Ultrasonics in Nitrogen, J. Acoust. Soc. Amer. 23, 472 (1951).

## APPENDIX A

## ACOUSTIC TRANSMISSION ACROSS 25 CM DUCT AT MACH 0.15

The propagation of sound waves through a Mach 0.15 flow was investigated over a wide range of frequencies and with several transducer configurations as indicated in the text. The parameters which led to the choice of 50 kHz as our operating frequency can be understood more clearly by studying signal and noise parameters over a wide range of conditions. The four major test configurations are displayed in Fig. A1. The direction of flow, the boundary layer thickness, and transmission direction are indicated in the figure. Also shown is the near field limit  $\frac{d^2}{\lambda}$  for frequencies at which data was taken. Roughly, the sound beam propagates with no spreading out to the near field limit. Beyond the near field limit spreading occurs and the intensity is a function of the angle of propagation. The near field is shown by parallel lines in Fig. A1 to indicate the parallel phase fronts. The far field pattern is indicated by an intensity versus angle pattern. The intensity is proportional to the radius vector drawn from the center of the transducer to the far field pattern.

The first set of photographs (A2-A5) shows a small transducer transmitting to a downstream transducer (upper left in Fig. A1). The flow offsets the beam in such a way as to increase the received signal as compared to the no flow signal. The second set of photographs (A6-A9) shows a small transducer transmitting to an upstream transducer (upper right in Fig. A1). The flow moves the beam in such a way as to decrease the received signal as compared to the no flow signal. The no flow signal with flow and flow noise is shown for each frequency. The flow noise was obtained by turning off the transmit signal and recording the receive output. The receiver noise with no flow was orders of magnitude below the flow noise displayed in the photographs.

The signal-to-noise for the upstream transmitter series is less than 1 at 10 kHz, increasing to about 50 at 40 kHz and reaching ~150 at 80 kHz. However, the phase coherence of the signal is optimum at ~50 kHz. The jitter in-phase in Fig. A4 (40 kHz) is about  $45^\circ$  while in Fig. A5 (80 kHz) the jitter increases to  $180^\circ$ . The phase jitter increase in the wavelength becomes smaller relative to either the large scale vorticity or the receiver transducer diameter.

The signal-to-noise ratio and phase jitter show a similar pattern for the downstream transmitter series. However, the signal-to-noise

- - - - Turbulent Boundary Layer

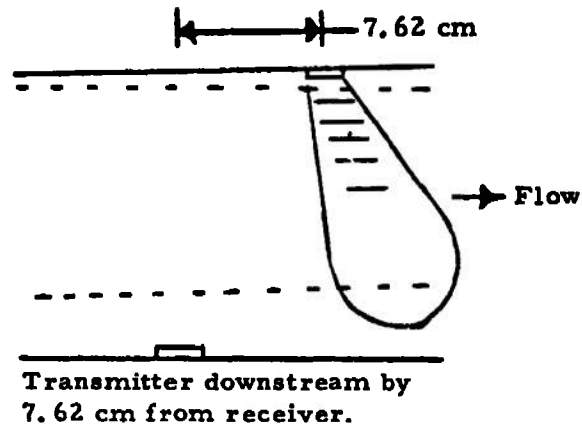
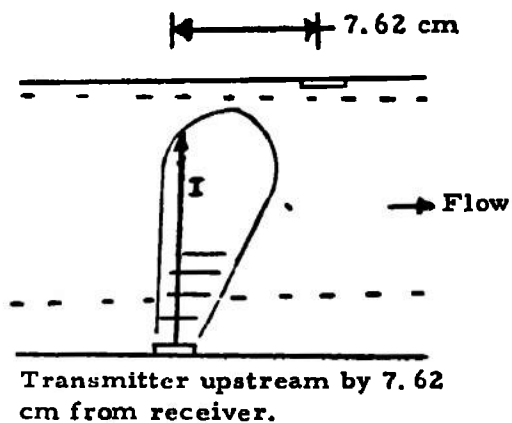
Near field  
limit  $1/4 \frac{d^2}{\lambda}$

→ 100 kHz

→ 80 kHz

→ 50 kHz

→ 10 kHz



→ 50 kHz

→ 10 kHz

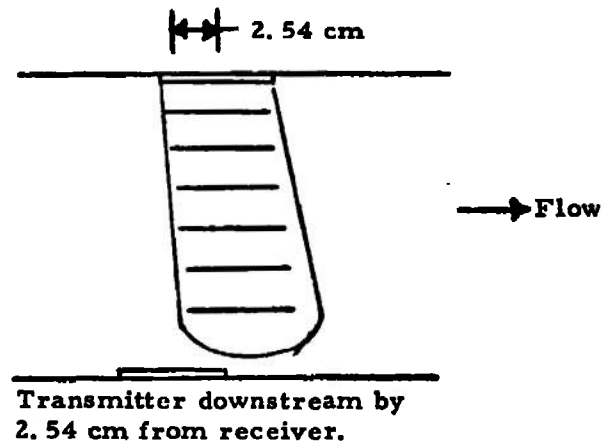
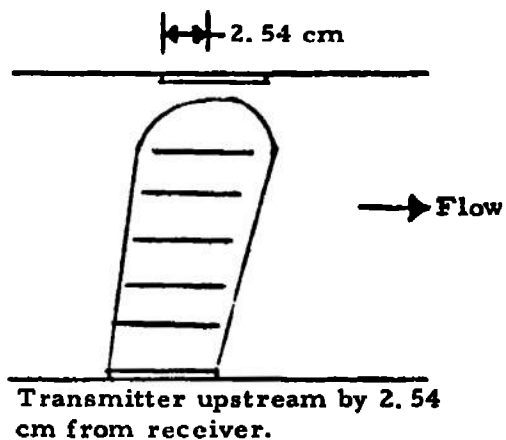


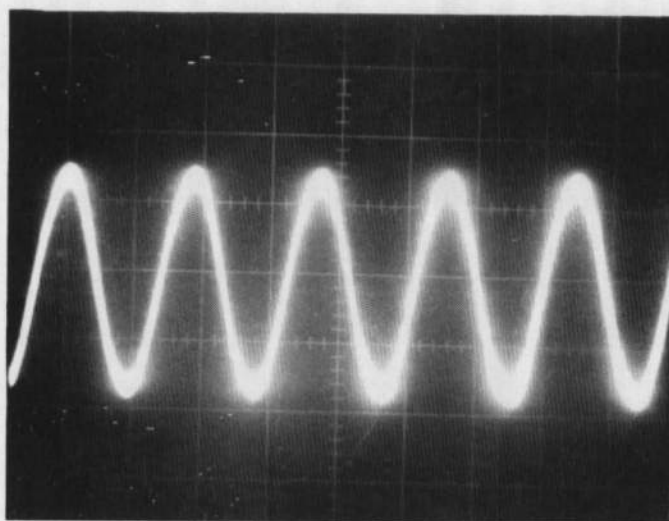
Fig. A1. Transducer mounting relative to flow direction and transducer size.

ratio is 4 at 40 kHz and 5 at 80 kHz. This is due to the fact that the flow pushes the beam further away from the transducer. The signal-to-noise ratio does not improve as quickly as one would expect with frequency because at 80 kHz the near field extends about 75% of the distance across the tube. Thus, the rays sufficiently angled upstream to reach the receiver have a very low intensity at 80 kHz compared to 50 kHz.

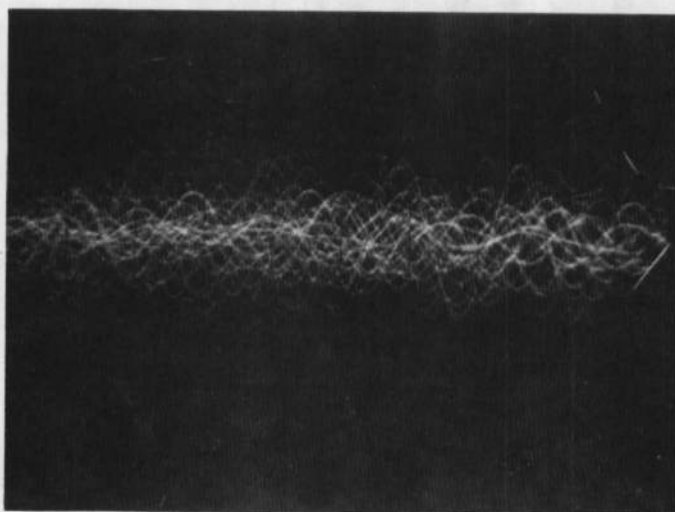
The final set of photographs shows signals obtained with large transducers offset by the distance the beam is expected to drift due to flow, 2.54 cm. The geometry for transmission with (lower left) and against (lower right) the flow is shown in Fig. A1. Note the signal-to-noise is 3 at 10 kHz for the large transducers since we are operating very close to the beam axis. In addition, the variation of signal amplitude with flow direction is very small at low frequencies since beam spread makes up for beam drift. However, at higher frequencies the beam is narrow and the downstream signal is larger than the upstream signal.

Over a hundred photographs of acoustic transmissions were taken, in addition to recorder traces of frequency response and signal-to-noise ratio. Since the absorption over large acoustic paths ( $> 10$  cm) drastically reduces the signal above 500 kHz, we generally concentrated on frequencies below 500 kHz. In addition, for turbulent flow large pathlengths include large vortices. This fact, together with the large number of wavelengths in the path, lead one to expect phase jitter. In practice, at 100 kHz across the 25.4 cm duct,  $180^\circ$  of phase jitter is clearly observable. However, the signal-to-noise ratio is relatively high. At lower frequencies,  $\sim 50$  kHz, the phase jitter is much smaller than the 100 kHz result, but the signal-to-noise ratio is poorer. Since phase jitter (or modulation noise) is undesirable for the proposed flowmeter application, the 50 kHz operating frequency is preferred to. In smaller ducts a higher frequency should be used to maximize signal-to-noise ratio, consistent with not exceeding allowable phase jitter.

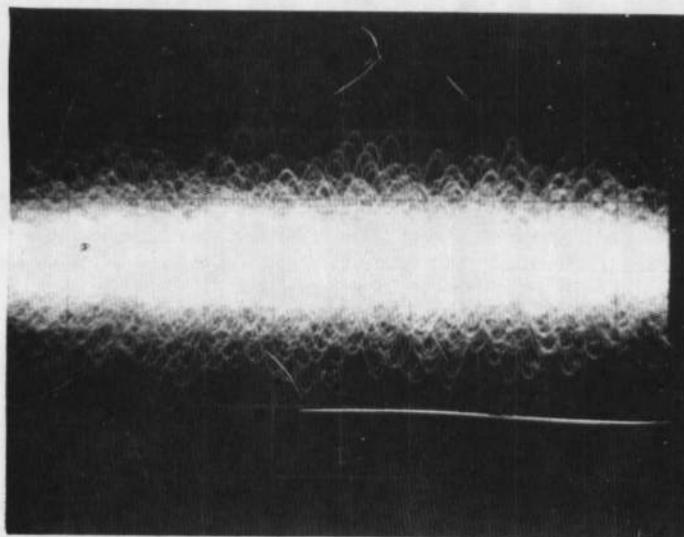
Based on the observed propagation over the wide range of frequencies obtained in the present tests, together with our previous work at megahertz frequencies, we were able to select the optimized measurement parameters for the 25 cm duct flowmeter problem. Furthermore, we are able to recommend the system described on pages 70-74. This system is expected to achieve  $\sim 1\%$  accuracy and  $\sim 1$  second response time, for the PWT or equivalent facilities.



100  $\mu$  V/cm  
No Flow Signal

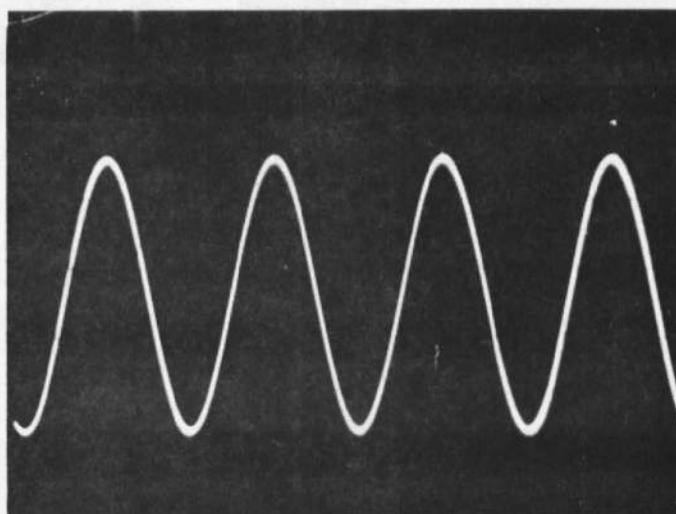


100  $\mu$  V/cm  
Flow Signal

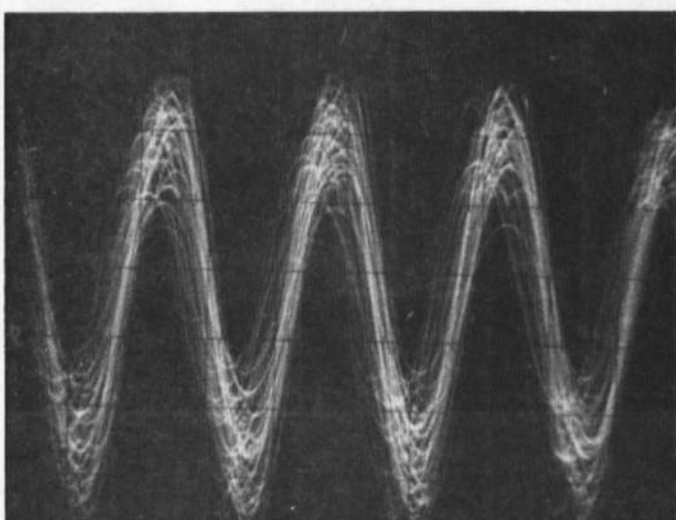


100  $\mu$  V/cm  
Flow Noise

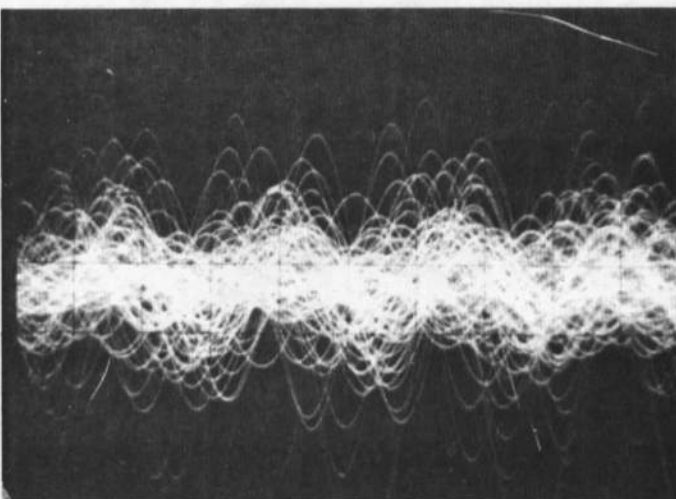
Fig. A.2. 2.54 cm transducers - transmitter upstream by 7.62 cm from receiver (10 kHz).



100  $\mu$  V/cm  
No Flow Signal



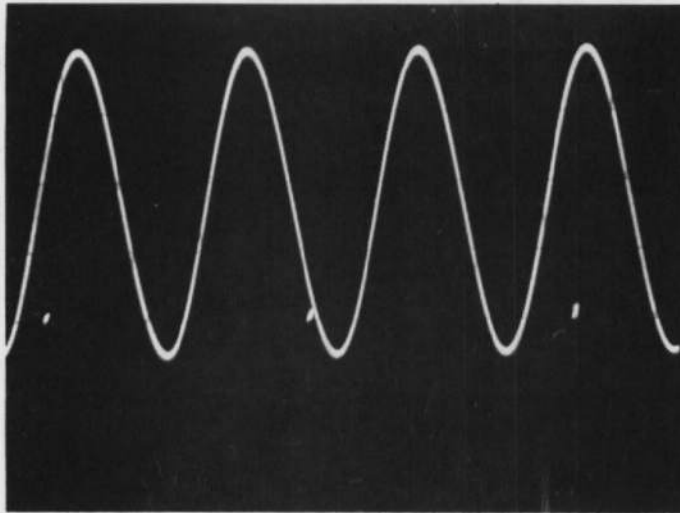
100  $\mu$  V/cm  
Flow Signal



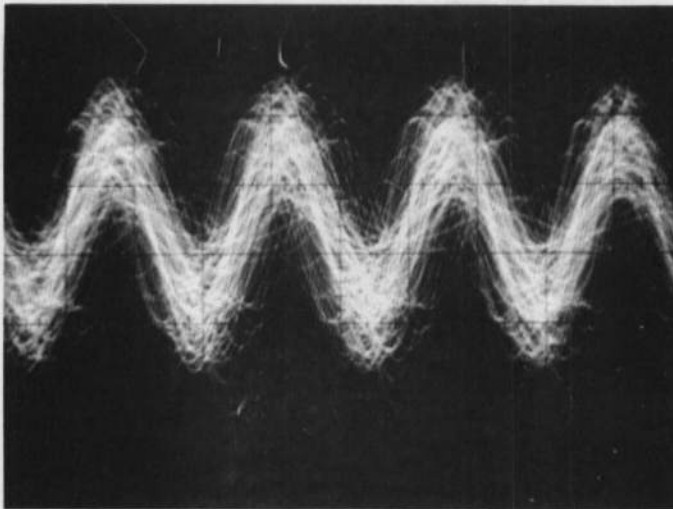
100  $\mu$  V/cm  
Flow Noise

Fig. A. 3. 2.54 cm transducers - transmitter upstream by 7.62 cm from receiver (20 kHz).

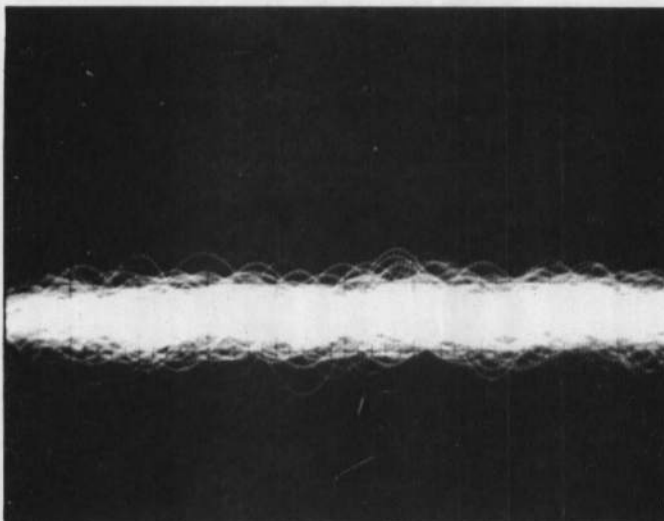




250  $\mu$  V/cm  
No Flow Signal

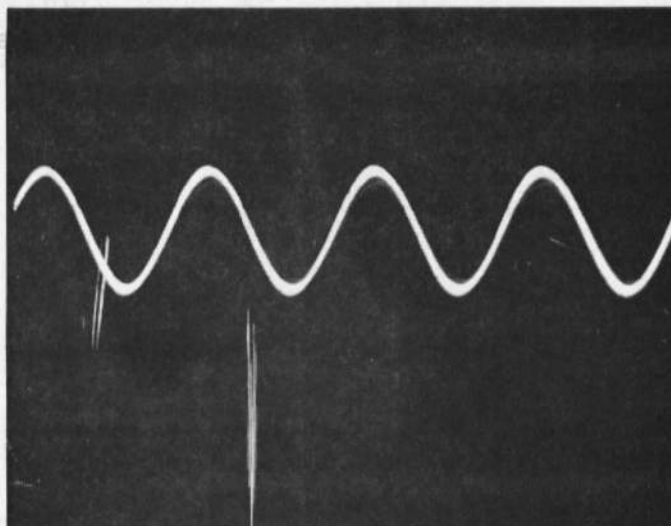


500  $\mu$  V/cm  
Flow Signal

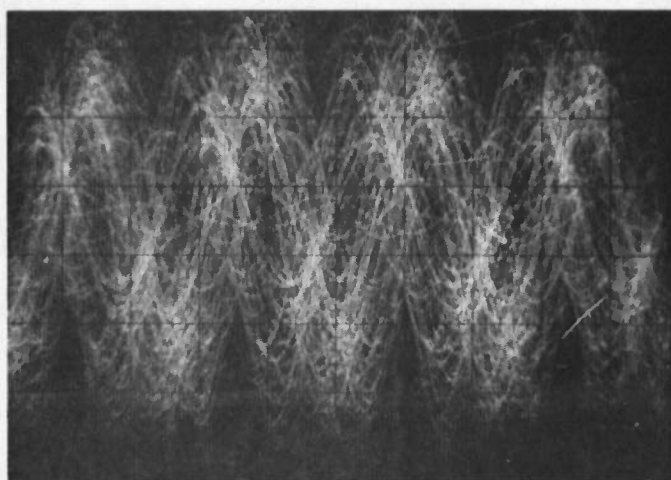


50  $\mu$  V/cm  
Flow Noise

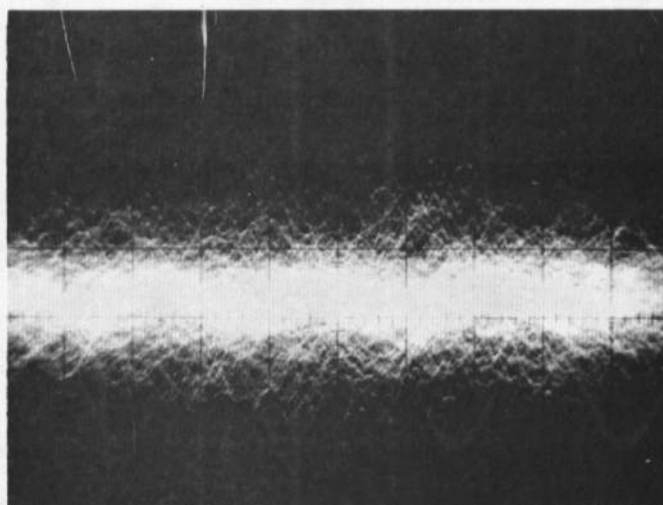
Fig. A. 4. 2.54 cm transducers - transmitter upstream by 7.62 cm from receiver (40 kHz).



250  $\mu$  V/cm  
No Flow Signal

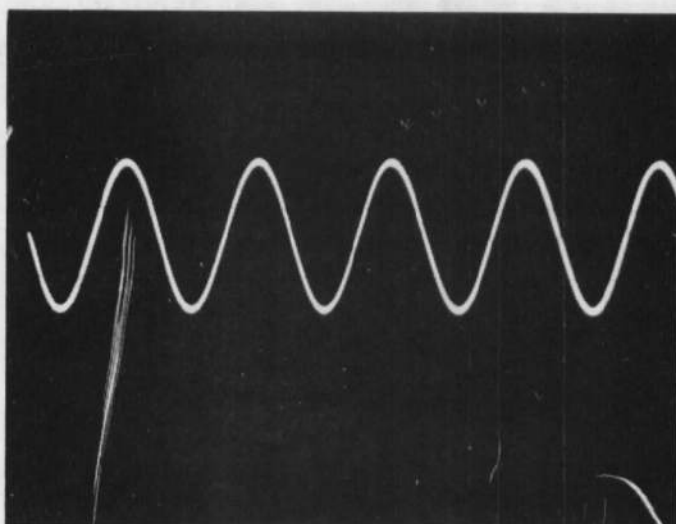


250  $\mu$  V/cm  
Flow Signal

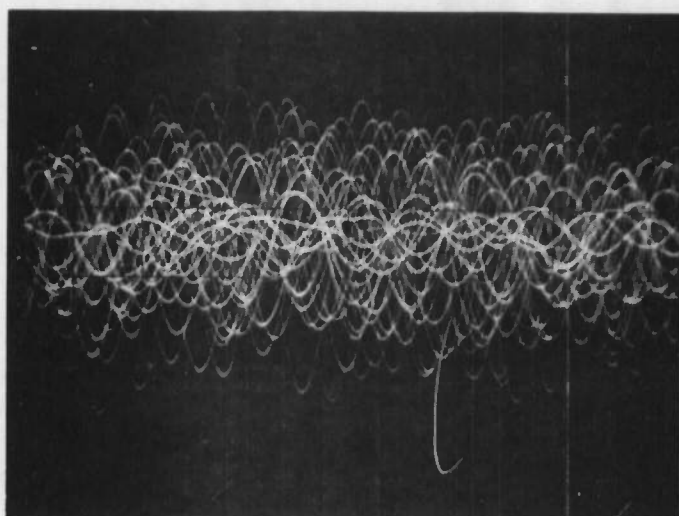


10  $\mu$  V/cm  
Flow Noise

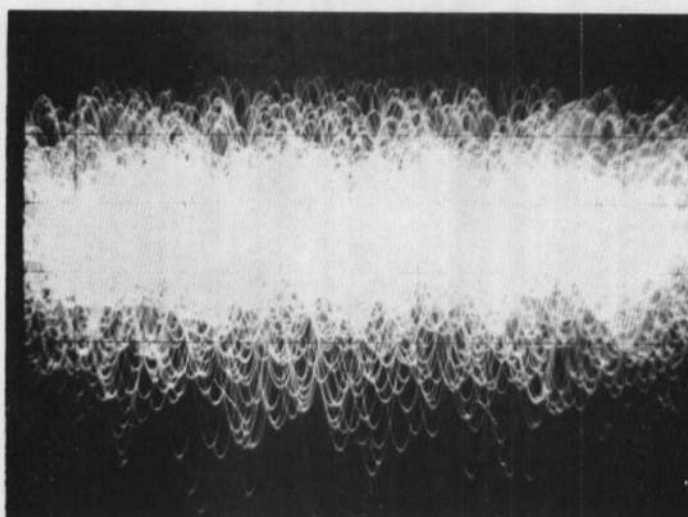
Fig. A. 5. 2.54 cm transducers - transmitter upstream by 7.62 cm from receiver (80 kHz).



25  $\mu$  V/cm  
No Flow Signal

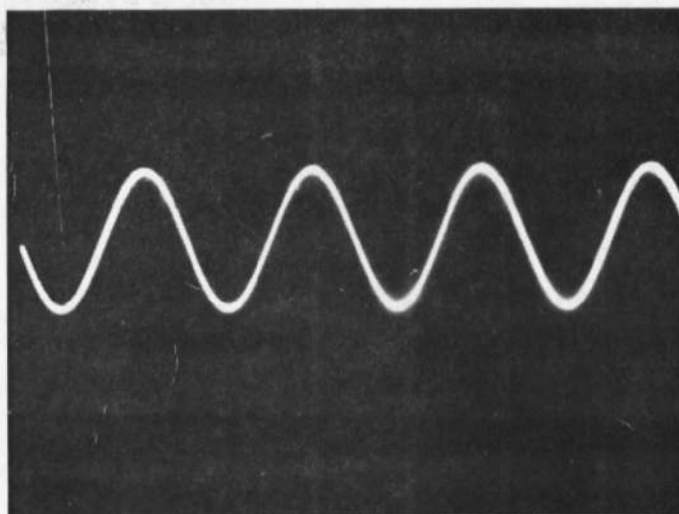


250  $\mu$  V/cm  
Flow Signal

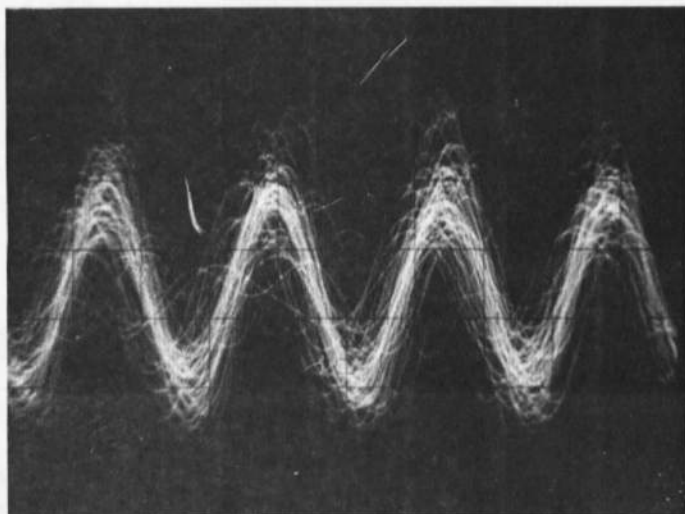


250  $\mu$  V/cm  
Flow Noise

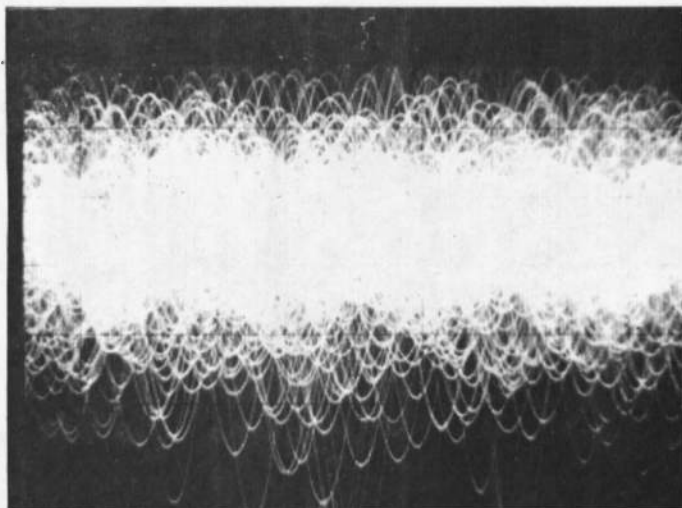
Fig. A. 6. 2.54 cm transducers - transmitter downstream by 7.62 cm from receiver (10 kHz).



250  $\mu$  V/cm  
No Flow Signal



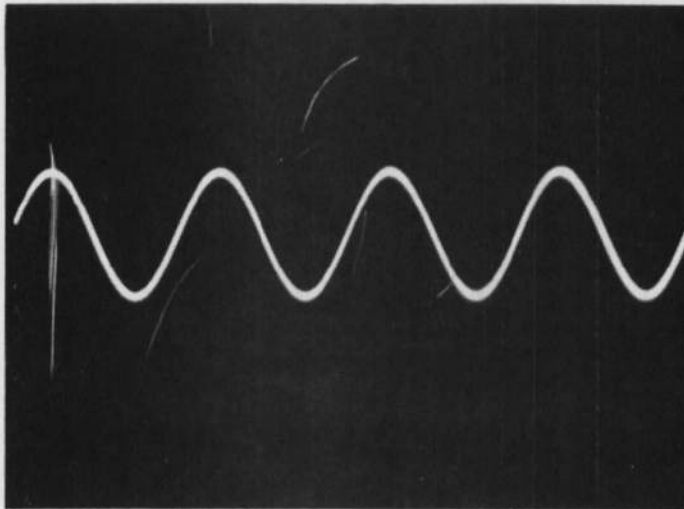
100  $\mu$  V/cm  
Flow Signal



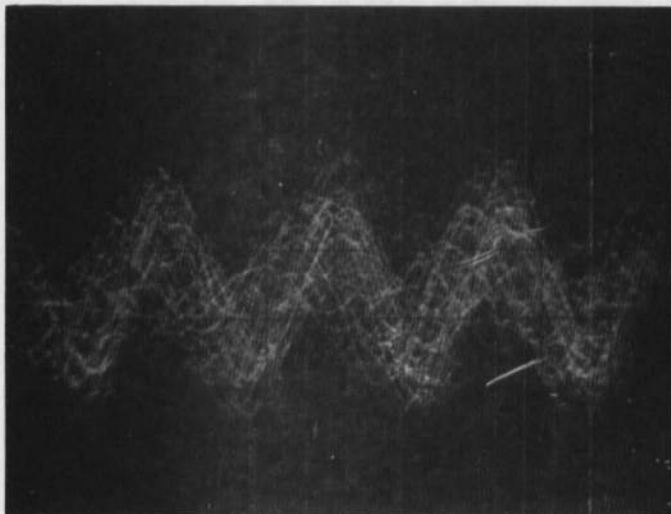
100  $\mu$  V/cm  
Flow Noise

Fig. A. 7. 2.54 cm transducers - transmitter downstream by 7.62 cm from receiver (20 kHz).

500  $\mu$ V/cm  
No Flow Signal



100  $\mu$ V/cm  
Flow Signal



100  $\mu$ V/cm  
Flow Noise

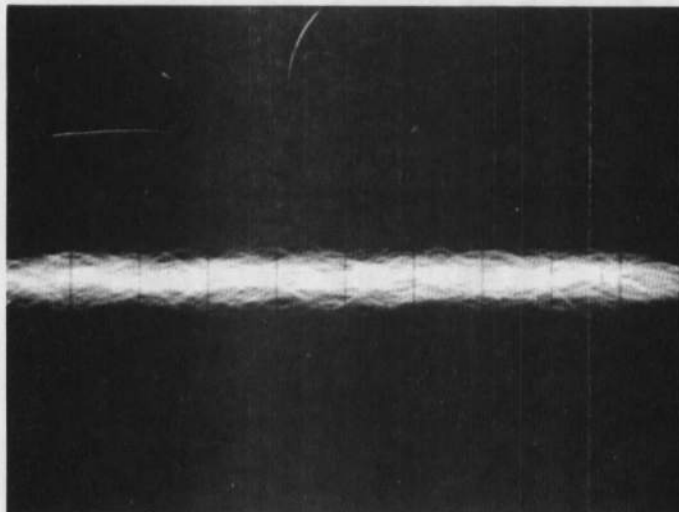
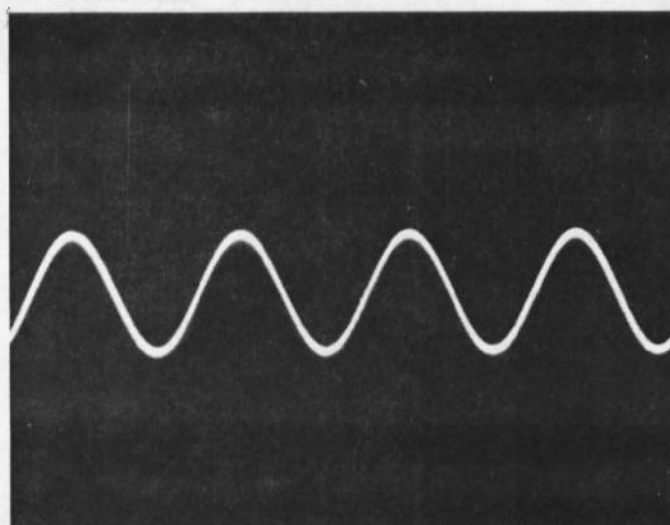
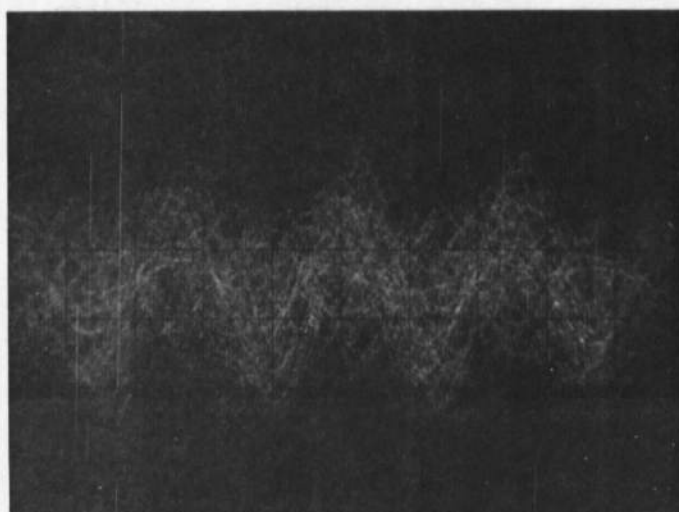


Fig. A. 8. 2.54 cm transducers - transmitter downstream by 7.62 cm from receiver (40 kHz).

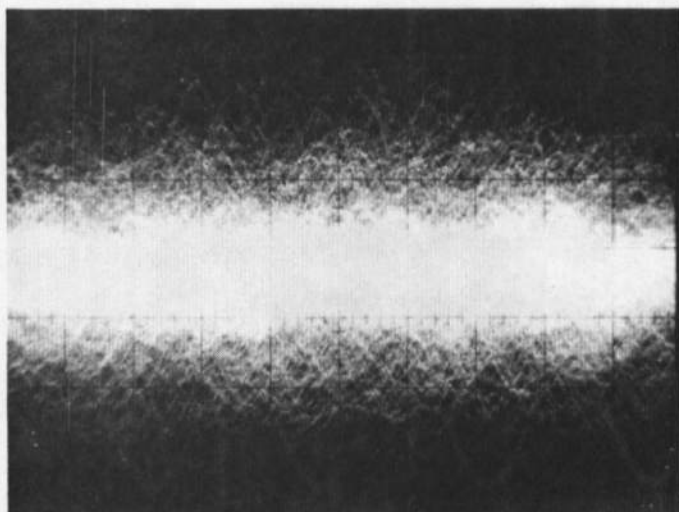




500  $\mu$  V/cm  
No Flow Signal

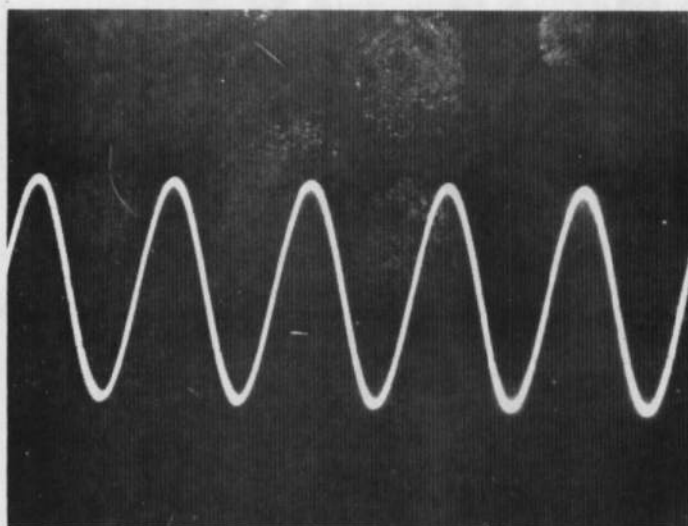


100  $\mu$  V/cm  
Flow Signal

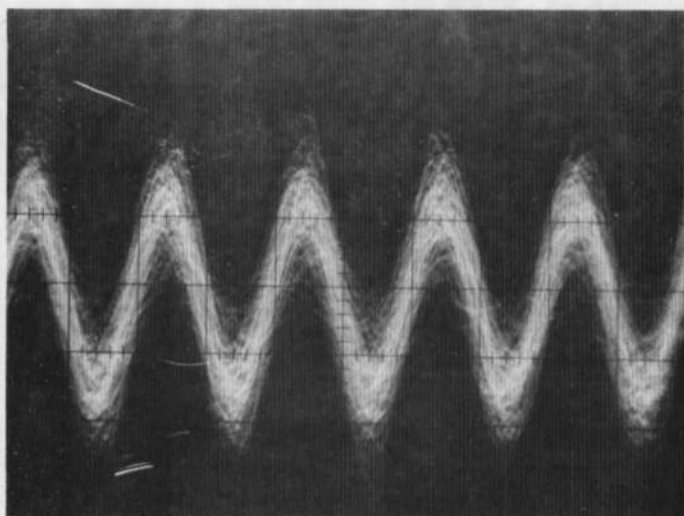


20  $\mu$  V/cm  
Flow Noise

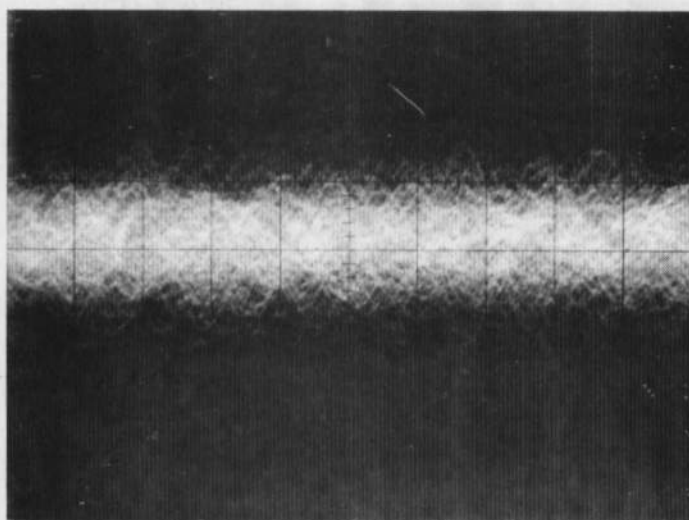
Fig. A. 9. 2.54 cm transducers - transmitter downstream by 7.62 cm from receiver (80 kHz).



5 mV/cm  
No Flow Signal

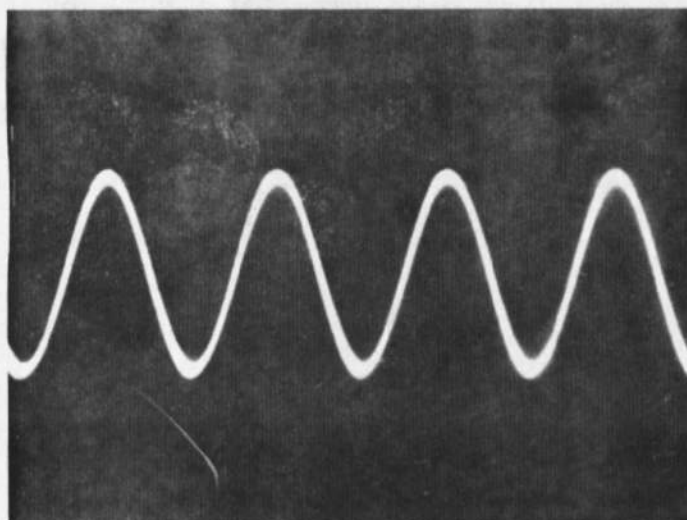


5 mV/cm  
Flow Signal

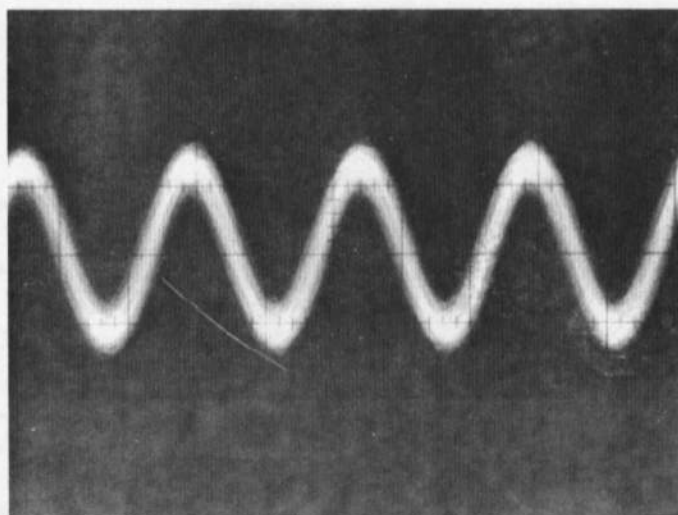


5 mV/cm  
Flow Noise

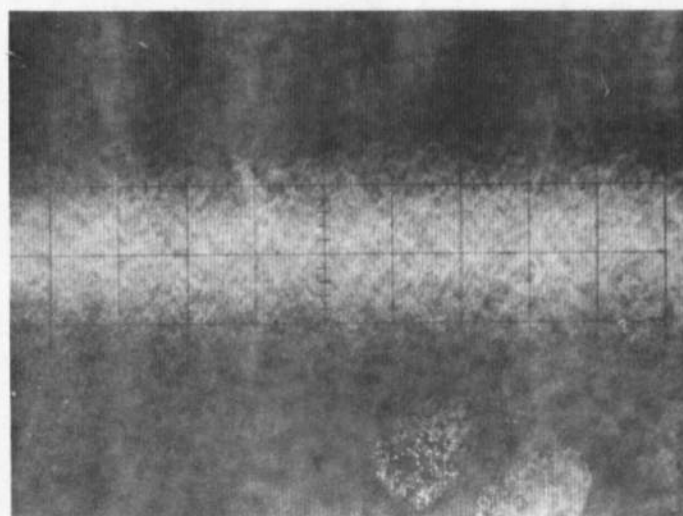
Fig. A.10. 6.35 cm transducers - transmitter upstream by 2.54 cm from receiver (10 kHz).



5 mV/cm  
No Flow Signal



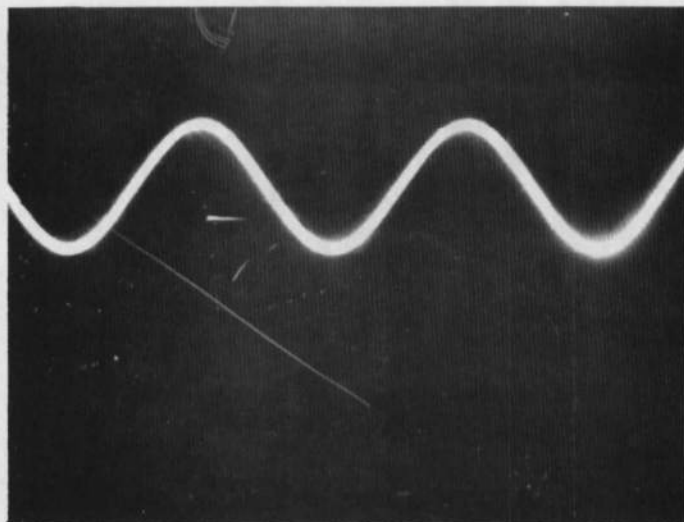
5 mV/cm  
Flow Signal



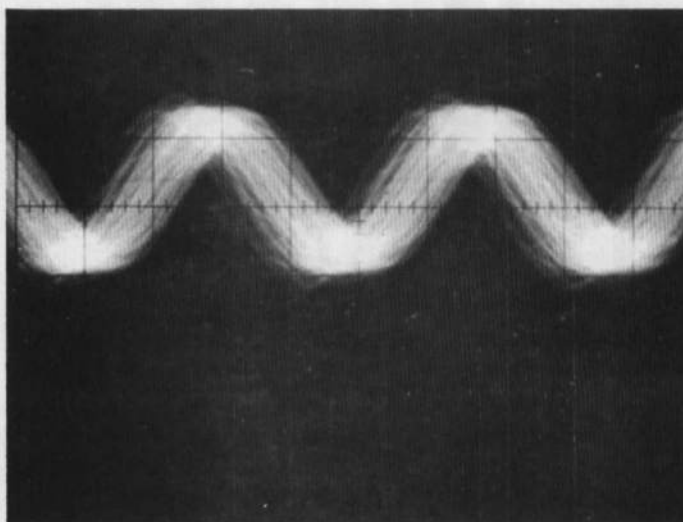
2 mV/cm  
Flow Noise

Fig. A.11. 6.35 cm transducers - transmitter upstream by 2.54 cm from receiver (20 kHz).

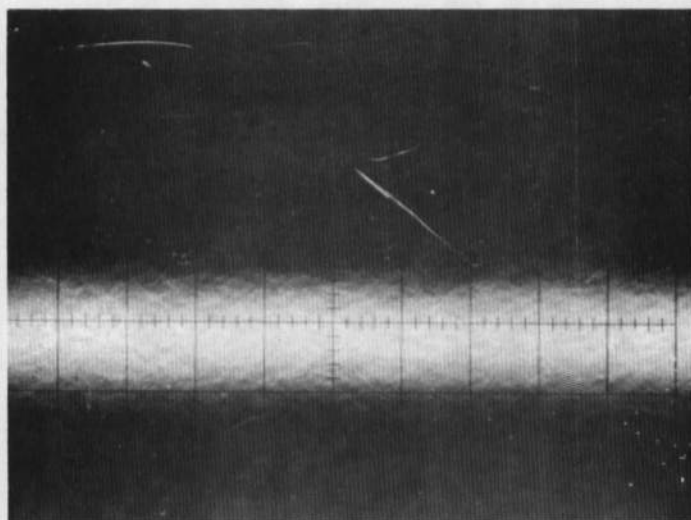




5 mV/cm  
No Flow Signal



5 mV/cm  
Flow Signal



1 mV/cm  
Flow Noise

Fig. A.12. 6.25 cm transducers - transmitter upstream by 2.54 cm from receiver (50 kHz).

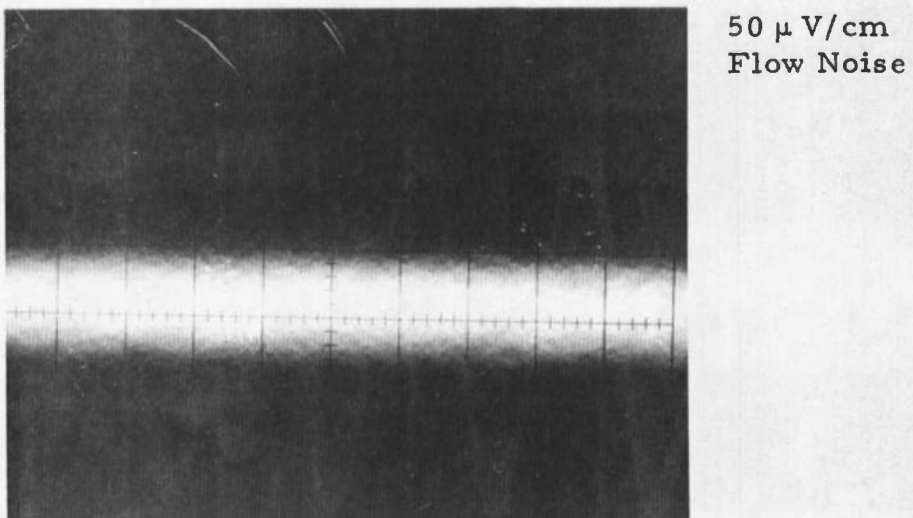
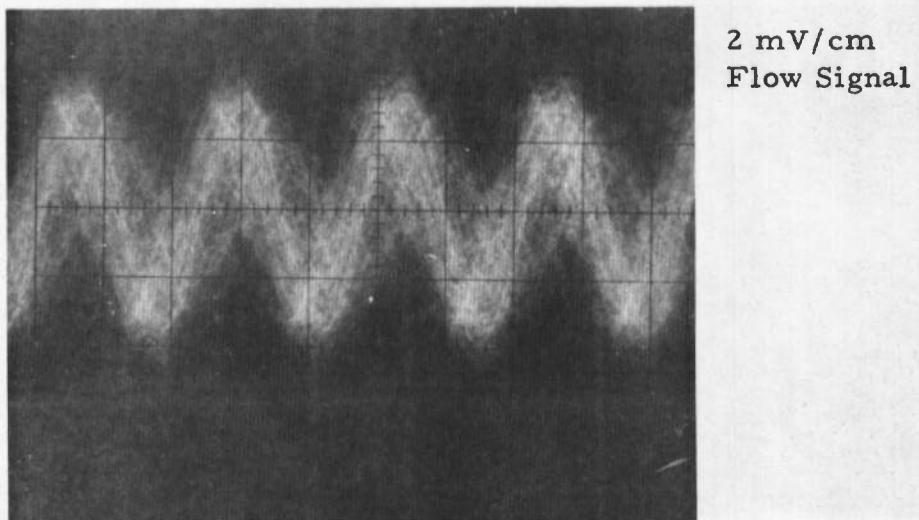
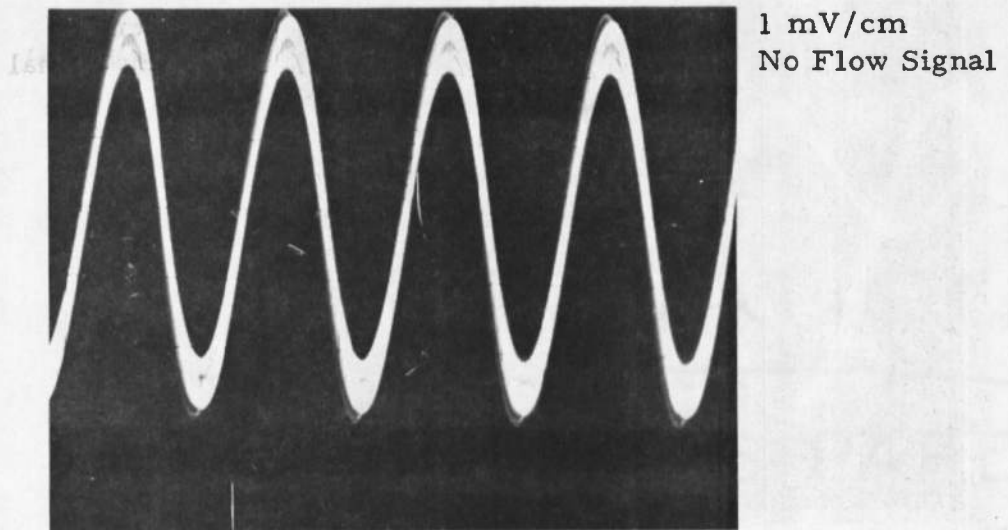
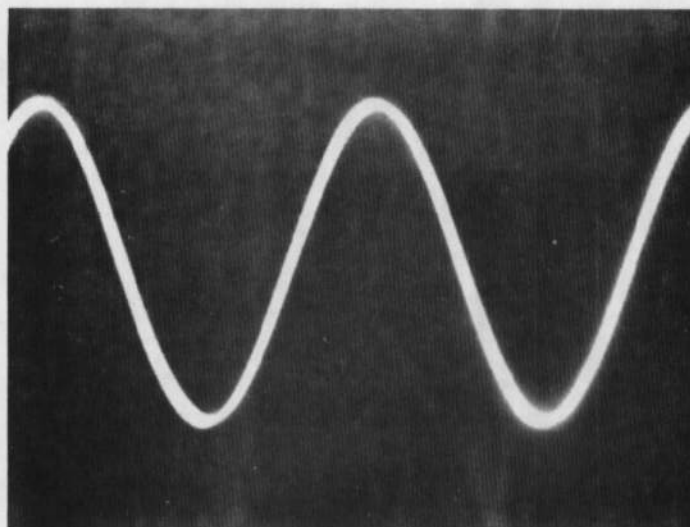
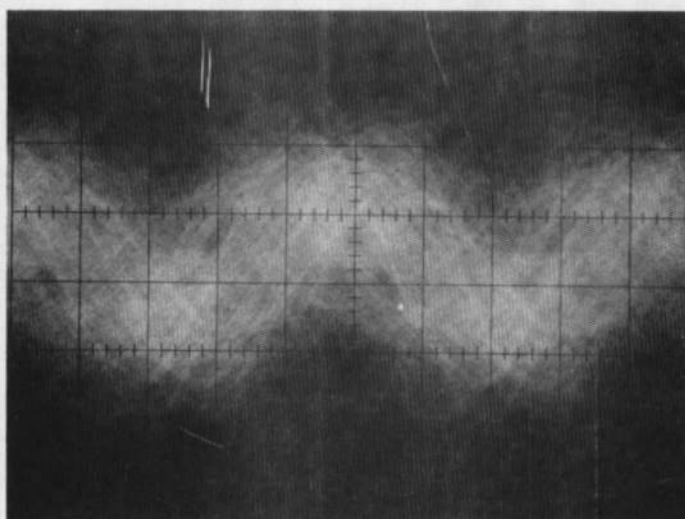


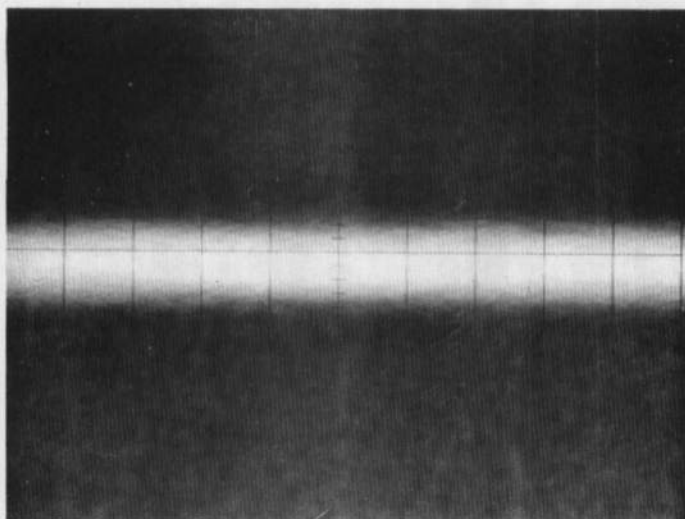
Fig. A.13. 6.25 cm transducers - transmitter upstream by 2.54 cm from receiver (82.2 kHz).



2 mV/cm  
No Flow Signal

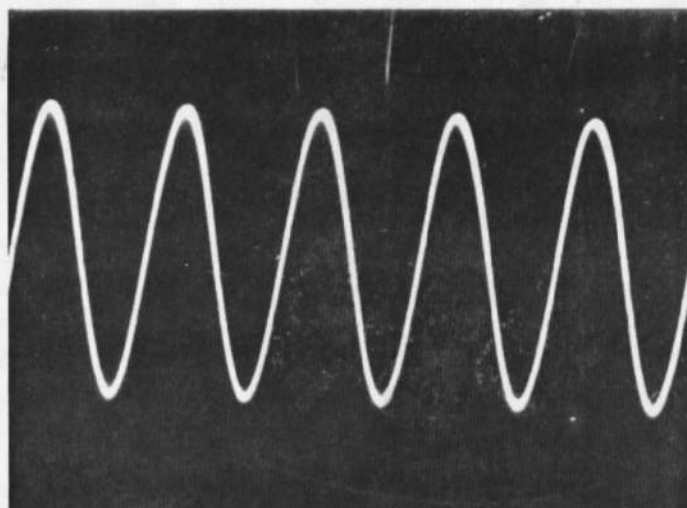


2 mV/cm  
Flow Signal

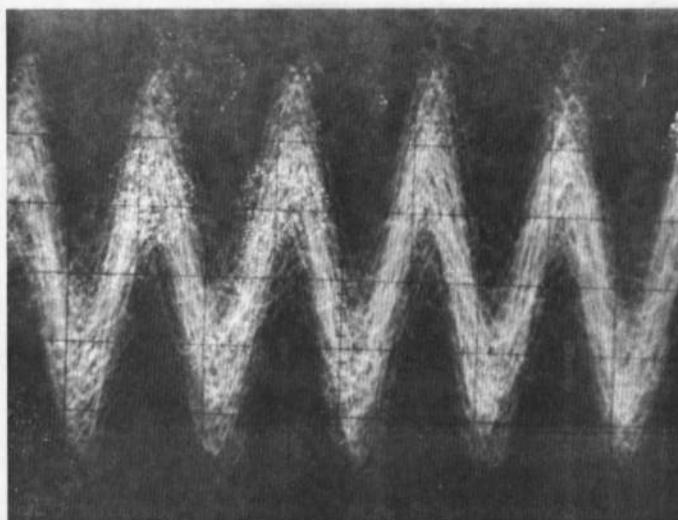


50  $\mu$ V/cm  
Flow Noise

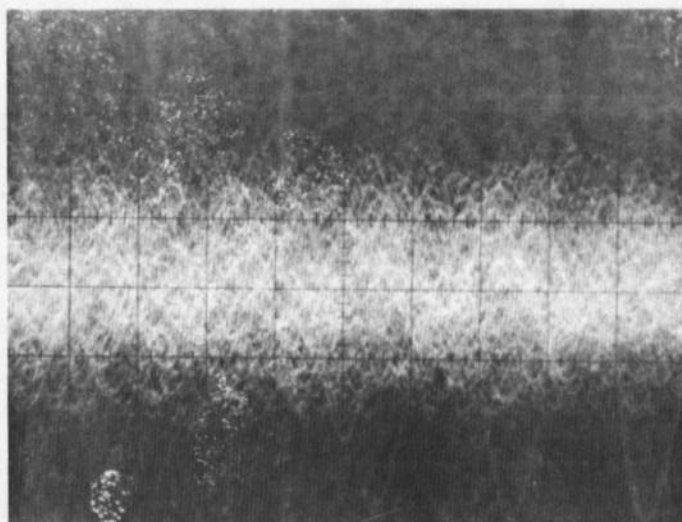
Fig. A.14. 6.25 cm transducers - transmitter upstream by 2.54 cm from receiver (99.4 kHz).



5 mV/cm  
No Flow Signal

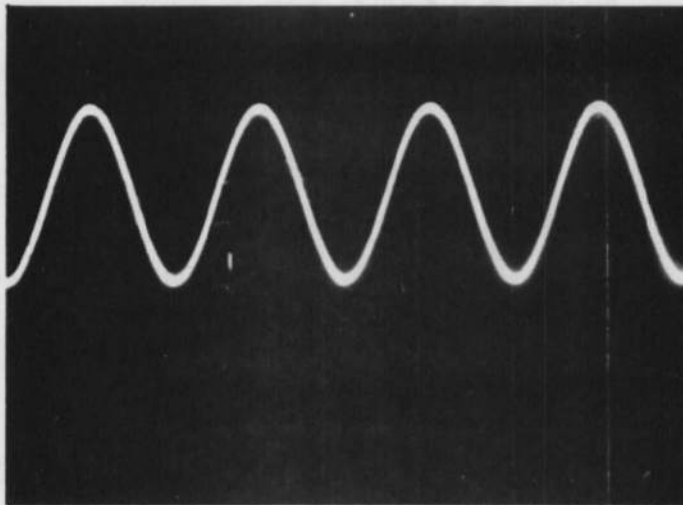


5 mV/cm  
Flow Signal

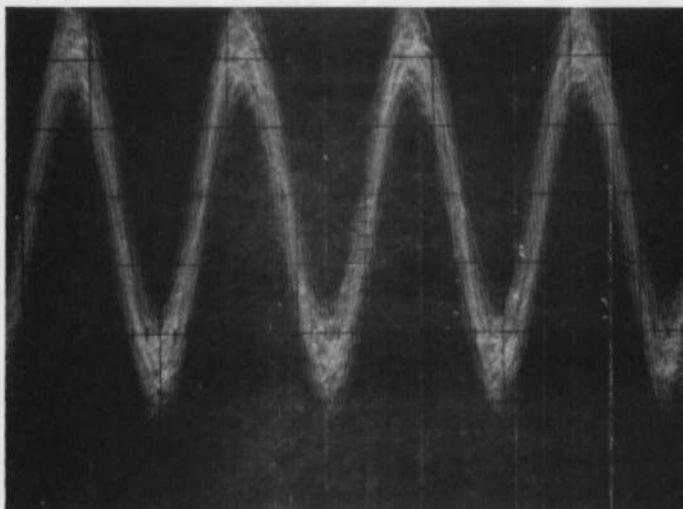


5 mV/cm  
Flow Noise

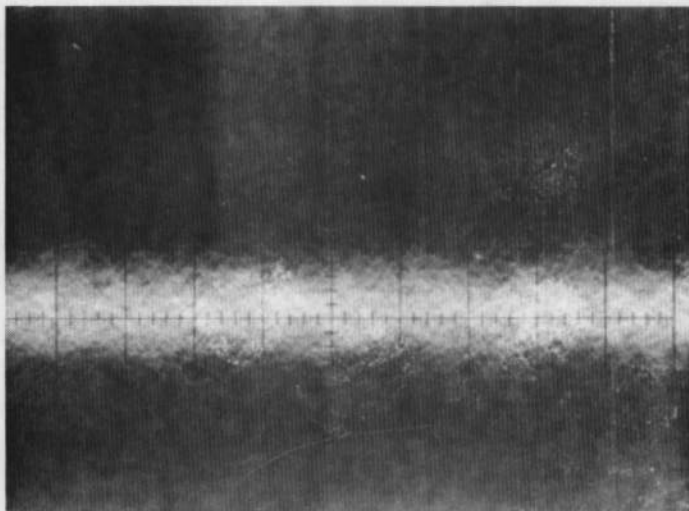
Fig. A.15. 6.25 cm transducers - transmitter downstream by 2.54 cm from receiver (10 kHz).



10 mV/cm  
No Flow Signal



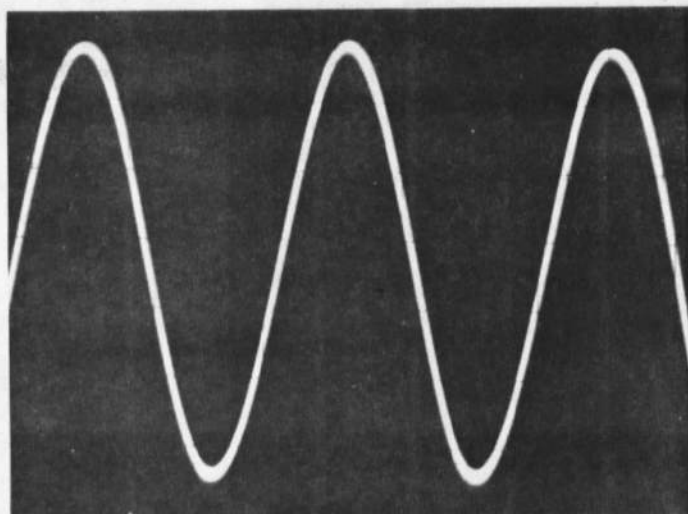
10 mV/cm  
Flow Signal



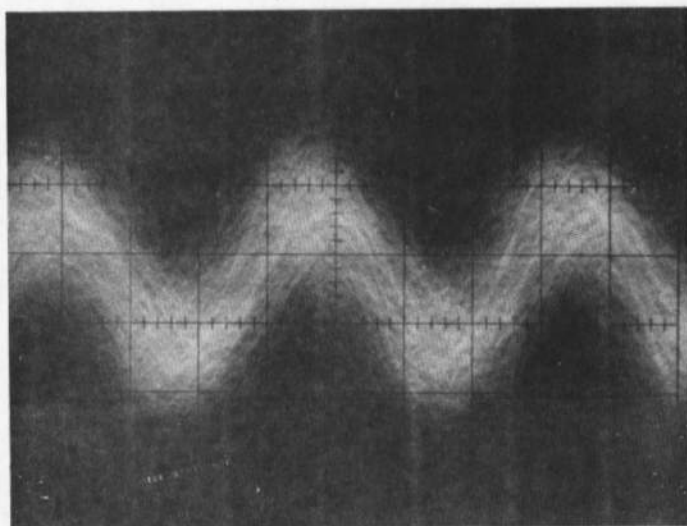
1 mV/cm  
Flow Noise

Fig. A.16. 6.25 cm transducers - transmitter downstream by 2.54 cm from receiver (20 kHz).

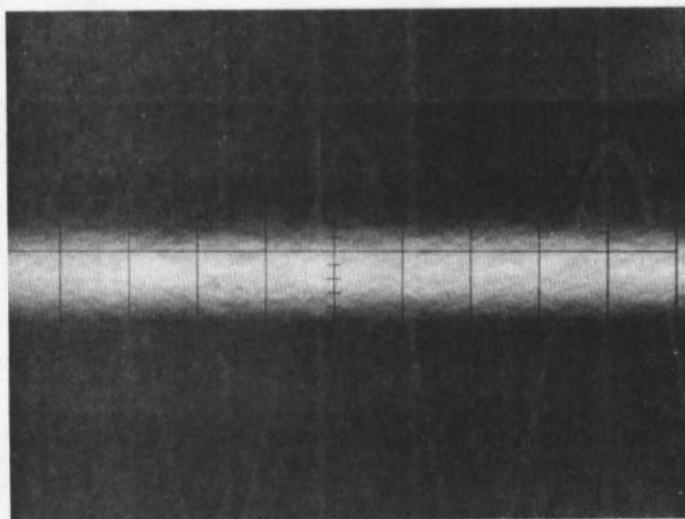




2 mV/cm  
No Flow Signal

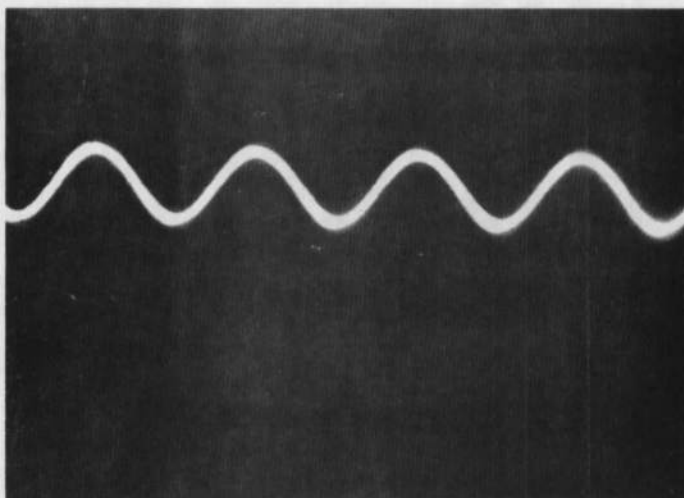


2 mV/cm  
Flow Signal

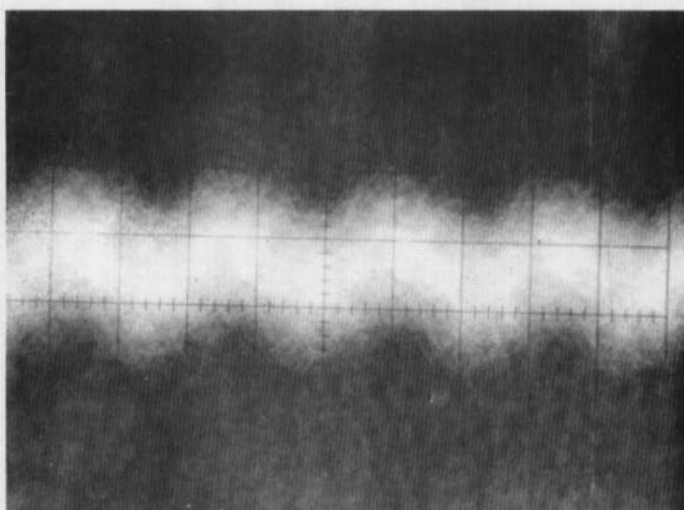


200  $\mu$ V/cm  
Flow Noise

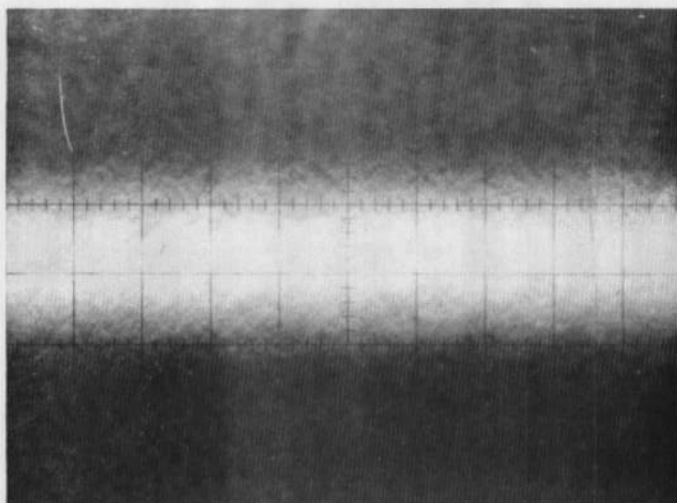
Fig. A.17. 6.25 cm transducers - transmitter downstream by 2.54 cm from receiver (50 kHz).



5 mV/cm  
No Flow Signal

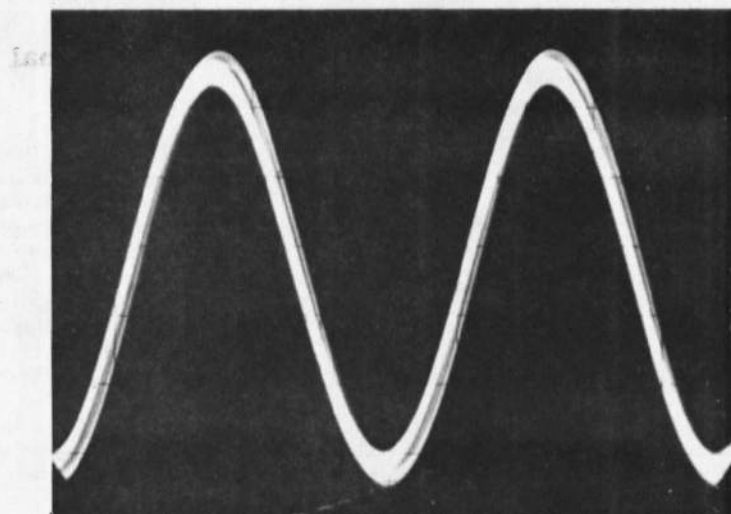


2 mV/cm  
Flow Signal

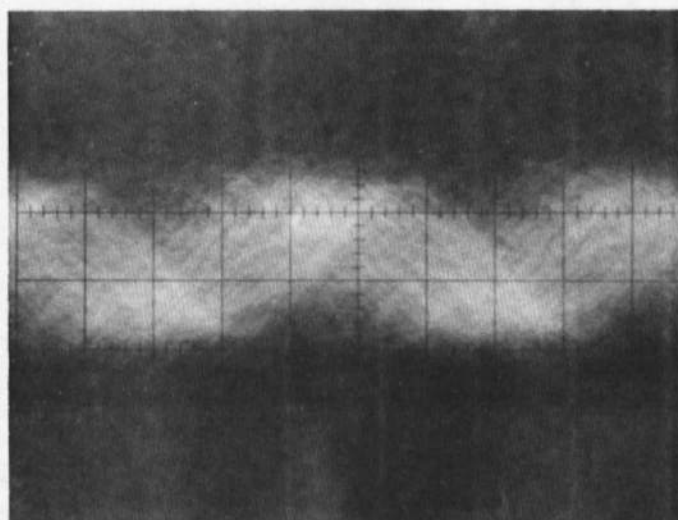


50  $\mu$ V/cm  
Flow Noise

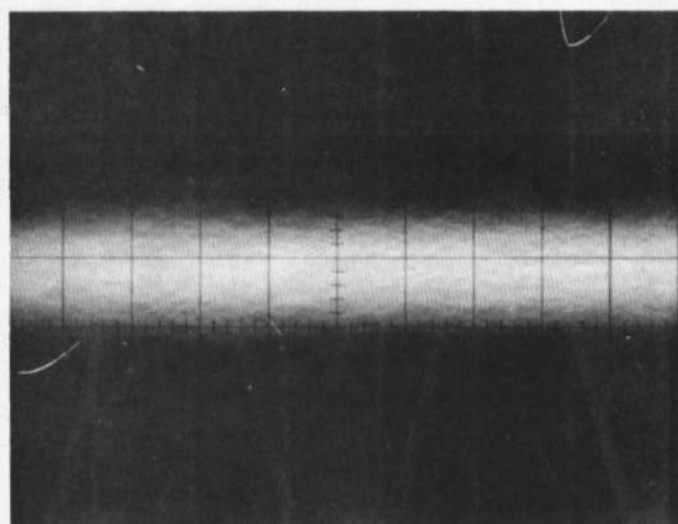
Fig. A.18. 6.25 cm transducers - transmitter downstream by 2.54 cm from receiver (82.1 kHz).



2 mV/cm  
No Flow Signal



2 mV/cm  
Flow Signal



50  $\mu$  V/cm  
Flow Noise

Fig. A. 19. 6.25 cm transducers - transmitter downstream by 2.54 cm from receiver (99.4 kHz).



## ULTRASONIC MASS FLOWMETER

L. C. Lynnworth and N. E. Pedersen  
Panametrics, Inc., Waltham, Massachusetts 02154

**ABSTRACT.** Development began on a new type of ultrasonic mass flowmeter for fuel flow in gas turbine engines. The fuel flowmeter consists of a flow velocimeter, densitometer, time intervalometer, and a metering section containing nonintrusive transducers. The velocimeter measures the phase difference between two coherent individually coded 5 MHz waves continuously transmitted obliquely upstream and downstream across a common path, yielding a phase difference proportional to  $v/c^2$ , where  $v$  = area-averaged flow velocity and  $c$  = sound speed. The densitometer consists of a stepped-diameter probe; the difference in echo amplitudes at the wetted end and at the dry step is a function of the acoustic impedance  $\rho c$  of the fuel where  $\rho$  is the fuel density. The time intervalometer measures the time  $T$  between two successive echoes, which time is proportional to  $1/c$ . The mass flow rate  $\dot{M}$  is  $\dot{M} = (K')(v/c^2)(\rho c)(1/T)$  where  $K'$  is a constant. The complete system was tested on various liquids at rates up to  $\sim 2300$  kg/hr. It was operated during and recalibrated after 104-hr exposure to a contaminated fluid flowing at  $\sim 860$  kg/hr. Response time was 20 ms. The flowmeter can operate in laminar, transitional and turbulent flow, and uses a novel method of weighting the profile. It is concluded that refinement of the present approach should be able to attain  $\dot{M}$  accuracy of 1%.

### Introduction

This paper is mainly concerned with the ultrasonic measurement of the mass flow rate of aviation fuels, presently for diagnostic purposes, and ultimately, for control purposes too. Those who are familiar with biomedical applications only may be surprised to hear that over 100 ultrasonic flowmeters have been used in industrial applications. Further, industrial test, measurement and control applications of ultrasonics cover over a dozen different parameters, with standard instruments available from many sources, some of which are listed in Table I.<sup>1,2</sup>

From the viewpoint of those responsible for diagnosing and controlling the performance of aircraft engines, it is important to know accurately the value of the fuel mass flow rate  $\dot{M}$ . The heating values of typical fuels such as JP-4, JP-5, Diesel fuel and Avgas grades from 80 to 145 octane are within about 1% of 19000 Btu/lb. Thus, the maximum power that can be extracted from these fuels is proportional to  $\dot{M}$ .

In engine diagnostic studies, one is interested in measuring engine performance from start-up, at relatively low flow rates of about 20 kg/hr, up to maximum running conditions where  $\dot{M} \approx 1000$  kg/hr in some engines. Thus, a range of  $\sim 50:1$  is of interest. Accuracy of better than 1% is desirable at high flow and  $\sim 5\%$  at the low end. For control, response times of  $\sim 10$ -30 ms are desired. Continuing to define the problem, the fuel composition may be an unknown mixture of two or more fuels. The fuel temperature may range between  $-55^\circ\text{C}$  to  $+70^\circ\text{C}$ . The fuel may be contaminated by iron oxide, sand and dirt particles having sizes up to 420  $\mu\text{m}$ , and by corrosive agents. The engine environment includes noise and vibration. The flowmeter measuring cell, nonintrusive transducers and electronics should be small, lightweight and rugged.

The main problem with previous (turbine) flowmeters has been clogging within ten hours under contaminated fuel flow. The present ultrasonic flowmeter employs recessed, nonintrusive transducers, and has

no rotating parts. Accordingly, it is not subject to clogging.

In the following, we describe a novel ultrasonic approach to this mass flowmetry problem, with consideration of the flow profile, and we summarize tests, results and conclusions based on this first year's work. A more complete account is available.<sup>3</sup>

### Ultrasonic Approach

In analyzing ultrasonic flow velocimeter approaches, one finds that a measurement of upstream minus downstream transit time (or phase) yields a term proportional to  $v/c^2$ , where  $v$  = flow velocity and  $c$  = sound speed, whereas a measurement of the difference between two frequencies which are reciprocals of these times responds to  $v$ , independent of  $c$ . Doppler shifts, however, are proportional to  $v/c$ . These outputs may be combined with fluid density ( $\rho$ ), characteristic impedance ( $\rho c$ ) and sound speed measurements to yield  $\dot{M}$ , the mass flow rate, as shown in Table II.

A two-frequency Doppler approach was selected at the beginning of this program, because at that time it appeared to offer, at least theoretically, the best way of measuring average flow velocity with minimum disturbance of simple pipelines. Calculations of the power scattered at 20 MHz from fuel contaminated according to MIL-E-5007C showed that scattering should be adequate even in fuels containing  $\sim 1\%$  of the specified contaminant. However, tests on uncontaminated liquid did not provide enough scatter to be detected with our equipment. Therefore we abandoned the Doppler approach and adopted a transmission approach. Interrogation was accomplished by transmitting a pair of 5 MHz continuous plane waves which ideally remain undistorted in the flowing liquid. These waves simultaneously traversed the same path, and sampled the entire cross section of flowing liquid such that  $v/c^2$  was determined. To separate upstream from downstream waves, each wave was phase-coded with a pseudo-random-noise code. We think this is the first such separation in an ultrasonic flowmeter.

Table I. Examples of industrial process control and quality control parameters and vendors of standard ultrasonic equipment for their measurement.

Parameter	Vendor
Flow . . . . .	Alma Instruments, Badger, Controlotronics, NUSonics, Saratoga Systems, Scarpa Labs, Tokyo Precision Instruments, Westinghouse.
Temperature . . . . .	J. Bell/Univ. of Aston (wire), Hewlett-Packard (quartz), Honeywell (fluidic), Panametrics (wire).
Pressure . . . . .	Columbia, Endevco, Kristal, PCB Piezotronics, Wallace & Tiernan.
Viscosity . . . . .	Bendix, Unipan Scientific Instruments.
Level . . . . .	Bindicator, Controlotronics, Delavan, Endress & Hauser, National Sonics, Raytheon.
Density . . . . .	ITT-Barton, National Sonics.
Thickness . . . . .	Automation Industries, Branson, Krautkramer, Magnaflux, Nortec, Panametrics.
Modulus . . . . .	Magnaflux, H. M. Morgan, Panametrics
Flaws . . . . .	See "Thickness"; and Holosonics, Shurtronics, Sonic Instruments, Tektran, Ultrasonoscope.
Fluids Composition . . .	NUSonics, Tracor.
Acoustic Emission . . .	Dunegan, Endevco, Nortec, Panametrics, Trodyne.
Leaks . . . . .	Dawe, Delcon (Hewlett-Packard).
Bubbles . . . . .	Vero Precision Engineering Ltd.

Table II. Comparison of output products of six combinations of continuous wave flow velocimeters and ultrasonic densitometers.

Densitometer	Reflection Coefficient	Resonant Frequency
Flow Velocimeter	( $\rho c$ )	( $\rho$ )
Doppler(v/c)	M	M/c
Phase Difference(v/c <sup>2</sup> )	M/c	M/c <sup>2</sup>
Frequency Difference(v)	Mc	M

To determine fuel density, we utilized the reflection of normally incident longitudinal wave pulses. At normal incidence the reflection coefficient for these plane waves depends only on the characteristic acoustic impedance of the adjacent media at the boundary. Since the fuel's characteristic impedance equals  $\rho c$ , if the probe's impedance  $Z_1$  is known, measurements of the reflection coefficient at the boundary, together with a measurement of sound speed  $c$  (or time interval  $T$ , where  $T$  is proportional to  $1/c$ ) enable one to determine the fuel density  $\rho$ . A separate transmission path normal to the fuel flow direction was utilized to measure a time interval  $T$ , which is inversely proportional to  $c$ , and independent of  $v$ . Combining these measurements, we have  $M = (K') (v/c^2) (\rho c) (1/T)$  where  $K'$  depends on the area of the cell's flow channel, and on the units of measure.

#### Reynolds Number and Flow Profile

If one interrogates the fluid with a wave that averages over the diameter, but not over the whole area, one measures  $v_d = v_a/K$ , where  $K$  is less than unity and depends on the Reynolds number  $Re$ . The diameter-averaged flow velocity  $v_d$  is larger than the area-averaged value  $v_a$  by 25% for laminar flow ( $Re < 2000$ ).  $K = 0.881 + 0.011 \log_{10} Re$  for turbulent flow for  $Re \geq 10^4$ . Fractional differences  $(v_d - v_a)/v_d = 1 - K$  are listed in Table III as functions of  $Re$ .

In many industrial situations, where flow is turbulent, temperature and composition of the process fluid are sufficiently constant so that Reynolds number can be estimated from  $v_a$ . Since  $K$  is relatively

Table III. Potential errors due to flow profile.<sup>1</sup>

Re	$< 2 \times 10^3$	$10^4$	$10^5$	$10^6$	$10^7$
K	.750	.925	.936	.947	.958
1-K	25%	7.5%	6.4%	5.3%	4.2%

insensitive to  $Re$ , the estimated  $Re$  is sufficient to determine  $K$  to a small fraction of 1%, which means  $v_a$  can be determined to that accuracy too. In our case, however, the combination of unknown fuel mixtures and wide temperature range prevent one from determining  $K$  to less than 1% from measurements of  $v_d$  alone. Can one measure  $v_a$  directly? Yes, provided one properly weights the entire flowing cross section. To a good approximation, it appears that one way this condition is met is by using a square flow channel, interrogated obliquely in the near field of a rectangularly-collimated transducer (Fig. 1a, b).

#### Flow Velocimeter - CW Phase Measurement

Similar to previous ultrasonic transmission flowmeters, the system to be described measures the phase difference between waves transmitted upstream and downstream. The two cw waves traverse virtually the same path at virtually the same time. The two waves have the same carrier frequency, yet can be separated, or identified, by the manner in which they are each modulated and then demodulated.

In Fig. 2, a 5 MHz crystal controlled oscillator signal is divided into two isolated channels. The waves in the upper and lower channels are phase coded by means of a dual coherent pseudo-random-noise code generator, producing a sequence of 1's and 0's such that the resulting code displays all the characteristics of perfect randomness. The length of the code, as well as the clock rate are arbitrarily variable. Each "1" produces a  $+90^\circ$  phase shift of the carrier, while each "0" produces a  $-90^\circ$  phase shift. The codes in the upper and lower channels are different. These pseudo-random sequences are orthogonal. The two 5 MHz waves are independently phase code modulated ( $C_1$  and  $C_2$ ) by the DBM's at the left. These are then fed, via circulators, to the

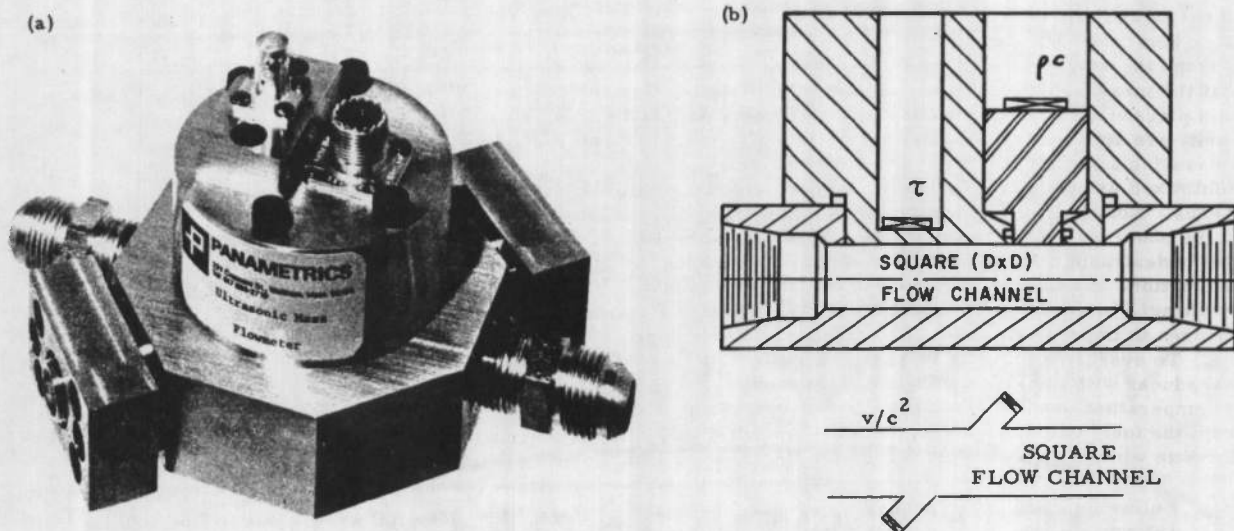


Fig. 1 (a) Ultrasonic mass flowmeter measuring cell; (b) Transducer locations.

two transducers. The received waves are fed (via the circulators) to the top and bottom DBM's on the right. The demodulating codes,  $C_{2d}$  and  $C_{1d}$  are also fed to these DBM's. The outputs of the DBM's are two cw signals, as well as wide band noise. The "noise" results from noncorrelation of unwanted signals from either the wrong channel or from stray reflections and reverberations within the pipe. Only that wave which is due to a reverberation-free straight-through-transmission results in a cw wave at the demodulator DBM's. We next go through a pair of tuned 5 MHz amplifiers which strip off most of the uncorrelated information, and finally feed into a pair of phase-locked loops.

Instead of phase-locked loops we used a standard phase meter. Another simplification involved using just one code for both directions.

#### Tests on Fuel and Contaminated Fluid

The main purpose of these tests, conducted at Avco-Lycoming between June and August 1972, was to determine the accuracy, reproducibility and linearity of the ultrasonic mass flowmeter system, and to demonstrate operation on uncontaminated fuel such as JP-4 and JP-5 as well as on a fluid contaminated in accordance with MIL-E-5007C. Response time was not determined in these tests, but was calculated from the system bandwidth to be 20 ms.

Test data for four successive runs in JP-5 are plotted in Fig. 3. These data exhibit linearity over the range indicated. Significantly, for 3 of 4 runs, the data are within  $\pm 4\%$  of one straight line. Disregarding the anomalous fourth run, these data are quite encouraging, in that they demonstrate the basic

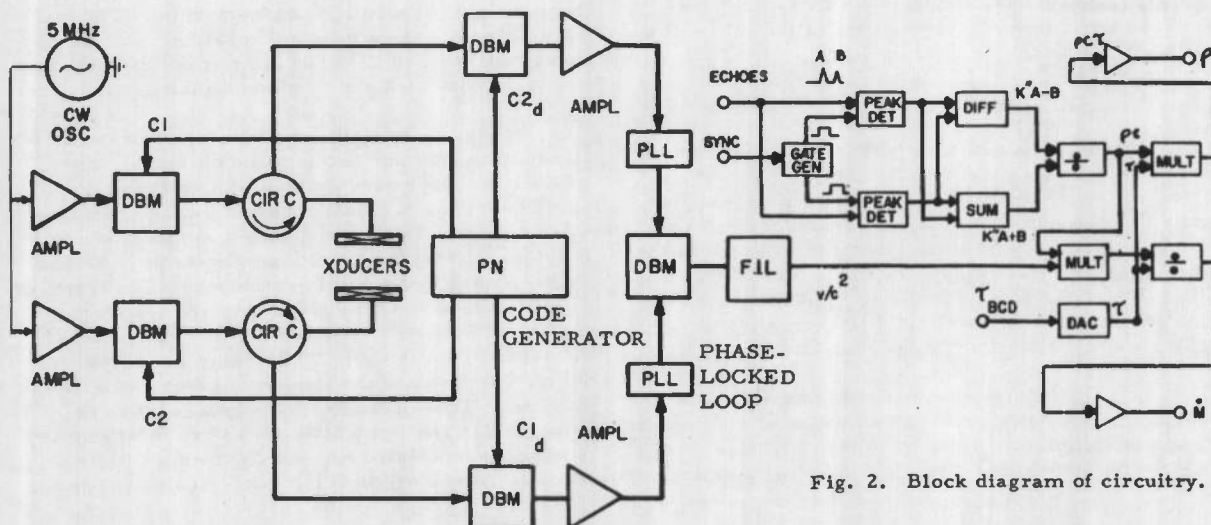


Fig. 2. Block diagram of circuitry.

linearity and reproducibility of the  $\dot{M}$  system. In a later test on JP-5, where  $\dot{M}$  ranged to  $\sim 2300$  kg/hr, (beyond the range of the present multiplier), we found that the measured phase angle could be approximated as a piecewise linear function. Departures from linearity are apparently due mainly to eddies in the measuring zone. It is expected that these can be minimized using a window, wedge, screen or other means. Nonideal inlet conditions may also contribute to the observed nonlinearity. Another deficiency was that undesirable circuit unbalances were produced by fluctuations in fuel temperature of a few degrees, or by changes in the acoustic radiation impedance due to changes in impedance of the fuel or transducer backing. To overcome this problem, one should choose a transducer with minimal variation in properties due to temperature, and should isolate the transducer from the fuel, using, for example, an attenuating acoustic window as a pad.

Following JP-4 and JP-5 tests, the cell (Fig. 1a) was operated with a contaminated fluid. Exposure totaled 104 hrs at  $\sim 860$  kg/hr, plus 16 hrs of filtered contaminant at this rate, plus soaks at no-flow totaling 428 hrs. Signal levels degraded somewhat during these tests, but not due to any fundamental deficiency. Endurance appears to be far in excess of the two 2.5-hour tests required for instruments in MIL-F-3615. The complete system was then retested on JP-4 at  $25^\circ\text{C}$  and  $33^\circ\text{C}$ , and again did not exhibit deficiencies attributable to the contaminant. Due to accuracy limitations of the phase meter available for these tests, performance of the flowmeter was correspondingly limited. However, phase meters are now available which should reduce this source of errors to less than 0.5% of range, and possibly to 0.25%. Assuming comparable accuracy for the densitometer, a system accuracy of 1% or better for  $\dot{M}$  appears attainable.

### Conclusions

- A pseudo-random-noise phase coding technique has been demonstrated which separates two continuous ultrasonic waves of the same frequency transmitted upstream and downstream over a common path. This technique provided a flow velocimeter

response time of 20 ms, a factor of 25 faster than the contractual objective of 0.5 s, and a range up to  $\sim 2300$  kg/hr.

- The ultrasonic mass flowmeter measuring cell has been demonstrated to operate without clogging, both during and after exposure to a fluid contaminated essentially in conformance to MIL-E-5007C. This exposure included over 100 hr at  $\sim 860$  kg/hr and over 400 hr soaking at zero flow.
- Immunity to uncertainties in Reynolds number or flow profiles appears achievable using the square flow channel wherein 100% of the fuel cross section is interrogated by a rectangular plane wave beam of ultrasound. This is the basis for accurate, linear response to flow velocity, independent of fuel composition, temperature, density or viscosity. In the present measuring cell, the observed departures from linearity appear to be due to nonideal inlet conditions, probably correctable with a flow straightener, and to eddies at the measuring region, probably correctable with flush-mounted acoustic windows, wedges, screens or other means.
- Based on the encouraging first results obtained with coded single fixed frequency waves, it appears that the use of two variable frequencies should work too, to measure  $v$  independent of  $c$ . This is the basis for an improved ultrasonic mass flowmeter, where both  $v$  and  $\rho$  are each measured independent of  $c$ . The product of their outputs is thus proportional to  $\dot{M}$ . Accuracies of 1% of range appear achievable.

### References

1. L. C. Lynnworth et al., Proc. First ISA Symposium on Flow, Pittsburgh (May 1971); J. L. McShane, *ibid*.
2. L. C. Lynnworth, Proc. 7th Int'l. Congress on Acoustics 4, 525-528, Akademiai Kiado, Budapest (August 1971).
3. L. C. Lynnworth, N. E. Pedersen and E. H. Carnevale, Ultrasonic Mass Flowmeter System, Final Rpt, Contract DAAJ02-71-C-0061 (1972).

### Acknowledgments

The authors gratefully acknowledge contributions from E. H. Carnevale, G. M. Elfbaum, K. A. Fowler, E. P. Papadakis, J. Bradshaw and R. Morris of Panametrics, J. L. DuBois and P. R. Kranz of Dytron, and J. L. Black, J. Balcher and R. Hohenberg of Avco-Lycoming. The encouragement and support of G. W. Hogg, S. B. Poteate, R. Hunthausen and others at USAAVLABS, Eustis Directorate, is sincerely appreciated.

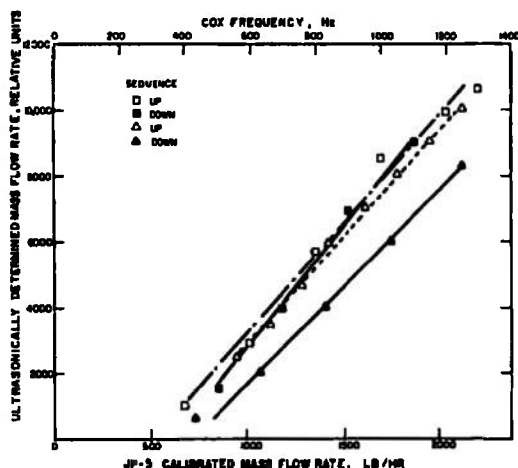


Fig. 3. Test results in JP-5.

Copyright by and reprinted with permission from the 1972 Ultrasonics Symposium IEEE Proceedings.

# ULTRASONICS SYMPOSIUM

## NONINTRUSIVE DYNAMIC FLOWMETER

N. E. Pedersen and L. C. Lynnworth  
Panametrics, Inc., Waltham, Massachusetts 02154

**ABSTRACT.** An ultrasonic dynamic flowmeter which combines nonintrusiveness, fast response, high accuracy and high resolution, was designed for use with cryogenic liquids and water. The flowmeter was designed to measure to 1% accuracy, the dynamic (1 to 100 Hz) as well as the steady flow velocity, averaged over the pipe area. The non-intrusive requirement is satisfied by using the vertically polarized component of obliquely incident shear waves, generated by transducers mounted outside the conduit. Compared to obliquely incident longitudinal waves, the choice of obliquely incident shear waves typically doubles the solid/liquid energy transmission coefficient, and doubles the refracted angle in the liquid. Calculations showed that one path was sufficient to obtain the area-averaged measurement of dynamic flow velocity to 1% accuracy. The electronic measuring system employs two different frequencies, each near 1 MHz. These frequencies are transmitted continuously, one upstream and the other downstream, over a common path. The frequencies are servoed such that the phase in each direction is maintained constant. By means of subtracting the two voltages corresponding to the two frequency deviations, an output signal is produced which is proportional only to fluid velocity and is independent of variations in sound speed.

### Introduction

According to references 1 and 2, many liquid-propellant rocket vehicles have experienced longitudinal vibration because of an instability arising from interaction of the vehicle structure with the propulsion system. The vibrations, nicknamed "pogo" after the jumping stick, have occurred principally in the first longitudinal structural mode during operation of the first liquid-propellant stage of a launch vehicle. Figure 1 illustrates a generalized representation of the effects of a typical instability. The vibration begins spontaneously, intensifies, and then dies away - typically in a period of 10 to 40 seconds. The frequency of vibration tracks that of the first structural mode. The frequency increases as propellant decreases. Less often, pogo vibrations have occurred in higher modes of longitudinal vibration, also, multiple periods of instability, each involving a different mode of vibration, have occurred during operation of a single vehicle stage. Vibrations have occurred in the frequency range of 5 to 60 Hz, with vibration amplitudes (zero to peak) as high as 17 g's at the input to payloads and 34 g's at an engine.

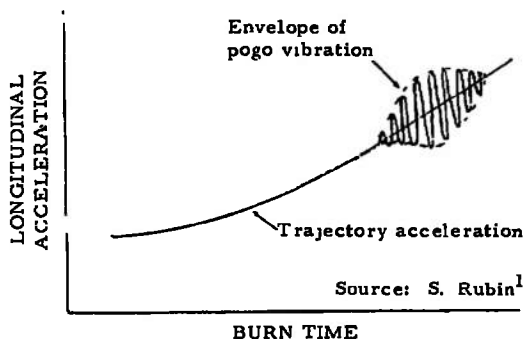


Fig. 1. Typical occurrence of pogo vibration.

1973 Ultrasonics Symposium Proceedings,  
IEEE Cat #73 CHO 807-8SU.

The brief account given below presents the ultrasonic and electronic main design considerations. Details are available in another report, NASA CR-112313.<sup>3</sup>

### Principal Design Requirements (LOX Region 1)

1. Nonintrusive - no measurable perturbation of flow profile by transducers.
2. Frequency response: 1 to 100 Hz.
3. Accuracy: errors <1% for area-average.
4. Resolution: 1% of oscillatory flow component, or 3 mm/s, whichever is greater (steady flow velocity  $\leq 5.5$  m/s).
5. Application: LOX,  $\sim 93$ K, 1.76 MN/m<sup>2</sup> ( $\sim 17$  atm), pipe ID = 30 cm.

### Transducer Mode and Orientation

In this section we consider the selection of the transducer vibration mode (longitudinal vs shear) and transducer orientation.

Refraction angles are readily computed from Snell's Law, provided sound speeds are known (Fig. 2). Historically, the problem of calculating sound energy transmission coefficients for solid/liquid interfaces and oblique incidence may be traced to Knott.<sup>4</sup> From the work of Firestone and Ling,<sup>5</sup> Mayer<sup>6</sup> and Garber,<sup>7</sup> it is seen that obliquely incident shear waves often, but not always, have an advantage regarding efficiency of energy transfer. In the cases cited, shear offers the transmission coefficient advantage at oblique incidence when the solid has a higher characteristic impedance than the liquid.

Using the Fortran IV G "ERRWAB" program listing provided to us as a courtesy by Garber and Union Carbide Corporation, Nuclear Division, Oak Ridge, we computed the energy ratios for LOX/aluminum and LOX/steel interfaces.



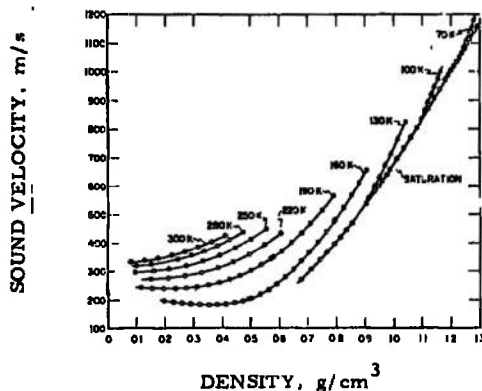


Fig. 2. Velocity of sound plotted against density for saturated liquid and compressed fluid oxygen, courtesy G. C. Straty and B. A. Younglove, NBS, J. Chem. Thermodynamics 5, 305 (1973).

For the present design purposes it is sufficient to plot transmission coefficients for an L wave incident from the liquid onto the solid (Fig. 3). One need only compare these energy curves to see that an incident shear mode would be coupled twice as efficiently as longitudinal. Further, comparing the LOX/pipe transmitted energy ratios for shear incident at  $60^\circ$ , the choice of aluminum over stainless steel yields an advantage of 4.3 dB per side. This advantage in signal, together with an observed "acoustic short circuit" noise advantage of over 20 dB, strongly favor the choice of an aluminum pipe over steel. (See also: LCL 1971 Patent #3,575,050.)

In the present design, it turned out to be convenient to separate the transmitter and receiver transducers on each side of the common path, as shown in Fig. 4. For oblique incidence, we again can make a comparison of shear versus longitudinal. Both modes share the advantage of avoiding the driving signal (except via stray capacitive pick-up) on the receiving transducer. However, if the shear wave elements are oriented at  $+45^\circ$  and  $-45^\circ$  to the plane of incidence, such that neighboring elements are vibrating orthogonally to one another, then theoretically there is no acoustic coupling between them.

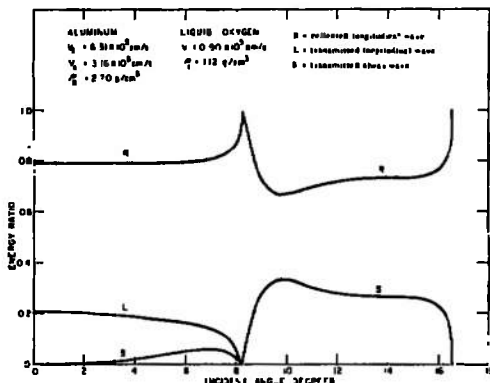


Fig. 3. LOX/aluminum energy coefficients.

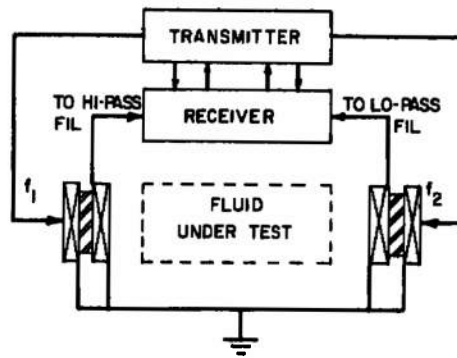


Fig. 4. Pair of orthogonally oriented shear wave transducers, on each side of fluid, may be coupled to fluid under test acoustically but separated electrically from each other by the sandwiched insulator.

#### Dynamic Flow Profile Analysis

The purpose of this analysis was to determine the value of the correction factor  $K$  required to convert an ultrasonic measurement averaged over a single path whose projection coincides with a diameter, to the desired area-averaged flow velocity. Thus,  $K v_{dia} = v_{area}$ . The analysis was conducted by Professor Forbes T. Brown of Lehigh University. While the "static  $K$ " is readily found in terms of Reynold's number to be about 0.95 at  $Re = 10^6$ , computation of the dynamic  $K$  is more complicated and depends on frequency.<sup>8</sup> For the Region 1 LOX conditions, and subject to assumptions stated in Ref. 3, it was found that  $K > 0.99$ , 1-100 Hz, and  $K > 0.995$  for 10-100 Hz. Thus, the dynamic profile is significantly flatter than the steady-state profile. Moreover the area-averaged dynamic flow velocity can be taken as  $0.995 v_{dia}$  with errors not exceeding 0.5%, over the dynamic frequency range of interest, 1-100 Hz.

#### Flow Cell Design

Based on electronic, ultrasonic and profile considerations, the cell design was configured as in Fig. 5. Measurements are made simultaneously over a common path. Four nonintrusive shear wave transducers are used, oriented  $\pm 45^\circ$  from the plane of incidence, with  $60^\circ$  angles of incidence obtained by the wedges.

#### Electronic System Design

To obtain a voltage output which is independent of sound speed but is proportional to fluid velocity, one can set the downstream and upstream phases equal to different integer constants:

$$\phi_1 = \frac{2\pi f_1 D}{\sin \theta} \frac{1}{c + v \cos \theta} = (2N-1) \frac{\pi}{2} \quad (1)$$

$$\phi_2 = \frac{2\pi f_2 D}{\sin \theta} \frac{1}{c - v \cos \theta} = (2M-1) \frac{\pi}{2} \quad (2)$$

Solving for  $f_1$  and  $f_2$ ,

$$f_1 = \frac{\sin \theta}{4 D} (2 N - 1) (c + v \cos \theta) \quad (3)$$

$$f_2 = \frac{\sin \theta}{4 D} (2 M - 1) (c - v \cos \theta). \quad (4)$$

The frequencies  $f_1$  and  $f_2$  are each composed of a fixed and variable component:

$$f_1 = f_{10} + F_1; f_2 = f_{20} + F_2, \quad (5)$$

where  $f_{10}$  and  $f_{20}$  are preset and fixed, and  $F_1$  and  $F_2$  are voltage controlled variables. This set of conditions is obtainable in a number of ways, e. g., through the use of a pair of Model 3100A Monsanto Digital Frequency Synthesizers. By means of the circuit of Fig. 6, the frequency  $F_1$  is controlled, via a first feedback loop, to maintain the condition given by Eq. (1), and the frequency  $F_2$  is controlled, via a second feedback loop, to maintain the condition given by Eq. (2).<sup>3</sup> We have, then:

$$F_1 = \frac{\sin \theta}{4 D} (2 N - 1) (c + v \cos \theta) - f_{10} \quad (6)$$

$$F_2 = \frac{\sin \theta}{4 D} (2 M - 1) (c - v \cos \theta) - f_{20}. \quad (7)$$

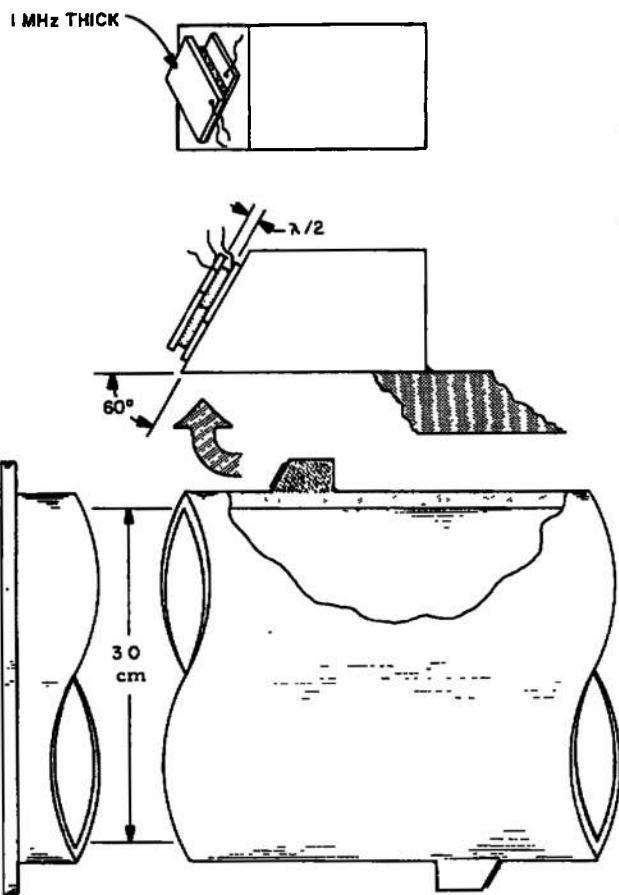


Fig. 5. Transducers mounted on pipe section.

The frequencies  $F_1$  and  $F_2$  are linearly proportional to their respective control voltages  $V_1$  and  $V_2$ , respectively. Thus  $F_1 = K_1 V_1$  and  $F_2 = K_2 V_2$ , where  $K_1$  and  $K_2$  are front panel adjustments on the Monsanto 3100A synthesizers. If we adjust the relationship between  $K_1$  and  $K_2$  such that  $K_2 = K_1 (2M-1)/(2N-1)$ , we can rewrite (6) and (7) in terms of  $V_1$  and  $V_2$ , respectively:

$$V_1 = \frac{1}{K_1} \frac{\sin \theta}{4 D} (2 N - 1) (c + v \cos \theta) - \frac{f_{10}}{K_1} \quad (8)$$

$$V_2 = \frac{1}{K_1} \frac{\sin \theta}{4 D} (2 N - 1) (c - v \cos \theta) - \frac{f_{20}}{K_1} \left( \frac{2 N - 1}{2 M - 1} \right). \quad (9)$$

Finally, subtracting (9) from (8), we obtain

$$(V_1 - V_2) = \frac{2 N - 1}{K_1} \frac{\sin \theta \cos \theta}{2 D} v - \frac{1}{K_1} \left[ f_{10} - \left( \frac{2 N - 1}{2 M - 1} \right) f_{20} \right] \quad (10)$$

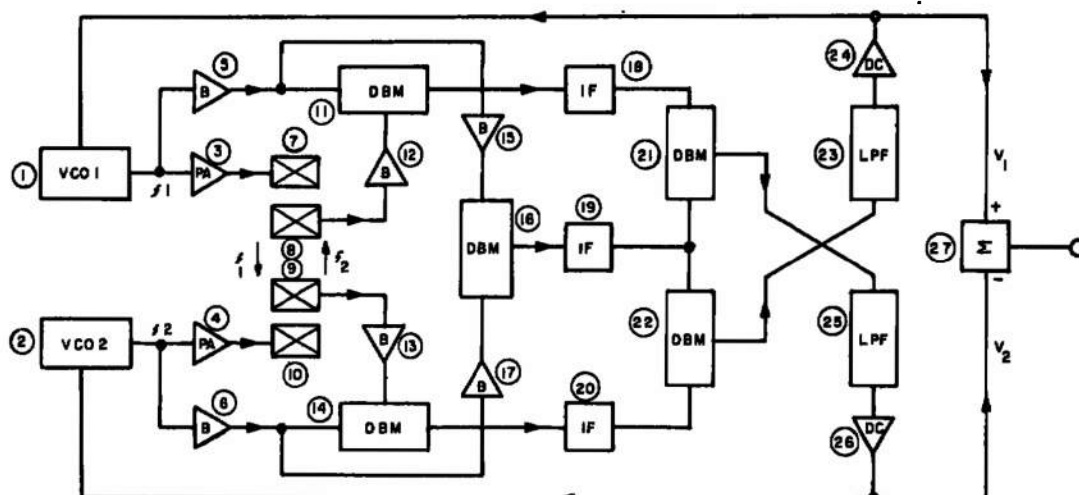
With regard to the term on the RHS of (10) we note that  $f_{10}$  and  $f_{20}$  are constants to within  $10^{-9}$  in the Monsanto units;  $M$  and  $N$  are invariants as is  $K_1$ . Therefore, this term is a constant which can be subtracted from  $(V_2 - V_1)$  under zero flow conditions in the case of measuring the steady state flow component, or neglected entirely if only a dynamic flow measurement is to be made. Variations in sound speed can also be measured if desired by adding Eqs. (8) and (9):

$$(V_1 + V_2) = \frac{2 N - 1}{K_1} \frac{\sin \theta}{2 D} c - \frac{1}{K_1} \left[ f_{10} + \left( \frac{2 N - 1}{2 M - 1} \right) f_{20} \right]. \quad (11)$$

The reason for providing a significant (~10%) separation between the frequencies of the upstream and downstream waves is that such a separation eliminates the need for a phase code modulation/demodulation scheme as is summarized in ref. 9. More conventional techniques suffice to isolate the received and transmitted waves at the transducer locations.

### Tests

Although the contract acknowledged below called for a design only, not tests, it was agreed to conduct a limited experimental program. The most significant experimental result was obtained using a four transducer arrangement connected electrically as in Fig. 6, and mounted in a cell similar to that used in an earlier program.<sup>9</sup> This test demonstrated stable, independent and simultaneous frequency servoing of both the upstream and downstream waves. Also, upon repetitive intentional interruption of either received signal, the system immediately locked onto the same total phase when the signal was reconnected. By filtering, one can separately read out both the dynamic (1-100 Hz) and dc flow components. These experimental results prove that a servoed frequency system can in fact be implemented. The number and type of constraints imposed upon the phases can be varied somewhat depending on the details of the application. For example, in another program,<sup>10</sup> constraints are chosen to provide an output voltage proportional to  $v/c$ , the Mach number. This number, when multiplied by the fluid's impedance  $\rho c$ , yields a final output proportional to mass flow rate. In general, one can arrange for the flow "velocimeter" to yield  $v$ ,  $v/c$ , or  $v/c^2$ .



LEGEND: PA = Power Amplifier; B = Buffer Amplifier; DC = DC Amplifier; IF = IF Amplifier.

Fig. 6. Block diagram of dynamic flowmeter electronic design.

We are now building a complete system for initial dynamic flow testing on liquid nitrogen at NBS-Boulder (pipe diameter ~10 cm), with subsequent testing at NASA-Huntsville (pipe diameter ~30 cm). Future applications may include ground tests for the space shuttle Orbiter, where dynamic flow velocity needs to be measured in liquid oxygen and hydrogen at various locations (NAS1-11756).

#### References

1. S. Rubin, NASA SP-8055, Prevention of Coupled Structure-Propulsion Instability (Pogo) (Oct. 1970).
2. S. Rubin, Prevention of Coupled Structure-Propulsion Instability (Pogo) on the Space Shuttle. Space Transportation System Technology Symposium (Cleveland), Vol. II-Dynamics and Aeroelasticity, NASA TM X-52876, pp. 249-262 (1970).
3. N. E. Pedersen and L. C. Lynnworth, NASA CR-112313 (R) (June 1972).
4. C. G. Knott, Phil. Mag. 48 (290), 64-97 (July 1899).
5. F. A. Firestone and D. S. Ling, Jr., Depts. of Physics and Engineering Research, Univ. of Michigan, Sperry Product Engineering Dept., Engineering Ref. File 5-1-1, Project M530, Reflection and Refraction of Supersonic Waves, The Raybender, pp. 24-57 (March 1945); R. C. McMaster (ed.), Nondestructive Testing Handbook, Vol. II, Ronald Press, Sect. 43, 19-23 (1959).
6. W. G. Mayer, Ultrasonics 3 (2), 62-68 (April-June 1965).
7. J. W. Garber, Ultrasonic Interactions at Liquid/Solid Boundaries, Union Carbide Rpt. No. Y-1540, Oak Ridge, Tenn. (July 1, 1966).
8. F. T. Brown, et al., Trans. ASME-J. Basic Engineering, 69-FE-11 (1969).
9. L. C. Lynnworth et al., Proc. 1972 IEEE Ultrasonics Symposium, 81-84; Proc. 1971 ISA Symposium on Flow, Pittsburgh, Pa.
10. L. C. Lynnworth, N. E. Pedersen and E. H. Carnevali, Final Report, Contract DAAJ 02-73-C-0054 (1974).

#### Acknowledgments

The authors acknowledge the encouragement and assistance of interested personnel at NASA-Langley, particularly T. D. Carpin. The cooperation of J. W. Garber and the Union Carbide Corporation, Nuclear Division, regarding use of their Fortran program and excerpts from Y-1540 is acknowledged. At Panametrics, E. H. Carnevale contributed to helpful discussions throughout the program; E. P. Papadakis programmed the LOX/metal cases of interest; K. A. Fowler built the transducers later used by J. E. Bradshaw and R. Morris to demonstrate the simultaneous servoing of the two frequencies transmitted upstream and downstream. J. G. Payne and S. Rubin of the Aerospace Corporation provided important design requirements and guidelines. B. A. Younglove of NBS-Boulder provided unpublished information on his cryogenic measurements. Professor F. T. Brown of Lehigh University computed the K factor for the dynamic profiles of main interest. This work was supported in part by NASA Contract NAS1-11756.

Construction of the flowmeter is now proceeding under Contract NAS1-12747.

Copyright by and reprinted with permission from the 1973 Ultrasonics Symposium IEEE Proceedings.



## APPENDIX D

ISA-authorized reprint from:

Flow - Its Measurement and Control in Science and Industry, Volume I.

Proceedings of the first interdisciplinary symposium, conducted 1971 in Pittsburgh, PA. Sponsored by American Society of Mechanical Engineers, American Institute of Physics, National Bureau of Standards, and ISA.

## NONINTRUSIVE ULTRASONIC MEASUREMENT OF FLOW VELOCITY AND MASS FLOW RATE

L.C. LYNNWORTH, N.E. PEDERSEN, E.P. PAPADAKIS\* AND J.H. BRADSHAW\*\*

*Panametrics  
Waltham, Massachusetts*

Four nonintrusive methods are analyzed for introducing ultrasonic waves into fluids within a pipe, without mechanically perturbing the inside of the pipe. In one method, obliquely incident shear waves are mode converted to longitudinal waves in the fluid. In a second method, wavefronts are diffracted into fluids at an angle. A third method involves beaming plane or focused waves across two separated paths, and measuring the correlation time between fluctuations in propagation over the two paths. A fourth method would use a fixed transducer array to control the sound distribution in the fluid. Other nonintrusive methods such as inserts, recesses or grooves require that the pipe be penetrated or its inside perturbed. Techniques are described which weight flow velocity proportional to cross-sectional area. Theoretically, this yields acoustic flow velocity readings which essentially do not require profile corrections for laminar, transitional or turbulent flow. One application of nonintrusive ultrasonic measurement of flow velocity, together with nonintrusive ultrasonic density compensation, is the measurement of mass flow rate  $\dot{M}$  of liquid fuels in a helicopter engine. Here, we demonstrated a transmission technique which employed phase-coded continuous waves and a refraction coefficient densitometer. The coded waves were separated and their phase difference was measured after upstream and downstream oblique transmission across square-channeled flow, over a common path between a pair of recessed, rectangularly-collimated transducers.

### INTRODUCTION

This paper is concerned with the analysis and design of flowmeters employing nonintrusive ultrasonic transducers for the measurement of fluid flow, sometimes without any penetration or perturbation of the container of the fluid. We shall limit the scope to analytic and experimental work done in our laboratory these past five years, and shall cover only the main points.

The user of a flowmeter usually seeks a precise, and sometimes accurate, measurement averaged over the full cross-sectional area of the fluid, and averaged over a time interval which may range from 10 ms in cases of aircraft engine control<sup>1</sup> or Pogo (flow oscillation) diagnostics,<sup>2</sup> to 24 hr in the case of pollution monitoring of stack exhausts.<sup>3</sup> There are also medical applications where flow velocity *profile* is to be determined,<sup>4</sup> and wind tunnel applications where profiles of *both* flow velocity and density are to be measured, to determine mass flow rates.<sup>5</sup> Accuracy requirements are usually in the 0.1 to 10 percent range. Mach numbers

range from less than  $10^{-3}$  to greater than 10; Reynolds number  $Re$  ranges from less than 100 to greater than  $10^7$ . Diameters range from  $\sim 1$  mm to tens of meters. Fluids are not always single-phase or homogeneous, and flow is not always unidirectional or steady.

Ultrasonics may offer the preferred approach to problems containing much of this complexity. One of the first details to be considered deals with data averaging, both area- and time-wise. Details of nonintrusiveness, precision, accuracy, reliability, response time, equipment versatility, complexity, maintainability, cost and other factors are also important.

### Average Flow Velocity

The ultrasonic measurement of flow velocity averaged across a single path which is a small fraction of the circular pipe area usually exceeds the true area-averaged flow velocity  $v$  by less than 8 percent for  $Re > 10^4$ , but by 25 percent for laminar flow.<sup>1,6,7</sup> We have found that one way to properly average the flow velocity profile is to measure transmissions across the entire fluid cross section in a rectangular or square flow channel, using rectangularly- or square-collimated plane waves.<sup>1</sup> Another way is to scatter a uniform plane wave

\*Present address: Ford Motor Co., Detroit, Michigan.

\*\*Present address: Gillette Co., Boston, Massachusetts.

## ACOUSTIC METHODS

off scatterers which are uniformly distributed, and measure the doppler shift.<sup>1</sup> These methods avoid assumptions about the flow profile. In some cases of unsteady flow, the major part of the flow has a profile so nearly flat that measurements over a single path should provide 1 percent accuracy.<sup>2</sup>

To achieve the highest accuracy in a given time interval, continuous waves potentially are best. Various electronic methods such as phase-code modulation, dual frequencies and fm have now been demonstrated, to separate upstream from downstream waves transmitted simultaneously over an essentially common path between a given pair of transducers.<sup>1,2,8</sup>

In any particular application, the optimum electronic approach generally cannot be selected independent of the details of the transducer mounting material and geometry - and vice versa. The selection also must recognize that different electronic flow velocimeter approaches respond primarily to  $v$ ,  $v/c$  or  $v/c^2$ , where  $c$  is the sound speed in the fluid.

We next present four nonintrusive transducer designs which, to our knowledge, originated in our laboratory.

## OBLIQUELY INCIDENT SHEAR WAVES

Obliquely incident vertically polarized ultrasonic shear waves can be mode-converted to longitudinal waves, and then transmitted diagonally across the conduit such that there is a substantial component of the longitudinal velocity in a direction parallel to the axis of flow of the fluid.<sup>9</sup> When this is achieved with transducers mounted external to the conduit there is no perturbation of the flow of the fluid stream, other than possibly thermal perturbation.

We demonstrated this noninvasive technique in water contained in a Cu pipe  $\sim 1.3$  cm diameter, and in a steel pipe 25 cm diameter, in the late sixties. Present applications involve cryogenic liquids, water and liquid sodium.

Figure 1 compares paths for longitudinal and shear waves incident at 45 deg in water. Note that the probes are flush-mounted inserts. If the fluid is water, and the insert probe (wedge) is made of acrylic, (a)  $L_L = 0.44D$ , and (b)

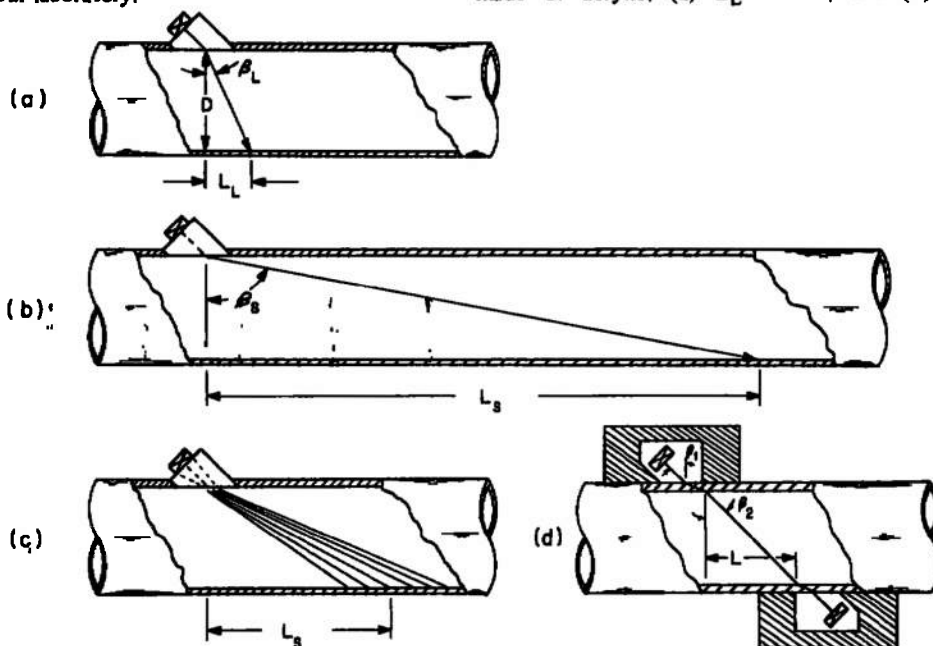


Fig. 1. Comparison of obliquely incident (45 degrees) longitudinal and shear waves.

## NONINTRUSIVE ULTRASONIC MEASUREMENT

$L_S = 5.67D$ , at room temperature. In (c) the focused incident wave permits the axial-projected path to remain constant by means of temperature-adaptive ray selection. In (d) we show a hybrid case. For some combinations of liquids and pipe wall materials, the 45 deg obliquely-incident longitudinal wave in the still liquid is refracted and mode-converted to a shear wave in the pipe wall. This shear wave reconverts to a single longitudinal wave in the flowing liquid. When the sound speeds are equal in the liquids in the transducer cavity and in the pipe,  $L = D$ .

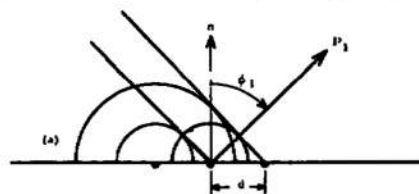
It can be seen that the shear waves are mode-converted by refraction at the interface into longitudinal waves, which are now transmitted at a much higher angle, typically twice that achievable with an incident longitudinal wave, through the fluid material. Since the ultrasonic waves being transmitted through the fluid have a significant component of velocity in a direction parallel to the axis of flow, the resolution of the measurement is increased by a factor of two or more. Further, obliquely incident shear, compared to obliquely incident longitudinal, may be coupled more efficiently into the fluid.<sup>10</sup> In the pipe itself, the slower, zigzagging shear wave is less troublesome than a zigzagging longitudinal and its mode-converting reverberations. At high temperature, the available transducer material (e.g.,  $\text{LiNbO}_3$ ) may be more efficient in shear than in longitudinal mode. Another advantage of using shear waves obliquely incident at a solid/liquid interface is that upstream and downstream waves can be generated and received by pairs of transducers polarized orthogonally at  $\pm 45$  degrees to the plane of incidence. This facilitates separation of the upstream and downstream waves even if they are transmitted continuously over a common path, at the same frequency.

## DIFFRACTION GRATING

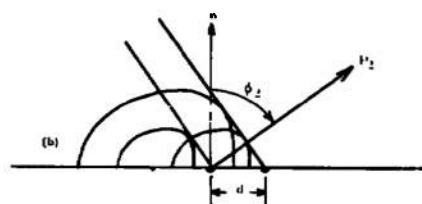
A second nonintrusive method of introducing ultrasound into the pipe (duct, channel) and to detect it is by means of ultrasonic diffraction gratings.<sup>15</sup> This method, used in dispersive delay lines, is advantageous from the point of view of sensitivity in one measurement scheme because the flow distorts and translates the Huygens wavelets radiated into the fluid in such a way as to steer the diffracted beams. Consider

the grating in Fig. 2. The circular Huygens wavelets in the no-flow condition are warped by laminar flow or translated (with distortion) by turbulent flow. The +1 diffracted order, radiating downstream as drawn, has its Poynting vector  $P$  steered more downstream, making its reception at the opposite side of the channel occur later than it would have under no-flow conditions. This result is opposite to the ordinary result in which the flow velocity causes the wave to arrive earlier in time. When angle  $\phi$  is large (approaching 90 degrees), the steering effect can be large.

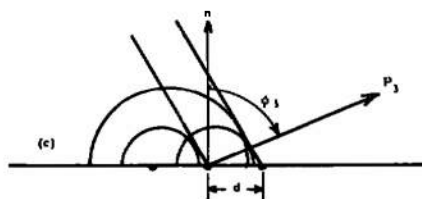
Reception is accomplished by a second diffraction grating, longer in extent and of the same spacing. The diffraction grating flowmeter could be operated in a pulsed rf mode with time-of-flight as the measured parameter. Another mode of operation is fm. The beam can be steered from the transmitter grating to a



Huygens wavelets for no flow. The Poynting vector  $P$  is generated at angle  $\phi$  defining the path of energy flow.



Wavelets for laminar flow



Wavelets for turbulent flow

Fig. 2. Analysis of wavelets launched by diffraction grating.

## ACOUSTIC METHODS

particular location on the receiver grating (or to a very small receiver) by changing the input frequency to compensate for the shifting of the Huygens wavelets by the flow. Readout would be the frequency generating the maximum received signal.

For thin-walled pipe, tubing, and ducts, the grating may be on the outside of the wall. Here, "thin-walled" is less than a wavelength. For thick-walled vessels, the grating should be on the inside (this may not always be "nonintrusive"). Screw threads are adequate gratings for transmission and reception in circular pipes. While the grating diffraction method of introducing a wave into a pipe (duct, channel) can be utilized for beam steering in the particular flowmeter scheme described above, it can also be used to introduce ultrasonic waves nonintrusively for other purposes. An endfire array ( $\phi = 90$  degrees) can be used for ordinary time-of-flight measurements or for doppler measurements. A principal limitation on this method is its extreme sensitivity to the boundary layer right next to the wall.

### NORMALLY INCIDENT LONGITUDINAL WAVES

This nonintrusive method involves beaming plane or focused waves across two axially-separated diameters.<sup>16</sup> Flow transit time between these two diameters is taken as the correlation time between fluctuations in propagation (velocity, scattering and/or attenuation) over said diameters.<sup>17</sup>

The method is illustrated schematically in Fig. 3. Provided the fluid wets or contacts the pipe with sufficient intimacy so ultrasound can be coupled across the interface, the acoustic part is relatively simple. One chooses a frequency high enough to yield directivity, and to attenuate the potentially troublesome acoustic short circuit around the pipe perimeter, yet not so high that attenuation in the fluid itself is excessive.

To reduce memory requirements in the correlation detector, one can periodically introduce a thermal or other disturbance. Naturally, within the spirit of the present "nonintrusive" approach, we suggest this perturbation be introduced noninvasively. For example, a high-

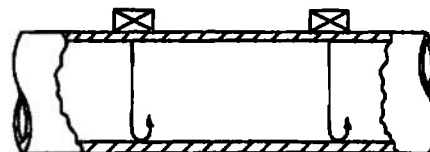


Fig. 3. Correlation time between longitudinal waves provides a measure of flow velocity.

intensity focused pulse introduced upstream will cause a slight temperature rise, and possibly cavitation near the axis.

As with other tagging techniques or correlation flowmeters reported in this Symposium, care must be exercised with regard to weighting and tag smearing.

### FIXED TRANSDUCER ARRAY

In this method of nonintrusive flow measurement, sound would be introduced into a section of pipe and detected by an array of fixed transducers.<sup>18</sup> The acoustic wavelength and pipe geometry determine the resultant mode. This mode ideally would weight each area element of the fluid's cross section equally. The array requires that a fixed acoustic wavelength,  $\lambda$ , be maintained within the pipe. The average velocity of the flow within the pipe is determined by measuring the frequency shift  $f \pm f'$  required to maintain  $\lambda$  (and applying profile corrections). Since the shifted frequency  $f' = (c \pm v)/\lambda$  due to flow velocity can be measured in either direction, the difference between the two can be extracted directly and is equal to  $\Delta f = (c + v)/\lambda - (c - v)/\lambda = 2v/\lambda$ . The array is composed of a row of transducers spaced and polarized such that the response due to sound "short-circuiting" through the walls of the pipe will be negligible around the operating frequency. The last transducer on each end is used for the transmitter of the up- and downstream sound and a sing-around oscillator is provided for each direction. The two frequencies are mixed to obtain the difference,  $\Delta f$ . Figure 4 illustrates this system schematically.

There are two conditions which should be considered when using this technique of flow measurement. First, the effective sound velocity in the fluid ( $c_f$ ) must be different from that in the pipe ( $c_p$ ). That is, if  $2n$  is the

## NONINTRUSIVE ULTRASONIC MEASUREMENT

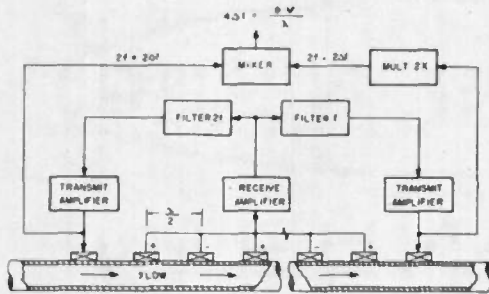


Fig. 4. Transducer array and sing-around flowmeter.

number of receive transducers and  $c_p/c_f = n'/n$  then  $n'$  should not be harmonically related to  $n$  (i.e.,  $n' \neq mn$ ) within the range  $c_f = c \pm v_{\max}$ . Secondly, the flow profile should be reasonably defined, consistent with accuracy requirements. (The fluid itself need not be homogeneous.) The type of profile correction is somewhat flexible, as the choice of acoustic mode (depends on pipe diameter to wavelength) or other considerations may make this correction unnecessary, or less critical than in other sing-around flowmeters which do not sample the entire fluid cross section. The authors have not yet demonstrated this method.

## RECESSED TRANSDUCERS

Recessed, nonintrusive transducers have been used by several earlier investigators. In our work on the helicopter engine fuel mass flowmeter, we used this approach, but not exactly in its usual form. Rather, we recessed the transducers behind a rectangular "sound port", to achieve a uniform weighting of the square-channeled flow intersected by the rectangularly-collimated sound beam.<sup>1</sup>

The hybrid designs of Fig. 5 retain the advantages of a transducer mounted outside the conduit, yet retain a beam direction which, like in the case of the usual recessed transducer, can be substantially or completely independent of sound speed in the fluid.

## MISCELLANEOUS INTERROGATION METHODS

Ultrasonic measurement of Mach number (Fig. 6a),<sup>11</sup> of the drawing speed of wire, particularly magnetostrictive wire (Fig. 6b), of

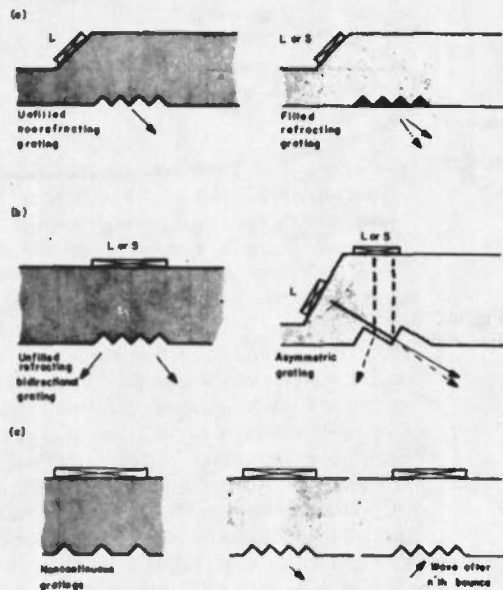


Fig. 5. Use of vee grooves to transmit over oblique paths.

fluid flow through permeable reflectors (Fig. 6c),<sup>12</sup> or between heat exchanger tubes offering limited access (Fig. 6d), are examples of special applications where ultrasonics offers a unique approach. Figure 7 illustrates a more general potential application, where ultrasound could measure  $v$  plus one or more other process variables.<sup>13</sup>

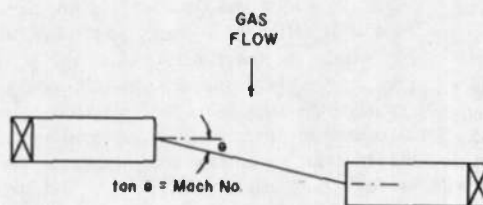


Fig. 6a. Approximate measure of subsonic gas flow velocity obtained at combustor exit by ratio of probe offset to gas path length.



Fig. 6b. Measurement of material velocity using guided extensional waves. Waves are introduced and detected magnetostrictively, without contact between coil and material.

## ACOUSTIC METHODS

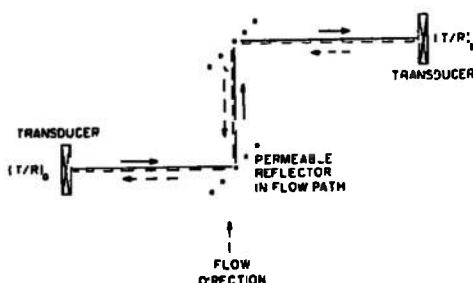


Fig. 6c. Reflectors for bidirectional interrogation of flow region using remote transducers.

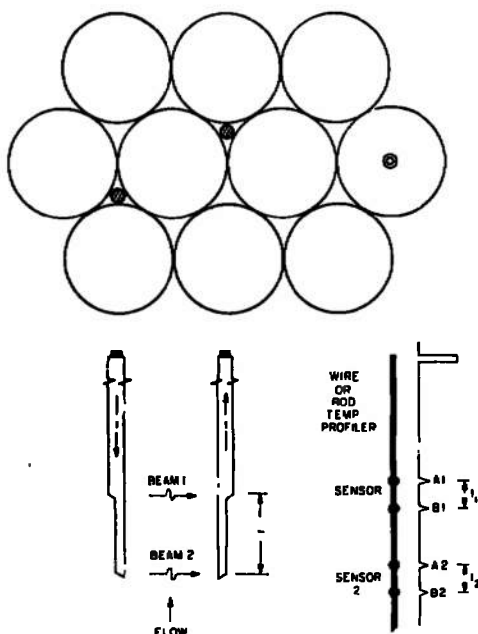


Fig. 6d. Correlation time between transmissions beamed over two parallel paths a distance  $L$  apart, provides a measure of flow. Multi-beveled probes are shown located in triangular cusps. Analogously, a single wire or rod may contain temperature-sensing zones spaced  $L$  apart. One would measure correlation time between  $t_1$  and  $t_2$ .

### MASS FLOWMETER FOR AVIATION FUELS

From the viewpoint of those responsible for diagnosing and controlling the performance of aircraft engines, it is important to know accurately the value of the fuel mass flow rate  $\dot{M}$ .<sup>1</sup> In 1972, we demonstrated a fuel flowmeter consisting of a flow velocimeter, densitometer, time intervalometer, and a metering section

containing nonintrusive transducers. The velocimeter measured the phase difference between two coherent individually coded 5 MHz waves continuously transmitted obliquely upstream and downstream across a common path, yielding a phase difference proportional to  $v/c^2$ . The densitometer consisted of a stepped-diameter probe; the difference in echo amplitudes at the wetted end and at the dry step is a function of the acoustic impedance  $\rho c$  of the fuel where  $\rho$  is the fuel density. The time intervalometer measured the time  $\tau$  between two successive echoes, which time is proportional to  $1/c$ . The mass flow rate is  $\dot{M} = (K)(v/c^2)(\rho c)(1/\tau)$  where  $K$  is a constant. The complete system was tested on various liquids at rates up to  $\sim 2300$  kg/hr. It was operated during and recalibrated after 104-hr exposure to a contaminated fluid flowing at  $\sim 860$  kg/hr. Response time was 20 ms. The flowmeter can operate in laminar, transitional and turbulent flow. It was concluded that refinement of this approach should be able to attain  $\dot{M}$  accuracy of 1 percent, despite a wide range of Reynolds numbers and other variables.<sup>1</sup> Work directed to attaining this performance is now in progress.

### CONCLUSIONS

Nonintrusive flow measurements are attractive because of their potential application to a variety of flowmetry problems where it is inconvenient or undesirable to penetrate the container, or to locate a sensor in the flow itself. A variety of ultrasonic transducer designs are now available which do not obstruct the flow. In some cases the transducers may be mounted outside the conduit, so that they do not disturb the flow profile in any significant way.

Depending on the details of the application, a transmission or a scattering approach may be preferred. It may even be desirable to incorporate both approaches in one modular system, to handle two-phase applications where scattering is not always sufficient to rely on a doppler system, yet may sometimes be so large as to interfere with a transmission measurement. Other factors such as area-averaging, range/resolution selection by frequency shift or multi-bounce transmission, accuracy and response

## NONINTRUSIVE ULTRASONIC MEASUREMENT

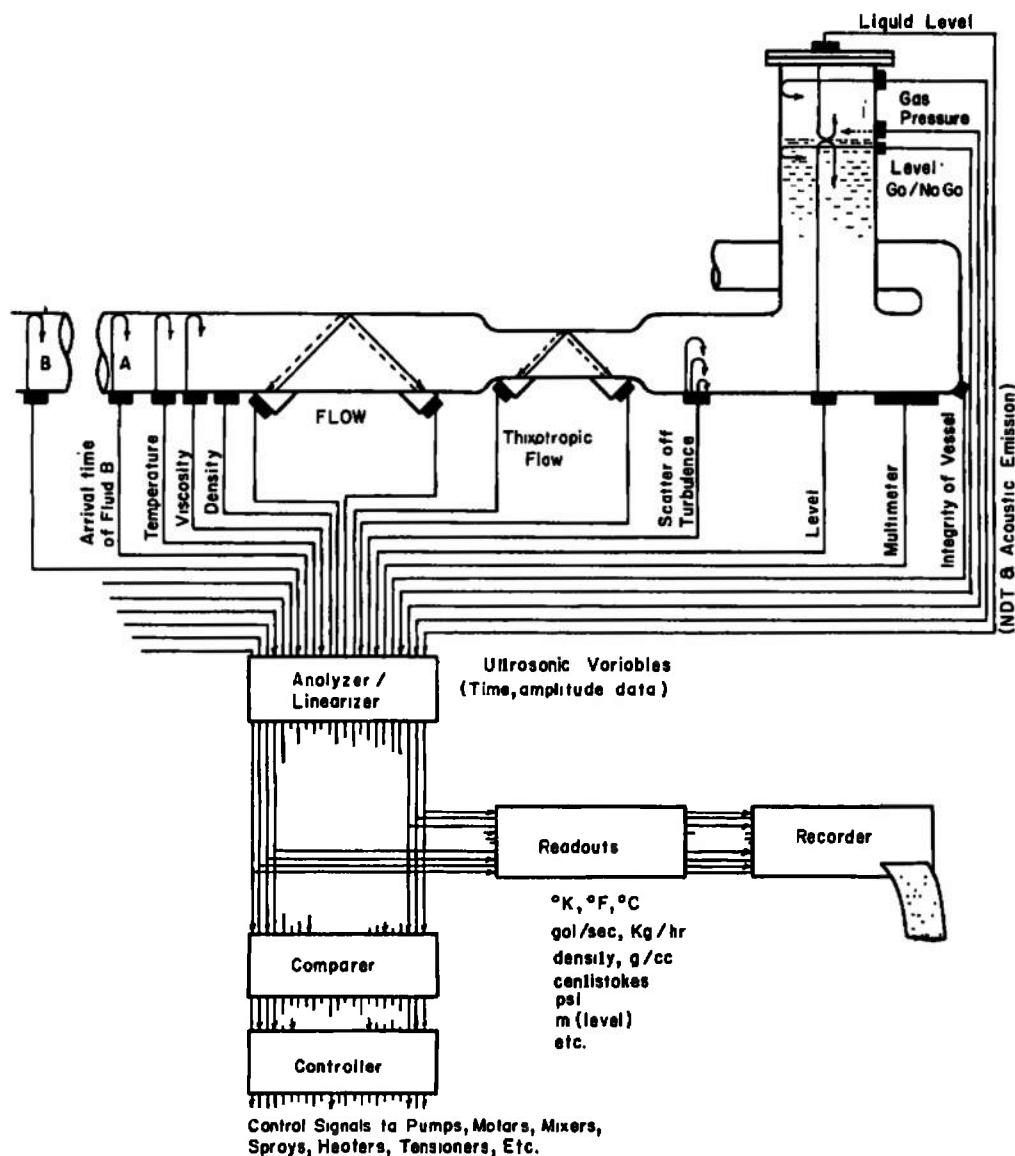


Fig. 7. Schematic of ultrasonic instrumentation system for fluid process measurement and control.

time requirements enter into the optimization of available flowmeter approaches for specific applications.

Analysis of specific applications such as measuring the steady flow of aviation fuels, and the oscillatory flow of cryogenic liquids, to absolute accuracies of 1 percent or better with a response time of about 10 ms, showed that, at least for these cases, the optimum approach

should include the use of cw or rf bursts, not pulses, transmitted upstream and downstream over a common path.

At this occasion of the First Symposium on Flow, it is instructive to look back ten years to a review which compared ultrasonic and other flowmeters with regard to maximum flow rate, accuracy, media, temperature, maximum pressure and viscosity.<sup>14</sup> The past decade has

## ACOUSTIC METHODS

witnessed experiments on a number of ultrasonic flowmeters, including successful applications in gases, liquids and airborne solids, primarily for industrial process control. Looking ahead to the seventies, we may anticipate ultrasonics' expanding role in human and ecological terms, based on measuring flow not only in a variety of industrial applications, but also in fluids in the human body and in the ecosphere.

## ACKNOWLEDGMENT

The authors acknowledge numerous helpful discussions with E.H. Carnevale of Panametrics, and with others outside Panametrics, for assistance in clarifying the technical and economic goals for improved flowmeters. Particular thanks are due Professors H. Schlichting and H. Blenk for guidance on the effects of boundary layers and inlet conditions on profiles. The encouragement of G. William Hogg and B. Poteate of the Eustis Directorate, and assistance of J.I. Black of Avco-Lycoming, J.L. DuBois and P. Kranz of Dytron, K.A. Fowler, R.E. Fisher, G.M. Elfbaum, J.E. Bradshaw, R. Morris and C.M. Barber of Panametrics in the design, construction and testing of various aspects of the Eustis mass flowmeter is also acknowledged. Helpful discussions with T. Carpini of NASA-Langley are acknowledged, relative to designing transducers and electronics to measure flow dynamics in liquid oxygen and liquid hydrogen. Contributions of Professor F.T. Brown of Lehigh University are also acknowledged.

## References

- <sup>1</sup>L.C. Lynnworth, N.E. Pedersen and E.H. Carnevale, Ultrasonic Mass Flowmeter System, USAAMRDL Tech. Rpt. 72-66, Contract DAAJ02-71-C-0061 (1972); L.C. Lynnworth and N.E. Pedersen, Ultrasonic Mass Flowmeter, in: *Proc. 1972 IEEE Ultrasonics Symposium*, 87-90, Boston, Mass. (Oct. 4-7, 1972).
- <sup>2</sup>N.E. Pedersen and L.C. Lynnworth, Design of a Nonintrusive Dynamic Flowmeter, Final Rpt., Contract NAS1-11756 (1973); Final Rpt., Contract NAS1-12747 (1974); *Proc. 1973 IEEE Ultrasonics Symposium*, 178-181, Monterey, Calif. (Nov. 5-7, 1973).
- <sup>3</sup>Environmental Protection Agency, Sol. No. DU-72-A118 (April 10, 1972).
- <sup>4</sup>A multiple gate pulse doppler flowmeter developed at Stanford University was reported at the 1971 IEEE Ultrasonics Symposium by F.D. McLeod and M. Anliker, and is abstracted in *IEEE Sonics and Ultrasonics* SU-19 (3), 401 (July 1972).
- <sup>5</sup>L.C. Lynnworth, N.E. Pedersen and C.A. Carey, Final Rpt., AEDC Contract No. F40600-73-C-0011 (1974).
- <sup>6</sup>J. Kritz, *ISA Proc.* 10, Part 2, 55-16-3, pp. 1-6 (1955); *Instruments and Automation* 28, 1912-1913 (1955).
- <sup>7</sup>E.M. Moffatt and K.I. Fetichehoff, Paper No. 2-10-126, *Proc. 1971 Flow Symposium*; J.L. McShane, *ibid*; *Instrum. Techn.* 18 (7), 44-48 (July 1971); Westinghouse Sci. Paper 71-1C6-FLOME-P1 (Aug. 13, 1971).
- <sup>8</sup>F. Noble, *Rev. Sci. Instrum.* 39 (9), 1327 (Sept. 1968); see also R.E. Fishbacher, Flowmeters, U.S. Patent No. 3,097,526 (July 16, 1963).
- <sup>9</sup>L.C. Lynnworth, Ultrasonic Testing Method, U.S. Patent No. 3,512,400 (May 19, 1970); Fluid Flowmeter, U.S. Patent No. 3,575,050 (April 13, 1971); *Materials Evaluation* 25 (12), 265-277 (1967); pp. 323-361, in: *Proc. 6th Symposium on Nondestructive Evaluation*, San Antonio (April 1967), Western Periodicals Co.
- <sup>10</sup>J.W. Garber, Ultrasonic Interactions at Liquid-Solid Boundaries, Rpt. Y-1540, pp. 15, 25, 32 (July 1, 1966); R.C. McMaster (ed.), *Nondestructive Testing Handbook*, Vol. II, Sect. 43, pp. 17-21 (1959).
- <sup>11</sup>S.S. Fam, L.C. Lynnworth, E.H. Carnevale and B.J. Spencer, Feasibility of Ultrasonic Determination of Turbine Inlet Gas Temperature, Test Rpt. for GE-Evendale, Ohio (July 17, 1969).
- <sup>12</sup>L.C. Lynnworth, E.H. Carnevale and D.R. Patch, U.S. Patent No. 3,636,754 (Jan. 25, 1972).
- <sup>13</sup>L.C. Lynnworth, et al., *IEEE Trans. Nucl. Sci.* NS-18 (1) Part 1, 351-362 (1971); Paper No. 04-19, in: *Proc. 5th Symposium on Temperature - In Measurement and Control in Science and Industry*, Washington, D.C. (21-24 June 1971); *Proc. 7th International Congress on Acoustics* 4, 525-528, Budapest, Akademiai Kiado (1971).
- <sup>14</sup>C.C. Miesse and O.E. Curth, *Product Engineering* (May 8, 1961).
- <sup>15</sup>Method conceived and demonstrated by E.P. Papadakis.
- <sup>16</sup>Method of nonintrusive measurement across one 25 cm diameter of a stainless steel pipe containing liquid sodium at ~350°C was demonstrated in May 1968 at Argonne National Laboratory by L.C. Lynnworth, K.A. Fowler and B.J. Spencer; reported in NYO-3906-4 (Sept. 1968); NYO-3906-13 (June 1972).
- <sup>17</sup>J. Coulthard, *Ultrasonics* 11 (2) 83-88 (March 1973).
- <sup>18</sup>Method due to J.H. Bradshaw.



## LIST OF SYMBOLS

$\alpha$	absorption coefficient for dry air; angle between direction of propagation and normal to phase front
$\alpha_c$	classical sound absorption coefficient due to thermal conductivity and viscosity
$\alpha_o$	angle of wave propagation relative to normal to transducer face
$\gamma$	specific heat ratio
$\delta^*$	displacement thickness of turbulent boundary layer
$\eta$	viscosity
$\theta$	angle
$\lambda$	wavelength
$\mu$	magnetic permeability
$\overline{\mu^2}$	index of refraction rms fluctuation
$\xi$	particle displacement in sound wave
$\rho$	density gm/cm <sup>3</sup>
$\tau$	correlation delay
$\psi_{xy}$	time correlation function
$\omega$	angular frequency ( $2\pi f$ ) of sound wave
$\omega_o$	convection frequency characteristic of boundary layer
$a$	electrical conductivity
$a_1$	correlation length of burbulence
$B_{rr}$	velocity correlation coefficient
$B_T$	thermal fluctuation correlation coefficient
$c$	sound speed

## LIST OF SYMBOLS (cont'd)

$d$	area density, $\text{gm/cm}^2$ ; transducer diameter
$D$	duct diameter
$f$	frequency of sound wave
$\Delta f$	frequency difference between two sound waves
$f_d$	doppler frequency
$k$	wave number of sound wave $\frac{2\pi}{\lambda}$
$l$	pathlength, length of shock formation
$L$	sound path
$L_z$	loss due to acoustic impedance mismatch
$L_\alpha$	loss due to absorption
$M$	Mach number
$\tilde{p}$	pressure fluctuation in sound wave
$P_{\max}$	maximum pressure acoustic wave which can be propagated a distance $l$ without shock formation
$P_r$	Prandtl number
$t$	time
$T$	Temperature
$T_o^2$	mean square temperature fluctuation of turbulence
$U_o$	maximum flow velocity
$v$	flow velocity (particle velocity)
$V_o^2$	mean square velocity fluctuation of turbulence
$x$	streamwise distance and beam drift distance
$Z$	normal distance from transducer face